

RADC-TR-89-196  
Final Technical Report  
October 1989

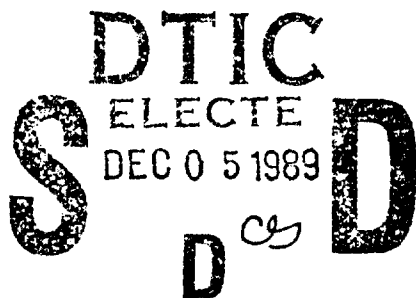
AD-A214 833



# MONOCHROMATOR CONFIGURATIONS FOR WAVELENGTH DIVISION MULTIPLEXING

Georgia Institute of Technology

Dr. Russell A. Chipman and Thomas Burleson



APPROVED FOR PUBLIC RELEASE; DISTRIBUTION UNLIMITED.

ROME AIR DEVELOPMENT CENTER  
Air Force Systems Command  
Griffiss Air Force Base, NY 13441-5700

UNCLASSIFIED

SECURITY CLASSIFICATION OF THIS PAGE

REPORT DOCUMENTATION PAGE				Form Approved OMB No. 0704-0188	
1a. REPORT SECURITY CLASSIFICATION UNCLASSIFIED			1b. RESTRICTIVE MARKINGS N/A		
2a. SECURITY CLASSIFICATION AUTHORITY N/A			3. DISTRIBUTION/AVAILABILITY OF REPORT Approved for public release; distribution unlimited.		
2b. DECLASSIFICATION/DOWNGRADING SCHEDULE N/A					
4. PERFORMING ORGANIZATION REPORT NUMBER(S)  N/A			5. MONITORING ORGANIZATION REPORT NUMBER(S)  RADC-TR-89-196		
6a. NAME OF PERFORMING ORGANIZATION Georgia Institute of Technology		6b. OFFICE SYMBOL (If applicable)	7a. NAME OF MONITORING ORGANIZATION  Rome Air Development Center (DCLW)		
6c. ADDRESS (City, State, and ZIP Code) Georgia Tech Research Corporation Centennial Research Bldg Atlanta GA 30332-0420			7b. ADDRESS (City, State, and ZIP Code)  Griffiss AFB NY 13441-5700		
8a. NAME OF FUNDING/SPONSORING ORGANIZATION  Rome Air Development Center		8b. OFFICE SYMBOL (If applicable)  DCLW	9. PROCUREMENT INSTRUMENT IDENTIFICATION NUMBER  F30602-81-C-0185		
8c. ADDRESS (City, State, and ZIP Code)  Griffiss AFB NY 13441-5700			10. SOURCE OF FUNDING NUMBERS		
			PROGRAM ELEMENT NO. 63726F	PROJECT NO. 2863	TASK NO. 92
			WORK UNIT ACCESSION NO. P1		
11. TITLE (Include Security Classification)  MONOCHROMATOR CONFIGURATIONS FOR WAVELENGTH DIVISION MULTIPLEXING					
12. PERSONAL AUTHOR(S) Dr. Russell A. Chipman, Thomas Burleson					
13a. TYPE OF REPORT Final		13b. TIME COVERED FROM Mar 87 TO Mar 88		14. DATE OF REPORT (Year, Month, Day) October 1989	
15. PAGE COUNT 136					
16. SUPPLEMENTARY NOTATION  Work was done at University of Alabama in Huntsville.					
17. COSATI CODES			18. SUBJECT TERMS (Continue on reverse if necessary and identify by block number)		
FIELD	GROUP	SUB-GROUP	Multiplexing Optical Multiplexing		
17	02		Wavelength Division Multiplexing Fiber Optics		
19. ABSTRACT (Continue on reverse if necessary and identify by block number)  The purpose of this work was to investigate the application of modified Czerny-Turner spectrographic optical systems to high channel density wavelength division multiplexing. A breadboard test system was constructed using off-the-shelf components and system performance was measured and evaluated. The results found using the breadboard system will be used to further develop measurement techniques for WDM systems and also to increase the performance of other high density systems. In parallel with the breadboard fabrication/evaluation, a series of lenses to increase system performance have been designed.					
20. DISTRIBUTION/AVAILABILITY OF ABSTRACT <input checked="" type="checkbox"/> UNCLASSIFIED/UNLIMITED <input type="checkbox"/> SAME AS RPT. <input type="checkbox"/> DTIC USERS			21. ABSTRACT SECURITY CLASSIFICATION UNCLASSIFIED		
22a. NAME OF RESPONSIBLE INDIVIDUAL James D. Denly, 1Lt. USAF			22b. TELEPHONE (Include Area Code) (315) 330-4092		22c. OFFICE SYMBOL RADC (DCLW)

DD Form 1473, JUN 86

Previous editions are obsolete.

SECURITY CLASSIFICATION OF THIS PAGE

UNCLASSIFIED

## Contents

<b>1</b>	<b>Executive Summary</b>	<b>4</b>
1.1	Contract Objectives . . . . .	4
1.1.1	First Objective: Research . . . . .	4
1.1.2	Second Objective: Fabrication and Measurement Methodology . . . . .	4
1.1.3	Third Objective: Establishment of Baseline Performances . . . . .	5
1.1.4	Fourth Objective: Lens Design . . . . .	5
<b>2</b>	<b>WDM Breadboard System</b>	<b>6</b>
2.1	Breadboard Hardware . . . . .	7
2.1.1	Diode Lasers and Power Supply . . . . .	7
2.1.2	Collimating Optics . . . . .	8
2.1.3	Diffraction Grating . . . . .	8
2.1.4	Imaging Lens . . . . .	8
2.1.5	Translating Fiber . . . . .	9
2.1.6	Photodetector . . . . .	9
2.2	Data Acquisition . . . . .	9
2.3	Alignment . . . . .	9
<b>3</b>	<b>WDM Performances</b>	<b>10</b>
3.1	Determination of Baseline Crosstalk and Insertion Loss Performance . . . . .	10
3.2	Insertion Loss and Crosstalk Measurements . . . . .	11
<b>4</b>	<b>Lens Design</b>	<b>14</b>
4.1	Objectives . . . . .	15
4.1.1	Aberration Requirements of Multiplexer Lenses . . . . .	15
4.2	Computer Design Experiments . . . . .	16
4.2.1	Optimization Methods . . . . .	16
4.2.2	Three Element Multiplexer Lens Optimization . . . . .	17
4.2.3	Four Element Multiplexer Lens Optimization . . . . .	17
4.2.4	Five and Six Element Multiplexer Lens Optimization . . . . .	17
4.3	<u>Final Designs</u> . . . . .	18
4.3.1	UAH Multi-mode WDM . . . . .	18
4.3.2	UAH Single-mode WDM . . . . .	18
<b>5</b>	<b>Bibliography</b>	<b>20</b>

<b>6</b>	<b>Appendices</b>	<b>23</b>
6.1	Appendix A: WDM Lens Design Documentation . . . . .	
6.2	Appendix B: July Presentation . . . . .	
6.3	Appendix C: Dispersive Elements . . . . .	
6.4	Appendix D: Optical Fibers . . . . .	

## List of Figures

1	<u>Picture of the Breadboard Experiment</u> . . . . .	6
2	<u>Block Diagram of the Breadboard Experiment</u> . . . . .	7
3	<u>Crosstalk Matrix Example</u> . . . . .	11
4	<u>Strip-chart Intensity Recording (I) of the Fiber Scan</u> . . . . .	12
5	<u>Strip-chart Intensity Recording (II) of the Fiber Scan</u> . . . . .	13
6	<u>Picture of the Best Focus Image</u> . . . . .	13
7	<u>UAH Single-Mode WDM</u> . . . . .	14
8	<u>UAH Multi-mode WDM</u> . . . . .	18
9	<u>UAH Single-Mode WDM</u> . . . . .	19

## List of Tables

<b>1</b>	<b>Ideal Multi-mode WDM Specifications . . . . .</b>	<b>4</b>
----------	--	----------

Accession For: ☒ NTIS CRA&I ☐ DTIC TAB ☐ Unannounced ☐ Just Published

By: ☐ Distribution

☐ Distribution Codes

☐ Distribution

☐ Distribution

A-1

QUALITY  
INSPECTED  
1

Wavelength Range	1200 - 1400 nm
Number of Channels	100
Fiber Diameter	6 $\mu$ m
Insertion Loss	2 dB
Crosstalk	30 dB
Channel Separation	1.0 nm
Laser Drift	0.05 nm
Optical Configuration	Czerny-Turner Monochromator

Table 1: Ideal Multi-mode WDM Specifications

## 1 Executive Summary

### 1.1 Contract Objectives

The objective of this contract was to explore modified Czerny-Turner spectrographic optical systems for applicability to fiber optic wavelength division multiplexing of large numbers of signals. Under this contract, a breadboard wavelength multiplexing test station has been constructed using off-the-shelf components. The breadboard will simultaneously allow the development of measurement methodologies and establish baseline performances. In parallel with the breadboard fabrication, a series of lenses suitable for WDM applications have been designed.

#### 1.1.1 First Objective: Research

The first objective of the contract was to develop a particular Czerny-Turner system configuration for fiber optic WDM applications. Based on system characteristics and performances' (discussed in Appendices A), the system detailed in this report was chosen for development.

Table (1) lists the specifications of an idealized wavelength multiplexer suitable for large numbers of channels. While these specifications are well in excess of present expectations or present capabilities, they represent an ideal system for which many applications exist.

#### 1.1.2 Second Objective: Fabrication and Measurement Methodology

The second objective of the contract was to assemble a breadboard wavelength multiplexer. The breadboard WDM determined baseline performance specifications for both the development of test methods and the next round of engineering. Development of test methodologies have been successful. Equipment is in place for measurements, at laser wavelengths, of insertion loss

for each fiber and the crosstalk between various laser wavelengths. The methodology involves scanning a fiber on a motorized translation stage across the image location (see Section 3).

### **1.1.3 Third Objective: Establishment of Baseline Performances**

The establishment of baseline performances have been successful for a sample multiplexer. For the present measurements, operating on a limited budget and short schedule, a TV projection lens was purchased to function as the imaging lens. This lens has the required large size (100 mm aperture) and short focal length (150 mm). This lens was designed for a completely different application and wavelength range: projecting visible wavelength, magnified television images on a screen. Of the lenses available for under \$500, this was the closest to our specifications. No detailed optical performance data or lens specifications were available for this, or any other similar lenses, to allow a modeling of the lens's performance in the optical design program. We purchased the lens and hoped for the best.

The present system has an image size of about 0.75 mm, more than ten times the image quality required for a multimode wavelength multiplexing system. The present wavelength multiplexer breadboard differs from our proposed design in several aspects. The WDM system was designed to be put together in a minimum period of time for approximately \$10,000 cost and was composed entirely of off-the-shelf components, some of which were completely unsuitable for WDM applications.

### **1.1.4 Fourth Objective: Lens Design**

The fourth major activity in this contract involved optical design studies of monochrometer configurations that were adaptable to wavelength multiplexing. Modified Czerny-Turner spectrograph systems with multi-element imaging lenses were analyzed for aberrations and for their suitability for this application.

This lens designing began in January 1987 and continued until November. Two optical design programs were used: CODE V from Optical Research Associates, Pasadena, California; and SYNOPSIS from Optical System Design, Inc., Booth Bay Harbor, Maine. These programs were run on the Microvax computer in the Lens Design Laboratory at the Center for Applied Optics.

The problem that off-the-shelf (OTS) lenses are completely unsuitable for wavelength multiplexing is exactly the reason that this configuration of WDMs have not been previously demonstrated successfully. This WDM configuration requires a custom lens (see Section 4). The lens design experiments have been quite successful in designing attractive lenses for wavelength multiplexing. We have successfully demonstrated a multi-mode imaging lens, which uses only spherical surfaces, as well as a lens suitable for a single mode fiber optic wavelength multiplexing, which incorporates aspheric surfaces (see Section 4.2.4). These lenses demonstrate the performance specifications desired for wavelength multiplexing systems, but have

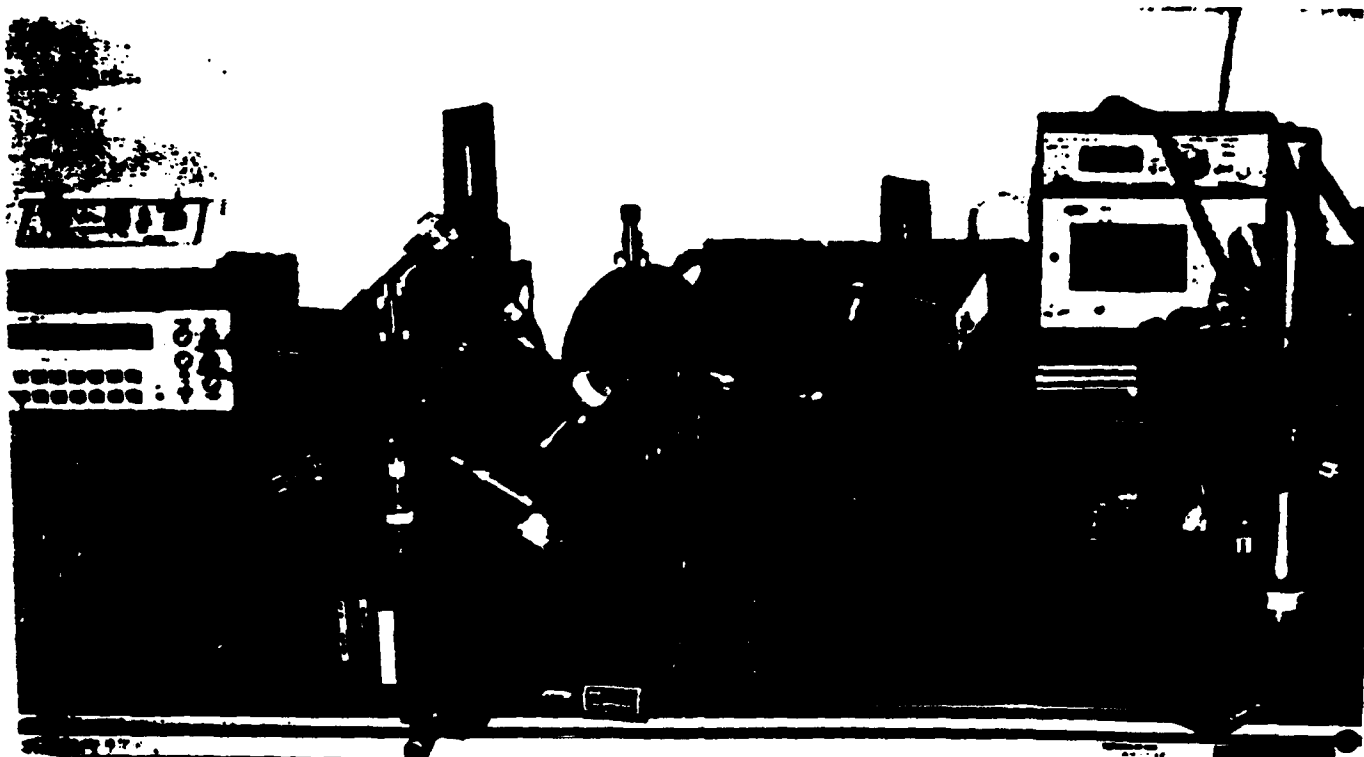


Figure 1: Picture of the Breadboard Experiment

not been engineered or studied to the point where we would recommend fabrication. More cost effective designs are undoubtedly possible given further work.

## 2 WDM Breadboard System

To demonstrate WDM concepts, a wavelength multiplexer breadboard was constructed based upon a modified Czerny-Turner spectrometer configuration. The Czerny-Turner spectrograph consists of 5 parts:

1. The entrance aperture, usually an entrance slit;
2. Collimating optics, usually a collimating mirror;
3. The diffraction grating;
4. Imaging optics, usually a second collimating mirror;
5. An exit slit or spectral focal plane.

Figures (1) and (2) respectively show the picture of our modified Czerny-Turner spectrograph, adapted for wavelength multiplexing, and a block diagram of the WDM system.

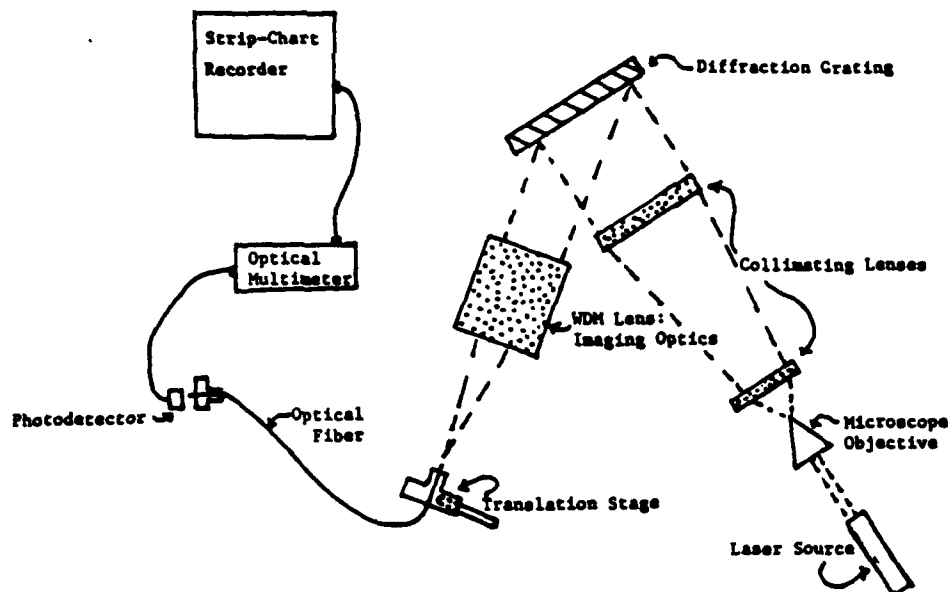


Figure 2: Block Diagram of the Breadboard Experiment

## 2.1 Breadboard Hardware

Section 2.1 describes the hardware that was utilized in the breadboard WDM system.

### 2.1.1 Diode Lasers and Power Supply

In order to demonstrate wavelength multiplexing, two continuous-wave diode lasers, with wavelengths of 1213 nm and 1292 nm, were purchased from M/A Com Laser Diode, Incorporated. Accompanied inside the design package of the laser diodes were:

1. Thermo-electric coolers for wavelength stability and longevity.
2. Thermistors for feedback temperature control of the TE coolers.
3. Micro-lens systems for pigtailed into optical fibers of 62.5  $\mu\text{m}$ .
4. Peak optical power output capabilities of 2.0 mW

A laser current supply was also purchased from M/A Com Laser Diode, Incorporated. This current supply incorporated a feature which allowed the current to slowly rise along a ramp function from 0 to 350 mA; to protect the diode lasers from large turn-on heatloads and stresses. Such a feature is essential in a power supply in order to discourage laser burnout and increase the longevity of the laser diodes.

### **2.1.2 Collimating Optics**

The design of the wavelength multiplexer breadboard required the collimating optics to operate, with a focal length of 150 mm, over a 1200-1400 nm range while outputting a 60 mm diameter beam. To avoid the expense of an F/2.5, 150 mm focal length, single-element collimating lens with a 60 mm diameter, a two-stage approach to collimation was utilized. The first stage was a small, short focal length, 3 element laser diode collimating lens. The laser was located just inside the focal point of this high quality lens so the transmitted beam would be slightly divergent (thus having a high f/number) and have insignificant aberrations. After propagating an additional 400 mm, the beam reached the desired diameter of 60 mm. A simple plano-convex lens of 1000 mm focal length performed the final collimation. The system, while diffraction limited and inexpensive, was unnecessarily long. A viable alternative for collimation would be the use of an off-axis parabolic mirror in the production WDM system. Reference is directed to Section 5.1, Appendix A for optical layouts which utilize parabolic mirrors for system size reduction.

### **2.1.3 Diffraction Grating**

For the breadboard WDM, an 830 line per mm, 52 mm square, high quality diffraction grating blazed at 1200 nanometers was purchased from Milton Roy, Inc. Compromises between channel separation, wavelength range, and spectral dispersion parameterized the incidence angle of the collimated light with respect to the grating normal. This corresponded to an angle of 14 degrees such that a central wavelength of 1300 nm would be diffracted at approximately 54 degrees. Both the angle of incidence and the angles of diffraction lie on the same side of 0 order... by the definition detailed in Appendix B, the grating is used in the -1 order. Incident radiation, ranging from 1200 to 1400 nm, is dispersed in angular range from 46 to 62 degrees. Scattered light from the diffraction grating is one of the principal concerns and major factors in the role of poor insertion loss and large crosstalk. With the grating illuminated in helium neon laser light, even scattering from a high quality grating is readily apparent. Efforts to measure the grating scatter with the scanning fiber technique have been somewhat hampered by the poor image quality from the imaging lens. Large scattering constrains crosstalk measurements to within a few tenths of a millimeter from the center of the image.

### **2.1.4 Imaging Lens**

The imaging optics (an OTS multi-element super projection TV lens), along with the diffraction grating, are two of the most critical elements in the wavelength multiplexing. However, unlike the diffraction grating, a suitable multiplexing lens is not readily available as an off-the-shelf item. After searching several optical suppliers for suitable lenses, we settled with a surplus TV projection lens from Edmund Scientific. Since we required a very short focal length, large

diameter lens of F2.5 or less, we could only afford a surplus lens and not one of the production laser scanning lenses currently on the market. The three-element lens purchased from Edmund Scientific had a 150 mm focal length and 100mm diameter. This lens, designed to project TV images on to a screen at 5 to 1 magnification, was not intended to focus collimated light. Thus, the lens displayed large amounts of spherical aberration. Due to poor construction, non-spherical surfaces, and mis-aligned optical elements, an extremely aberrated wavefront was obtained. This OTS lens was determined to be the very weak link in our optical system.

### **2.1.5 Translating Fiber**

The motorized translation stage moved an optical fiber across the image point. The light coupled into the fiber illuminated to a photodetector for intensity measurements. In turn, this allowed a quantitative evaluation of the fiber-optic WDM system. To collect the light in the image plane of the multiplexer, a 62.5 micron diameter fiber was used. To perform insertion loss and crosstalk measurements this fiber was mounted on a motorized newport translation stage which scanned the image plane in the direction of dispersion, see Section (3). Two other translating adjustments, one along focus and one perpendicular to the direction of focus, allowed precise positioning of the fiber.

### **2.1.6 Photodetector**

The output end of the translating fiber was positioned to illuminate a Photodyne chopped light multimeter, Model 33XLC. The multimeter is a precise measuring instrument designed to measure the output power of an optical source by coupling the output end of a fiber to the appropriate sensor head. In our case, the sensor head would be sensitive in the near-infrared spectrum to both CW or modulated light. Additionally, while possessing power measurement capabilities, the multimeter can also act as a driver for optical radiation source such as LEDs.

## **2.2 Data Acquisition**

The detected intensities in the breadboard were routed from the analog output of the fiber radiometer to a strip chart recorder. The strip chart recorder coordinates were aligned with respect to the fiber scanning speed to allow position in the image plane to be read off the strip chart recorder. The y-axis of the strip chart recorder was calibrated using known light levels projected onto the fiber optic radiometer.

## **2.3 Alignment**

The wavelength multiplexer was aligned along an axis established by a helium neon laser. Great pains were taken to assure proper centering of all elements with respect to the optical axis in

order to minimize aberrations. The first element inserted was the diffraction grating, oriented at zero degrees retro-reflecting in the zero order. The second element inserted was the large plano convex imaging lens, since this lens had the largest tolerance on its position. Thus this lens could be moved with small affects to beam aberrations. A short focal length laser diode lens was inserted next. This lens required precision centering. The Boys-points ghost images resulting from multiple reflections were centered on the beam by tilting and decentering the lens. Then, the grating was rotated to 14 degrees and the first order beam was aligned through the center of the large imaging lens. By observing the beam's path through the imaging lens, decentrations between the lens elements of the imaging lens were readily apparent. Principle planes of the imaging lens were found, and large aberrations were immediately apparent in the focusing beam. A Foucault test revealed .9 mm of spherical aberration. A negative, 600 mm focal length, plano-concave lens was inserted into the beam. The result was a spherical aberration correction of .25 mm.

### 3 WDM Performances

#### 3.1 Determination of Baseline Crosstalk and Insertion Loss Performance

As previously mentioned in Section 1.1.2, multiplexer metrology techniques were developed for insertion loss and crosstalk measurements. The scanning fiber system concept works as follows. The system, operating in a demux mode, utilizes a single laser to illuminate the input fiber. This light diffracts from the grating and is brought to focus by the imaging lens at the focal plane. Presented on the image plane will be one bright monochromatic image as well as associated scattered light. To measure insertion loss and crosstalk, an single optical fiber scans across an image and maps the intensity profile of light coupled into the fiber. This mapping of the intensity profile simultaneously includes:

1. The peak intensity
2. The image width and broadening effects due to aberrations
3. The scattered light due to the grating, lenses, and mounts

The peak intensity coupled into the fiber is the minimum insertion loss for that fiber at that particular wavelength. In fiber optics communications, insertion loss and crosstalk are usually described in terms of decibel power. Decibel units: the logarithmic transformation of the basic optical power units, watts; are useful in compressing power measurement data that has a wide dynamic range. Decibel power, represented in units of decibels (dB), is defined as

$$dB = 10 * \log(P_{out}/P_{in}) \quad (1)$$

Fiber #1	3.0dB	10.8dB	15.1dB	27.3dB
Fiber #2	11.4dB	2.9dB	10.5dB	15.4dB
Fiber #3	15.7dB	11.3dB	2.1dB	10.9dB
Fiber #4	29.0dB	16.2dB	10.3dB	3.2dB

1280nm:      1290nm:      1300nm:      1310nm:  
 $\lambda_1$              $\lambda_2$              $\lambda_3$              $\lambda_4$

Figure 3: Crosstalk Matrix Example

As the fiber scans across the image, data is taken on the sensitivity of the insertion loss to wavelength drift or misalignment of the fiber. As the fiber scans further from the peak of the image, further data is acquired on the full width at half maximum of the image and its aberrations. As the fiber scans further from the peak, it scans across the locations where other fibers will be located for wavelength multiplexing. Thus, the crosstalk from the test wavelength into these other wavelength channels is measured in a single pass of the scanning fiber.

In practice, this test would be repeated for a set of test wavelengths across the wavelength range of the multiplexer to measure the wavelength dependence of the insertion loss and develop a matrix of crosstalk values. A possible example of such a crosstalk matrix is shown in Figure (3).

### 3.2 Insertion Loss and Crosstalk Measurements

The scanning fiber was carefully positioned on the peak of the image, located at the focal plane of the WDM lens. The x-axis, the direction along the axis of dispersion, was outfitted with a translating stage which moved the fiber across the image plane. The y-axis had a differential micrometer to insure precise positioning of the fiber on the center of the image. A third positioning micrometer was located along the optical/z- axis. The fiber was moved across the helium neon laser image and the data recorded on the chart recorder. The recorded data contained the intensity of the light coupled into the fiber, which could then be compared

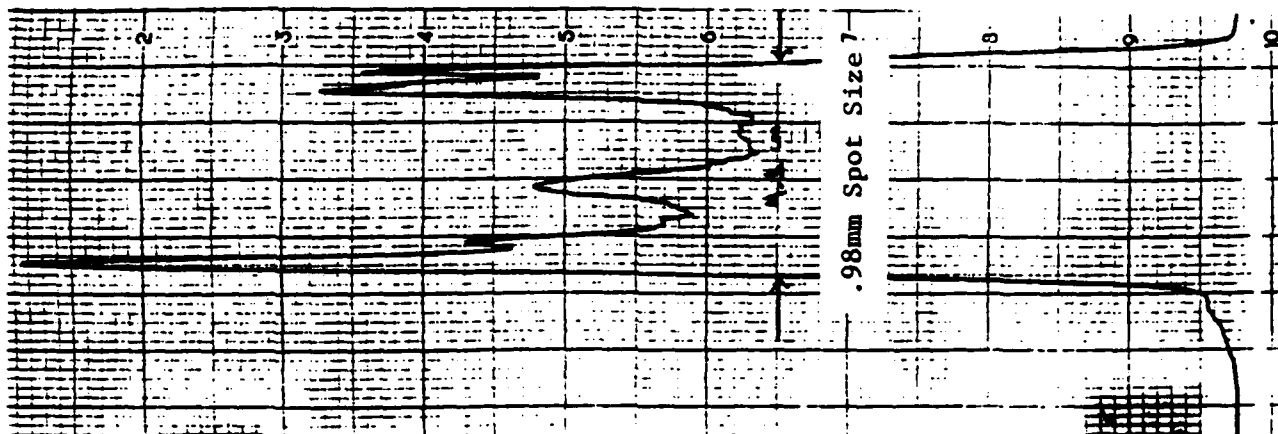


Figure 4: Strip-chart Intensity Recording (I) of the Fiber Scan

with the reference intensity of the focus laser beam at the entrance aperture of the multiplexer. The image size was determined, through an analysis of the translation stages, scan speed, and the image width at half maximum intensity, to be 1 mm in diameter, see Figure (4). Such a large image resulted from a large amount of spherical aberration and other aberrations that arise predominately from the imaging lens. Scans were taken with and without the lens (which functioned as an aberration corrector). Once the new focus was found, a new image trace was obtained (Figure (5)). A photograph of this new aberrated image in the image plane is shown in Figure (6). The measured insertion line for this 3/4mm diameter image is 22 dB.

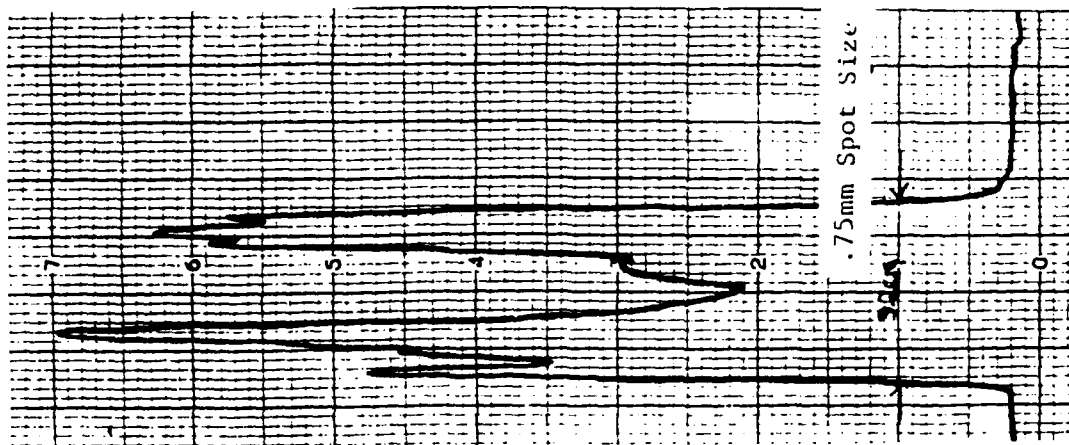


Figure 5: Strip-chart Intensity Recording (II) of the Fiber Scan



Figure 6: Picture of the Best Focus Image

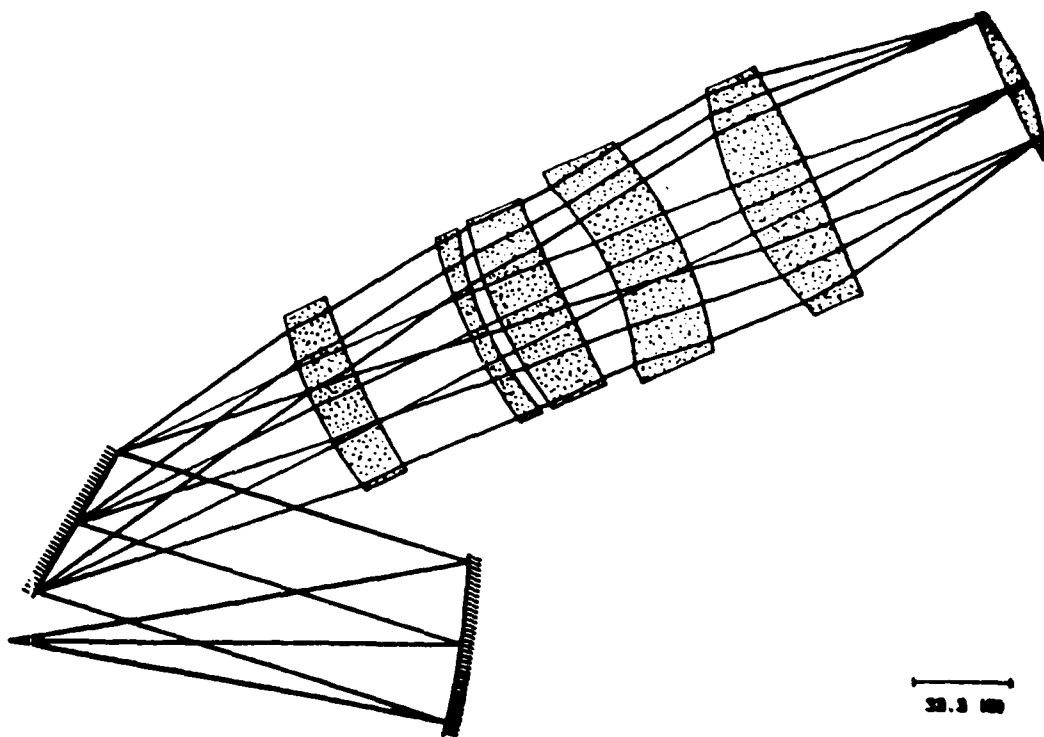


Figure 7: UAH Single-Mode WDM

## 4 Lens Design

Figure (7) shows a layout of the final lens design achieved under this WDM contract. The WDM design is a modified Czerny-Turner monochromator, a relatively standard design except for the imaging lens, which is located between an array of fibers and the diffraction grating. The system performs in one direction as a mux (light emergent from multiple fibers is multiplexed/coupled into a single fiber), and in the opposite direction as a demux (light emergent from one fiber is demultiplexed/coupled into many fibers).

With the time constraints imposed on this contract, a final, production-ready optical design was not achieved. However, substantial progress has been made towards this goal. Approximately five months of graduate student time and two weeks of principal investigator time have been devoted to achieve the present lens design status.

The WDM imaging lens has very special characteristics that are specific to wavelength multiplexing.

- Chromatic aberration insensitivity
- No requirement for a flat image field
- Remote aperture stop (the diffraction grating): heightens astigmatism and coma.

As stated previously, suitable standard or off-the-shelf (OTS) lenses do not exist for this particular application. A large fraction of the effort on this contract has been devoted to

exploring suitable lens designs. The lens shown in Figure (7) dates the level of our lens design progress.

#### **4.1 Objectives**

The objective of this optical design is to:

1. Collimate the beam from a single fiber onto the diffraction grating;
2. Select a diffraction grating with the appropriate angular dispersion and efficiency for the 1300 nm region;
3. Image each of these collimated beams with sufficient image quality that insertion loss remains a constant.

The first two objectives are easily attained. Light from a single fiber is well collimated by either a parabolic mirror or a high quality laser diode collimating lens. A suitable choice of grating frequency with respect to lase angle will assure near optimum efficiency at any desired wavelength. The third requirement for image quality among all the diffracted beams presents the unique challenge.

##### **4.1.1 Aberration Requirements of Multiplexer Lenses**

The lens, in a mux or demux system status, which lies between the array of fibers and the diffraction grating will be referred to as the WDM lens. This lens possesses several unusual characteristics:

- For demux system staus, a single object point, the input optical fiber transmits all the wavelengths.
- The collimating lens, or parabola, needs only function over this small field of view (defined by the numerical aperture of the fiber); thus a relatively simple design is possible.
- The chief rays between the grating and the image plane, for all the wavelengths, intersect at the center of the diffraction grating. Thus, the area of the grating that is illuminated by incident collimated light acts as the system stop.

In a Czerny-Turner spectrograph, a certain minimum distance is required between the diffraction grating and the WDM lens in order to prevent vignetting of the beam incident on the diffraction grating. In the present designs, this distance is about 2/3 of the focal length of the WDM lens. Since the WDM lens is removed from the diffraction grating, the multiplexer has a removed stop. Lenses with removed stops, (for example eyepieces) generally have serious problems with coma and astigmatism.

Due to the light dispersion that occurs at the diffraction grating, different wavelengths take different paths through the WDM lens. Light at 1300 nm travels directly through the center of the lens, while the 1200 nm beam is dispersed closest to the collimating mirror and the 1400 nm beam closes to the outside. Since each wavelength forms its own image, there is never a requirement that two wavelengths must focus at exactly the same distance or location, i.e. no requirement for the correction of lateral or longitudinal chromatic aberration. Because we are imaging into fibers, it is not necessary to have a flat focal plane, as would be required with a CCD detector or a glass photographic plate. We are free to form the image on any surface shape, provided that the fiber location is suitable for proper light coupling.

The lens needs to be a fairly fast lens, at least  $F/2.8$ , to efficiently couple into a multi-mode fiber (as previously mentioned, this constraint arises from the numerical aperture of the fiber), but the lens also needs to have a long focal length so that the linear dispersion at the image plane will be large. However, a long focal length, fast lens must have a large diameter. This is a compounded requirement because moving the removed stop further increase the diameter. While this is intrinsically expensive, everything in the multiplexer design forces the WDM lens towards a very large aperture.

No standard or off-the-shelf lenses are suitable for this particular multiplexing application. The described combination of requirements are quite unique. Lenses most similar to the WDM lens are those lenses used in pre-objective laser scanning systems, where a laser beam reflects off a rotating mirror through a scanning lens. Such lenses typically work with a single wavelength over a flat field of view and are designed to have  $F/\theta$  distortion characteristics. A typical cost, for a 4" diameter,  $F/\theta$  scanning lens, is approximately \$3,000 per single lens.

## 4.2 Computer Design Experiments

The computer-aided design of the wavelength multiplexer proceeded as follows.

1. The off-axis collimating mirror and diffraction grating were configured in the program.
2. A three element lens of the appropriate focal length, 150 mm, was inserted into the CAD program as a starting point for the WDM lens.

At this point the design of the collimating lens and diffraction grating was frozen... all effort was focused on the optimization of the WDM lens.

### 4.2.1 Optimization Methods

A merit function, set up to describe the quality of a WDM lens, used the RMS spot size associated with the 1200, 1300, and 1400 nm images. Each of these images was treated as a separate zoom position using the zoom options of the optical design programs. The zoom option

allowed each image to be evaluated with respect to a reference ray of the correct wavelength. The effective focal length of the WDM lens was constrained to 150 mm to prevent the scale of the lens from running away.

#### **4.2.2 Three Element Multiplexer Lens Optimization**

A combination of lens curvatures and thicknesses were designated as optimization variables. The optimization routines of CODE V or SYNOPSIS were invoked and the program was allowed to vary these variables until a minimum of the merit function was located. If no improvement was found, practice dictated a return to the original lens. A different combination of optimization variables or some change to the starting point of the lens would then be utilized. If a substantially improved lens was achieved during optimization, this lens would be used as a starting point for further optimization experiments. The starting point first chosen utilized a three element air spaced Cook Triplet lens with high index glasses for the first and last elements. During optimization these power of the lenses changed such that the first positive lens bent towards the diffraction grating, the last positive lens bent towards the image plane, and the middle negative lens remained virtually unaffected, see Appendix A. This configuration never produced images smaller than 1 mm at the edge wavelengths. The principal problem originated from the negative lens in the center not having enough spherical aberration to correct for the large amounts of spherical aberration generated from the two outer lenses.

#### **4.2.3 Four Element Multiplexer Lens Optimization**

Next, the positive lens with the larger power: the element closest to the image, was split into two positive lenses and optimization continued. This provided a roughly three-fold improvement in design, and several weeks of work trying different glasses, different starting points, and reversing the orientation of some of the lenses, finally led to the four-element design contained in the July progress report. This lens had image quality of a few tenths of a millimeter at the edge wavelengths... still not adequate for multimode wavelength multiplexing applications. Furthermore, the lens continued to have problems with large amounts of astigmatism and residual spherical aberration.

#### **4.2.4 Five and Six Element Multiplexer Lens Optimization**

The next approach was to utilize a 5-element lens: positive, negative, positive, negative, positive lens configuration. This allowed two negative lenses to share the task of balancing the spherical aberration of the system. While the curvatures on the positive lenses were minimized in order to reduce higher order aberrations. Additionally, the negative lenses were positioned very close to the more steeply curved surfaces in order to further reduce higher order aberrations. Several lens orientations were tried as starting points on Synopsys, but the

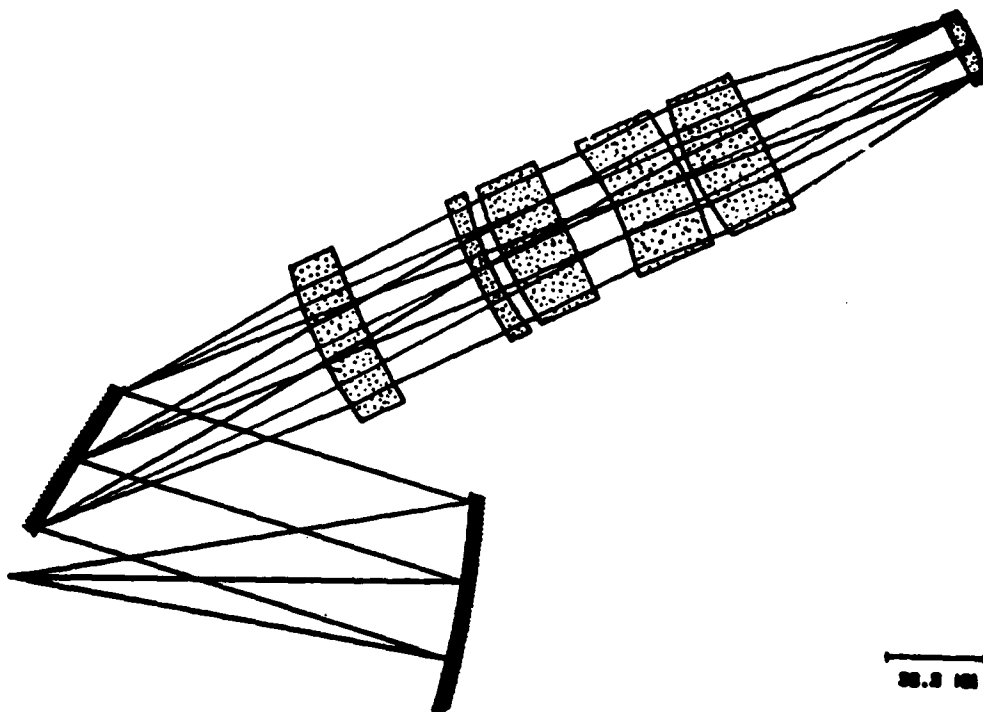


Figure 8: UAH Multi-mode WDM

performance requirements for a multi-mode lens were not achieved. At this point, the lens data was transferred to the CAD program: CODE V.

Re-initializing optimization procedures, via Code V, resulted in further performance improvements. Finally it was decided to add a thick lens at the image plane. This field lens would have a back curvature equal to the curvature of the image plane; the front curvature and thickness were allowed to vary to provide a very field-specific astigmatism correction. This astigmatic correction would result from the use of a thick block of glass at an angle (other than normal incidence) to the incident light. Furthermore, the corrector lens was allowed to de-center itself, while the remainder of the WDM lenses maintained a radially-symmetric optical system. This set of optimizations led to the multi-mode wavelength multiplexer lens design.

### 4.3 Final Designs

#### 4.3.1 UAH Multi-mode WDM

Shown in Figure 8 is the optical layout of a Multi-mode WDM designed by the CAD program CODE V. The lens design incorporates only *spherical* lenses. Inquiries for system specifications and performance are directed to Appendix A.4. System performance analysis utilized spot diagrams and ray aberration plots for both the sagittal and tranverse ray fans.

#### 4.3.2 UAH Single-mode WDM

To achieve further image quality improvements from those of the Multi-mode WDM, an aspheric was added to a flat surface near the center of the lens (surface 13), and allowed to vary into a conic surface. This improved image quality, after several optimization runs, by a factor

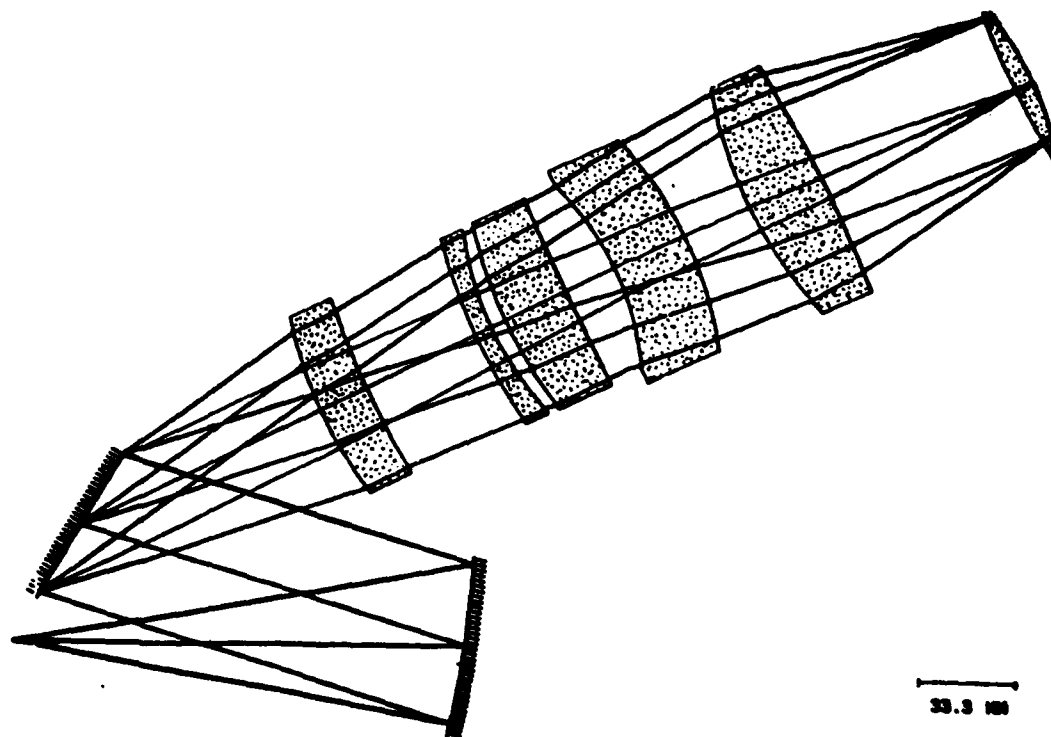


Figure 9: UAH Single-Mode WDM

of 2. Surface 17 was then changed to a toroidal surface in order to allow the sagittal and tangential radii to differ. Re-initializing the optimization program resulted in a factor of 5 in image quality improvement. Shown in Figure 9 is the optical layout of a Single-Mode WDM. Analysis of transverse ray aberration plots and spot diagrams show single-mode capabilities. The diffraction modulation transfer function plots show that for the wavelength range specified (1400 nm - 1200 nm) the system's performance is diffraction limited. Inquiries for system specifications and performance are directed to Appendix A.5.

## 5 Bibliography

Kielkopf J., "Echelle and Holographic Gratings Compared for Scattering and Spectral Resolution." Applied Optics, Vol. 20, No. 19, pg. 3327, Oct. 1, 1981.

Brown, R.A., Hillard, R.L., and Phillips, A.L., "Actual Blaze Angle of the Bausch & Lomb R4 Echelle Grating." Applied Optics, Vol. 21, No. 2, pg. 167, Jan. 15, 1982.

Cash, W., "Echelle Spectrograph at Grazing Incidence." Applied Optics, Vol. 21, No. 4, pg. 710, Feb. 15, 1982.

Liller, W., "High Dispersion Stellar Spectroscopy with an Echelle Grating." Applied Optics, Vol. 9, No. 10, pg. 2332, Oct. 1970.

Bussard, A.B., and Pulfrey, R.E., "Wavelength Division Optical Multiplexer/Demultiplexer." Applied Optics, Vol. 26, No. 17, pg. 3482, Sept. 1, 1987.

Hutley, M.C., "Diffraction Gratings, Techniques of Physics: 6," Academic Press, 1982.

Sternberg, R.S., and James, J.F., "The Design of Optical Spectrometers," Chapman and Hall Ltd., 1969.

Basch, E.E.B., Editor, "Optical-Fiber Transmission," Howard W. Sams & Co., 1987.

Okoshi, T., "Recent Advances in Coherent Optical Fiber Communication Systems," Journal of Lightwave Technology, Vol. LT-5, No. 1, pg. 44, Jan. 1987.

Suh, S.Y., "Pulse Width Modulation for Analog Fiber-Optic Communications," Journal of Lightwave Technology, Vol. LT-5, No. 1, pg. 102, Jan. 1987.

Kimura, T., "Coherent Optical Fiber Transmission," Journal of Lightwave Technology, Vol. LT-5, No. 4, pg 414, Jan. 1987.

Stanley, I.W., Hill, G.R., and Smith, D.W., "The Application of Coherent Optical Techniques to Wide-Band Networks," Journal of Lightwave Technology, Vol. LT-5, No. 4, pg. 439, Jan. 1987.

Sollberger, A., Heinamaki, A., Melchior, H., "Frequency Stabilization of Semicon-

ductor Lasers for Applications in Coherent Communication Systems," Journal of Lightwave Technology, Vol. Lt-5, No. 4, pg. 485, Jan. 1987.

Shen, T.M., Agrawal, G.P., "Computer Simulation and Noise Analysis of the System Performance of 1.55 Micron Single-Frequency Semiconductor Lasers," Journal of Lightwave Technology, Vol. LT-5, No. 5, pg. 653, May 1987.

The Photonics Design and Applications Handbook, Book 2, 33rd Edition, pg. H-76, h-108, 1987.

Ishikawa, H., Soda, H., "Distributed Feedback Laser Emitting at 1.3 Micron for Gigabit Communication Systems," Journal of Lightwave Technology, Vol. LT-5, No. 6, pg. 848, June 1987.

Shafer, A.B., Megill, L.R., Droppleman, L., "Optimization of the Czerny-Turner Spectrometer," Journal of Optical Society of America, Vol. 54, pg. 879, 1964.

Seya, M., Namioka, T., "Optical Properties of a System Consisting of a Mirror and a Grating," Applied Optics, Vol. 8, pg. 450, 1972.

Hill, R.A., "A New Plane Grating Monochromator with Off-Axis Paraboloids and Curved Slits," Applied Optics, Vol. 8, No. 3, pg. 578, 1969.

Czerny, M., Turner, A.F., Z. Physics, Vol. 61, pg. 792, 1930.

Kudo, K., "Optical Properties of Plane Grating Monochromator," Journal of Optical Society of America, Vol. 55, pg. 153, 1965.

Chupp, V.L., Frantz, P.C., "Coma Canceling Monochromator with No Slit Mismatch," Applied Optics, Vol. 8, No. 5, pg. 925, 1969.

Fastie, W.G., Journal of Optical Society of America, Vol. 42, pg. 641, 1952.

Murty, M.V.R.K., "Optimization for Coma and Anamorphic Effects in Double Monochromators," Applied Optics, Vol. 60, No. 8, pg. 1022, 1970.

Schroeder, D.J., "Optimization of Converging Beam Grating Monochromators," Applied Optics, Vol. 11, NO. 7, pg. 1637, 1972.

Aspnes, D.E., "High-Efficiency Concave Grating Monochromator with Wavelength Independent Focusing Characteristics," Journal of Optical Society of America, Vol. 72, No. 8, pg. 1056, 1982.

Chipman, R.A., "Monochromator Designs with Aberration Corrected Grating," SPIE 1980 International Lens Design Conference (OSA), Vol. 237, pg. 439, 1980.

## **6 Appendices**

**6.1 Appendix A: WDM Lens Design Documentation**

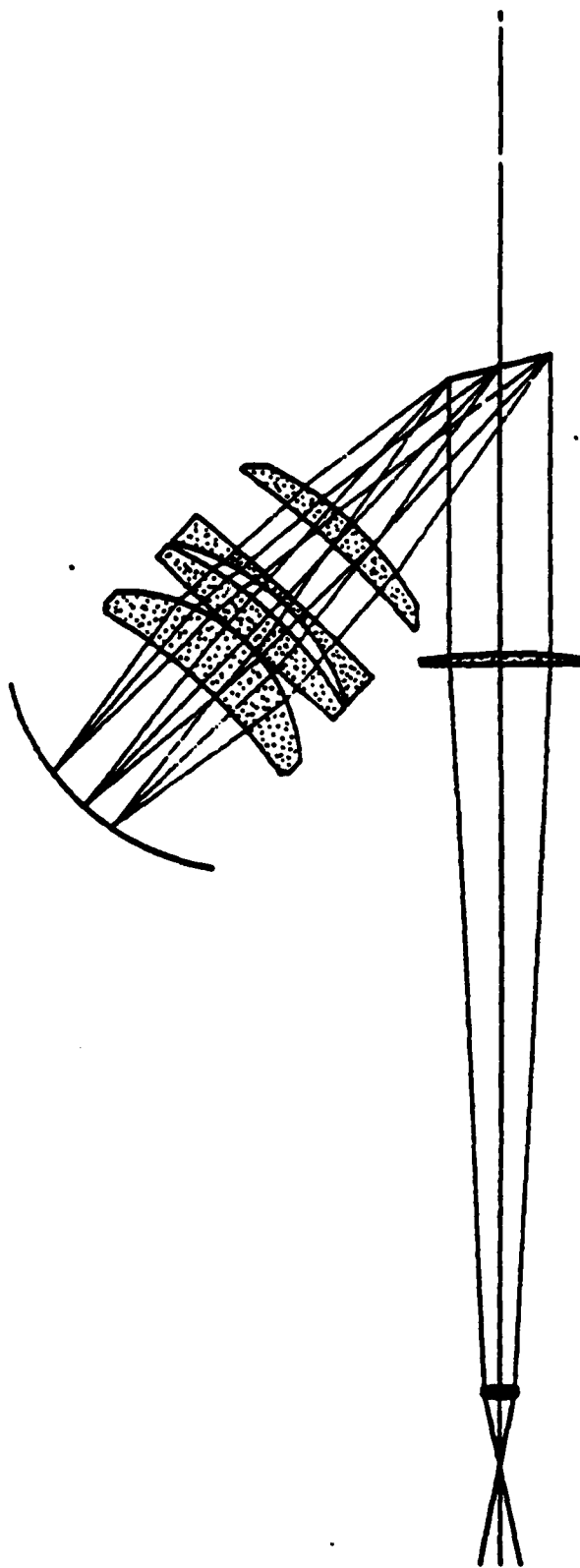
**6.2 Appendix B: July Presentation**

**6.3 Appendix C: Dispersive Elements**

**6.4 Appendix D: Optical Fibers**

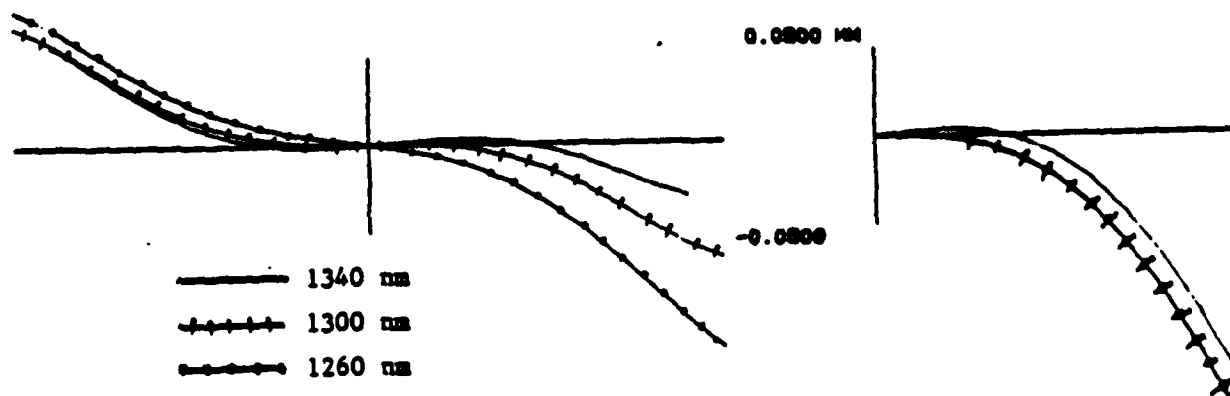
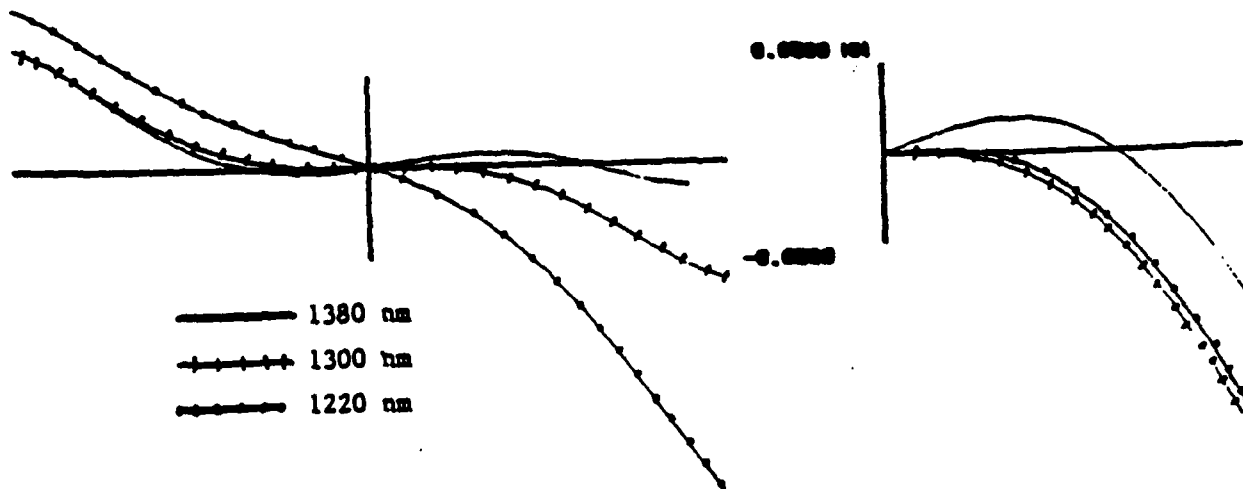
**Appendix A: WDM Lens Design Documentation**

## **1.1 Four-Element WDM System**



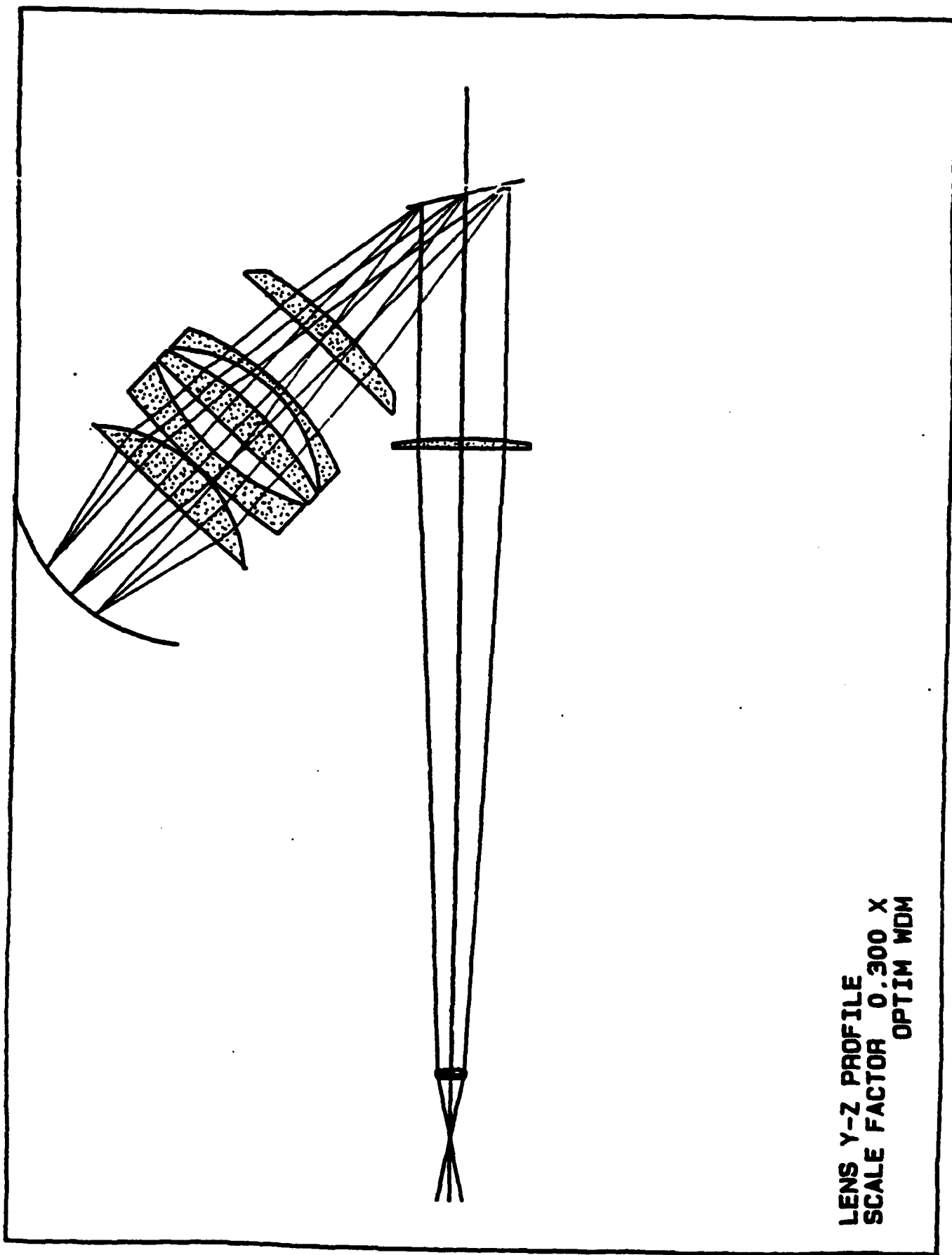
LENS Y-Z PROFILE  
SCALE FACTOR 0.250 X  
WAVELENGTH DIVISION DEMULTIPLEXER

# Ray Aberrations



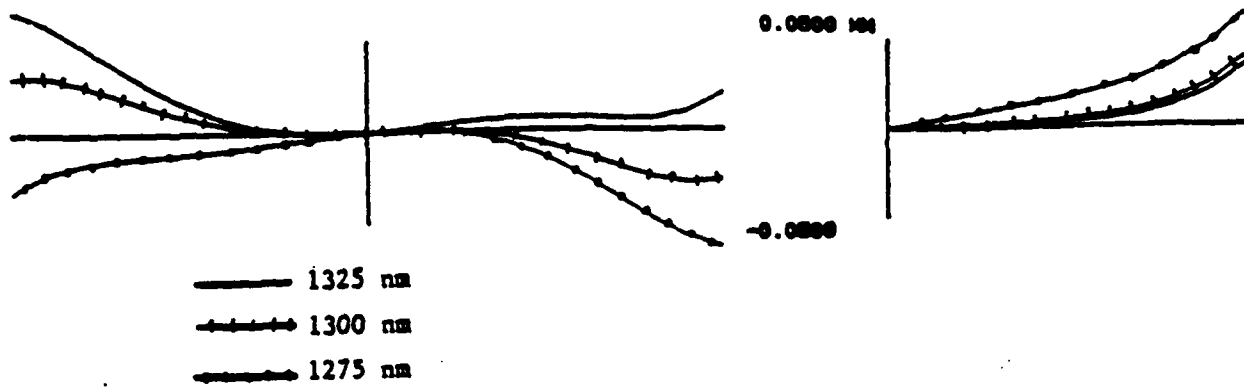
WAVELENGTH DIVISION DEMULTIPLEXER

## **1.2 Five-Element WDM System (A)**



LENS Y-Z PROFILE  
SCALE FACTOR 0.300 X  
OPTIM WDM

# Ray Aberrations



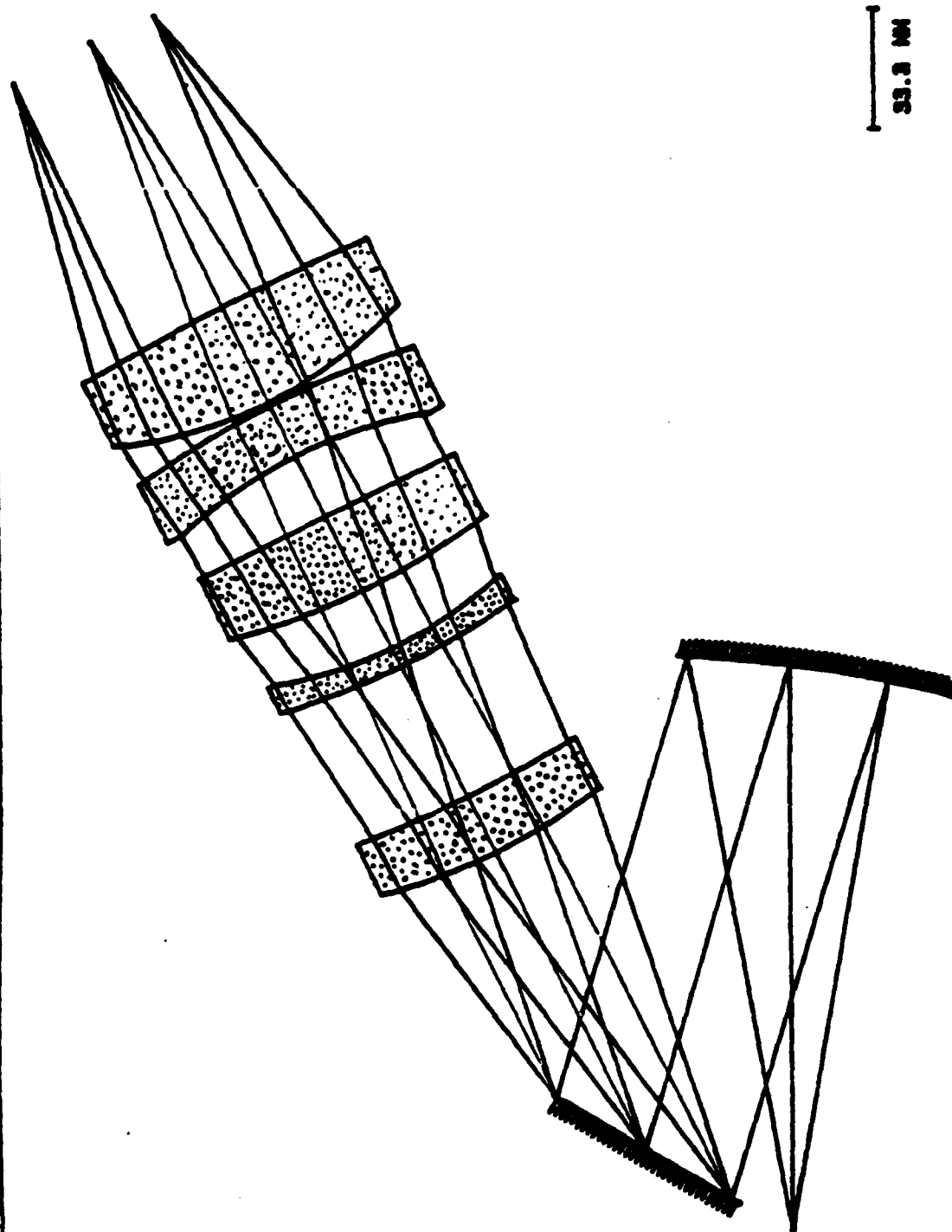
OPTIM WDM

### **1.3 Five-Element WDM System (B)**

DEC-87

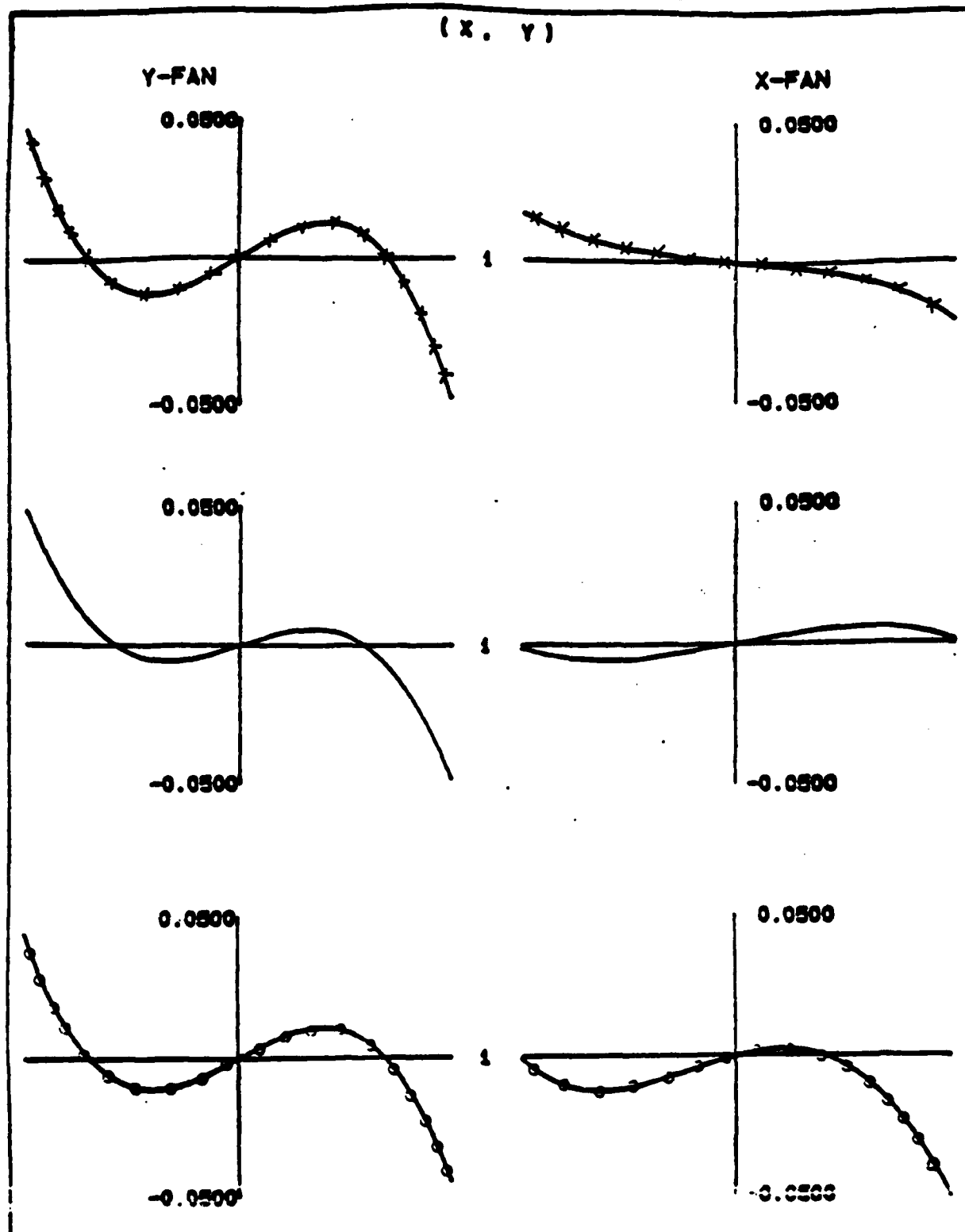
SCALE 0.600

UAH WDM System



# RAY ABERRATIONS

(X, Y)



UAH WDM System

RAY ABERRATIONS (MILLIMETERS)

Scale: 50 microns DEC-67

x x x x x x 1400.0 nm  
 ————— 1300.0 nm  
 o o o o o o 1200.0 nm

# SPOT DIAGRAM

FIELD  
POSITION

.00, 0.00  
0.0, 0.0 DS

1400 nm

.00, 0.00  
0.0, 0.0 DS

1300 nm

.00, 0.00  
0.0, 0.0 DS

1200 nm

DEFOCUSING

0.00000

UAH WDM System

SCALE: 1 INCH = 0.05000 MM

UAE WDM Specifications:

ELEMENT	RADIUS	THICKNESS	GLASS	CCY	THC	GLC
OBJECT:	INFINITY	150.000000				
STOP:	INFINITY	0.000000		100	100	
				100	100	
SURFACE 3:	INFINITY	150.000000		100	100	SU
XDE:	0.000000	YDE:	0.000000			
XDC:	100	YDC:	100			
ADE:	0.000000	BDE:	16.750000	CDE:	0.000000	
ADC:	100	BDC:	100	CDC:	100	
SURFACE 4:	-300.00000	0.000000	REFL	100	100	
CON:						
K :	-1.000000	KC :	100			
SURFACE 5:	INFINITY	-140.000000		100	100	
XDE:	44.166400	YDE:	0.000000			
XDC:	100	YDC:	100			
ADE:	0.000000	BDE:	0.000000	CDE:	0.000000	
ADC:	100	BDC:	100	CDC:	100	
SURFACE 6:	INFINITY	0.000000	REFL	100	100	
GRATING:						
K :	0.000000	KC :	100	IC :	YES	
:0.000000E+00	B :	0.000000E+00	C :	0.000000E+00	D :	0.000000E+00
AC :	100	BC :	100	CC :	100	DC :
GRO:	1	GRS:	0.001205			
GRX:	1.000000	GRY:	0.000000	GRZ:	0.000000	
XDE:	0.000000	YDE:	0.000000			
XDC:	100	YDC:	100			
ADE:	0.000000	BDE:	14.000000	CDE:	0.000000	
ADC:	100	BDC:	100	CDC:	100	
SURFACE 7:	INFINITY	90.000000		100	100	
XDE:	0.000000	YDE:	0.000000			
XDC:	100	YDC:	100			
ADE:	0.000000	BDE:	-56.832850	CDE:	0.000000	
ADC:	100	BDC:	100	CDC:	100	
SURFACE 8:	168.05273	16.850000	SF11_SCHOTT	0	100	
SURFACE 9:	349.22549	39.760000	AIR	0	100	
SURFACE 10:	225.32423	5.500000	BK7_SCHOTT	0	100	
SURFACE 11:	116.44133	17.700000	AIR	0	100	
SURFACE 12:	206.15224	22.330000	SF11_SCHOTT	0	100	
SURFACE 13:	-2554.25777	18.000000	AIR	0	100	
SURFACE 14:	-125.93124	15.000000	BK7_SCHOTT	0	100	
SURFACE 15:	-271.85781	1.000000	AIR	0	100	
SURFACE 16:	118.58561	28.000000	SF11_SCHOTT	0	100	
SURFACE 17:	-725.38697	79.821115	AIR	0	0	
IMAGE:	-169.22474	0.000000		0	100	
XDE:	0.000000	YDE:	0.000000			DAR
XDC:	100	YDC:	100			
ADE:	0.000000	BDE:	0.756355	CDE:	0.000000	
ADC:	100	BDC:	0	CDC:	100	

Entrance Pupil Diameter:	52.00000	mm
Wavelengths:	1400.00 nm	1300.00 nm      1200.00 nm
XAN	0.00000	
YAN	0.00000	
VUX	0.00000	
VLX	0.00000	
VUY	0.00000	
VLX	0.00000	

# REFRACTIVE INDICES

GLASS CODE:	1400.00	1300.00	1200.00
SP11_SCHOTT	1.746999	1.748879	1.750962
BK7_SCHOTT	1.502511	1.503712	1.504922

No solves defined in system

# ZOOM DATA:

	POS 1	POS 2	POS 3
WTW W1	30	0	0
WTW W2	0	30	0
WTW W3	0	0	30
REF	1	2	3

This is a decentered system. If elements with power are decentered or tilted, the first order properties are probably inadequate in describing the system characteristics.

	Position 1	Position 2	Position 3
--	------------	------------	------------

# INFINITE CONJUGATES:

Effective Focal Length	-382.9082	-380.0032	-376.7397
Back Focal Length	424.6924	421.1402	417.1476
Front Focal Length	-575.6281	-573.2362	-570.5492
F/Number	-7.3636	-7.3078	-7.2450

# AT USED CONJUGATES

Reduction Ratio	0.8996	0.8979	0.8958
F/Number	2.6338	2.6286	2.6227
Object Distance	150.0000	150.0000	150.0000
TT	343.9611	343.9611	343.9611
Image Distance	79.8211	79.8211	79.8211
Optical Axis Length	114.1400	114.1400	114.1400

# PARAXIAL IMAGE

Height	0.0000	0.0000	0.0000
Thickness	80.2162	79.9538	79.6537
Field Y-Angle	0.0000	0.0000	0.0000

# ENTRANCE PUPIL

Diameter	52.0000	52.0000	52.0000
Thickness	0.0000	0.0000	0.0000

# EXIT PUPIL

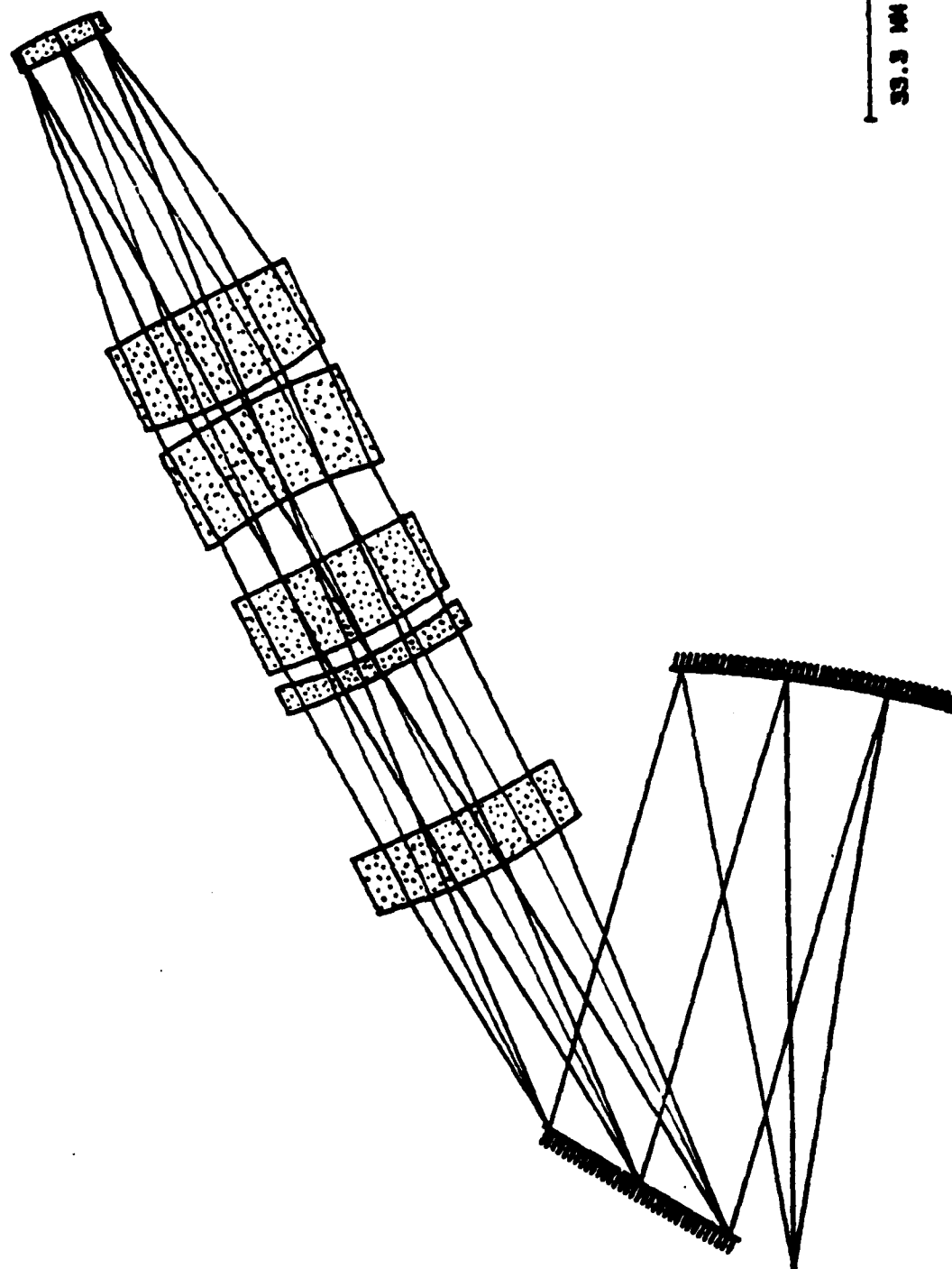
Diameter	34.5904	34.4712	34.3362
Thickness	169.9815	169.2329	168.3824
Stop Diameter	52.0000	52.0000	52.0000

#### **1.4 UAH Multi-Mode WDM System**

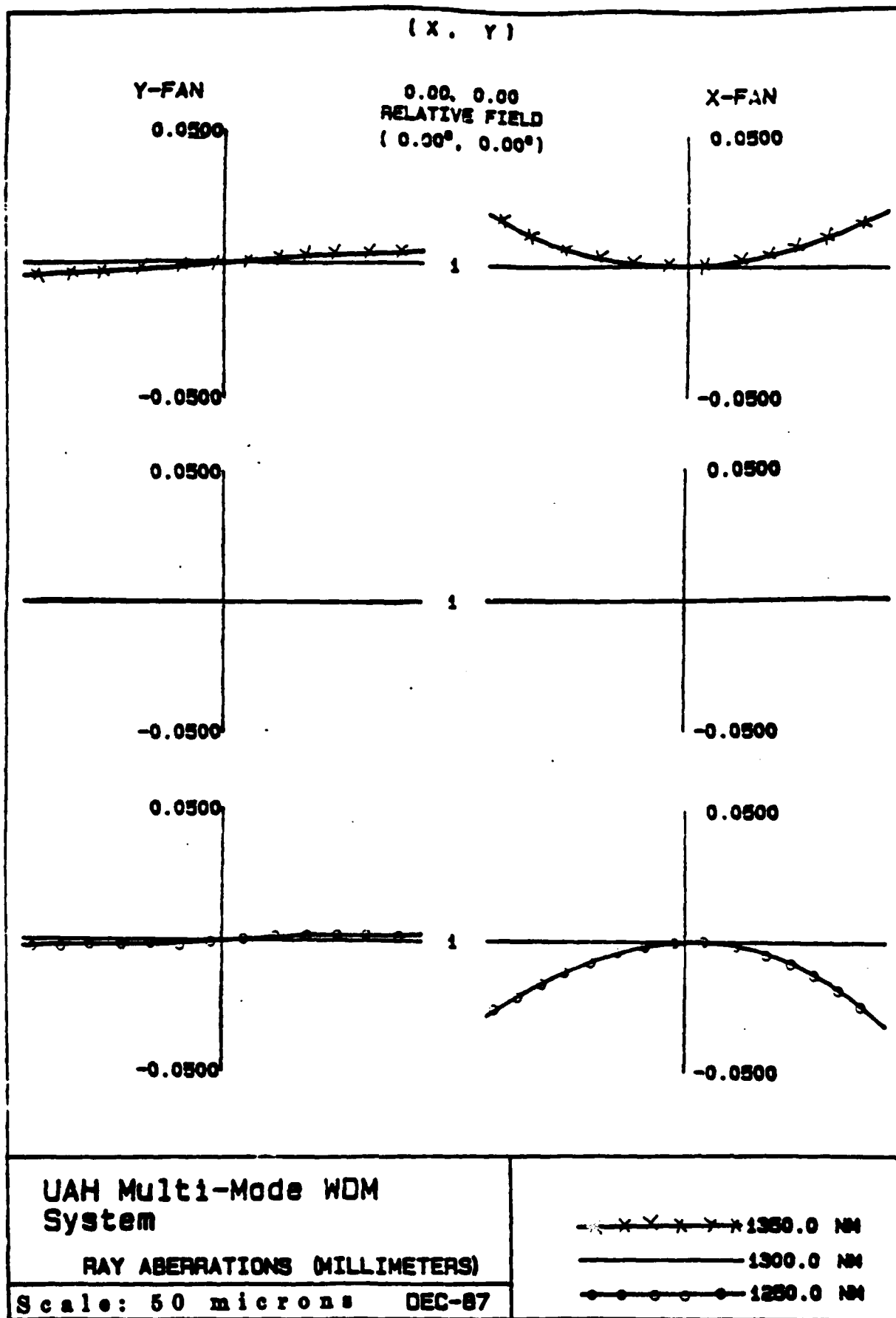
DEC-87

SCALE 0.600

UAH Multi-Mode WDM System



# RAY ABERRATIONS



# SPOT DIAGRAM

FIELD  
POSITION

.00, 0.00  
0.0, 0.0 DG

1350 nm

.00, 0.00  
0.0, 0.0 DG

1300 nm

.00, 0.00  
0.0, 0.0 DG

1250 nm

DEFOCUSING

0.00000

UAH Multi-mode WDM System

SCALE: 1 INCH = 0.05000 MM

# UAM Multi-mode WDM System Specification Input:

	RADIUS	THICKNESS	GLASS	CCY	THC
Object:	INFINITY	150.000000	100	100	
Stop:	INFINITY	0.000000	100	100	
Surface 2:	INFINITY	-150.000000	100	100	
Surface 3:	INFINITY	150.000000	100	100	
XDE:	0.000000	YDE:	0.000000		
XDC:	100	YDC:	100		
ADE:	0.000000	BDE:	16.750000	CDE:	0.000000
ADC:	100	BDC:	100	CDC:	100
Surface 4:	-300.00000	0.000000	REFL	100	100
Parabolic mirror:	CON:				
	K :	-1.000000	KC :	100	
Surface 5:	INFINITY	-140.000000		100	100
XDE:	44.166400	YDE:	0.000000		
XDC:	100	YDC:	100		
ADE:	0.000000	BDE:	0.000000	CDE:	0.000000
ADC:	100	BDC:	100	CDC:	100
Surface 6:	INFINITY	0.000000	REFL	100	100
Grating:					
K :	0.000000	KC :	100	IC :	YES
A :0.000000E+00		B :0.000000E+00		C :0.000000E+00	D :0.000000E+00
AC :	100	BC :	100	CC :	100
GR0:	1	GRS:	0.001205	GRZ:	0.000000
GRX:	1.000000	GRY:	0.000000		
XDE:	0.000000	YDE:	0.000000		
XDC:	100	YDC:	100		
ADE:	0.000000	BDE:	14.000000	CDE:	0.000000
ADC:	100	BDC:	100	CDC:	100
Surface 7:	INFINITY	90.000000		100	100
XDE:	0.000000	YDE:	0.000000		
XDC:	100	YDC:	100		
ADE:	0.000000	BDE:	-56.832850	CDE:	0.000000
ADC:	100	BDC:	100	CDC:	100
Surface 8:	149.65942	17.283206	SF11_SCHOTT	0	100
Surface 9:	280.83863	41.307700	AIR	0	100
Surface 10:	203.77882	5.954313	BK7_SCHOTT	0	100
Surface 11:	109.98355	5.432801	AIR	0	100
Surface 12:	173.47261	22.720352	SF11_SCHOTT	0	100
Surface 13:	2651.80673	18.180511	AIR	0	100
Surface 14:	-106.49135	26.000000	BK7_SCHOTT	0	100
Surface 15:	-203.32729	2.991443	AIR	0	100
Surface 16:	115.70657	25.961943	SF11_SCHOTT	0	100
Surface 17:	-767.18389	73.347788	AIR	0	0
Surface 18:	367.33235	6.221046	SF11_SCHOTT	0	0
Image:	-79.87601	0.000000		0	100
XDE:	0.000000	YDE:	0.000000	DAR	
XDC:	100	YDC:	100		
ADE:	0.000000	BDE:	1.311379	CDE:	0.000000
ADC:	100	BDC:	0	CDC:	100

## SPECIFICATION DATA

Entrance Pupil Diameter: 52.00000 mm  
Wavelength: 1350.00 nm 1300.00 nm 1250.00 nm  
XAN 0.00000  
YAN 0.00000  
VUX 0.00000  
VLX 0.00000  
VUY 0.00000  
VLY 0.00000

# REFRACTIVE INDICES

GLASS CODE	1350.00 nm	1300.00 nm	1250.00 nm
SF11 SCHOTT	1.747919	1.748879	1.749889
BK7 SCHOTT	1.503112	1.503712	1.504314

No solves defined in system

## ZOOM DATA

	POS 1	POS 2	POS 3
WTW W1	1	0	0
WTW W2	0	1	0
WTW W3	0	0	1
REF	1	2	3

This is a decentered system. If elements with power are decentered or tilted, the first order properties are probably inadequate in describing the system characteristics.

## INFINITE CONJUGATES

	Position 1	Position 2	Position 3
Effective Focal Length:	-380.6252	-380.0000	-379.3375
Back Focal Length:	612.3236	610.5767	608.7139
Front Focal Length:	-394.2420	-393.8835	-393.5051
F/number:	-4.1877	-4.1785	-4.1688

## AT USED CONJUGATES

Reduction Ratio:	0.8916	0.8909	0.8902
F/number:	2.6102	2.6083	2.6063
Object Distance:	150.0000	150.0000	150.0000
TT:	345.4011	345.4011	345.4011
Image Distance:	6.2210	6.2210	6.2210
Optical Axis Length:	189.1801	189.1801	189.1801

## PARAXIAL IMAGE

Height:	0.0000	0.0000	0.0000
Thickness:	6.4603	6.2333	5.9900
YAN:	0.0000	0.0000	0.0000

## ENTRANCE PUPIL

Diameter:	52.0000	52.0000	52.0000
Thickness:	0.0000	0.0000	0.0000

## EXIT PUPIL

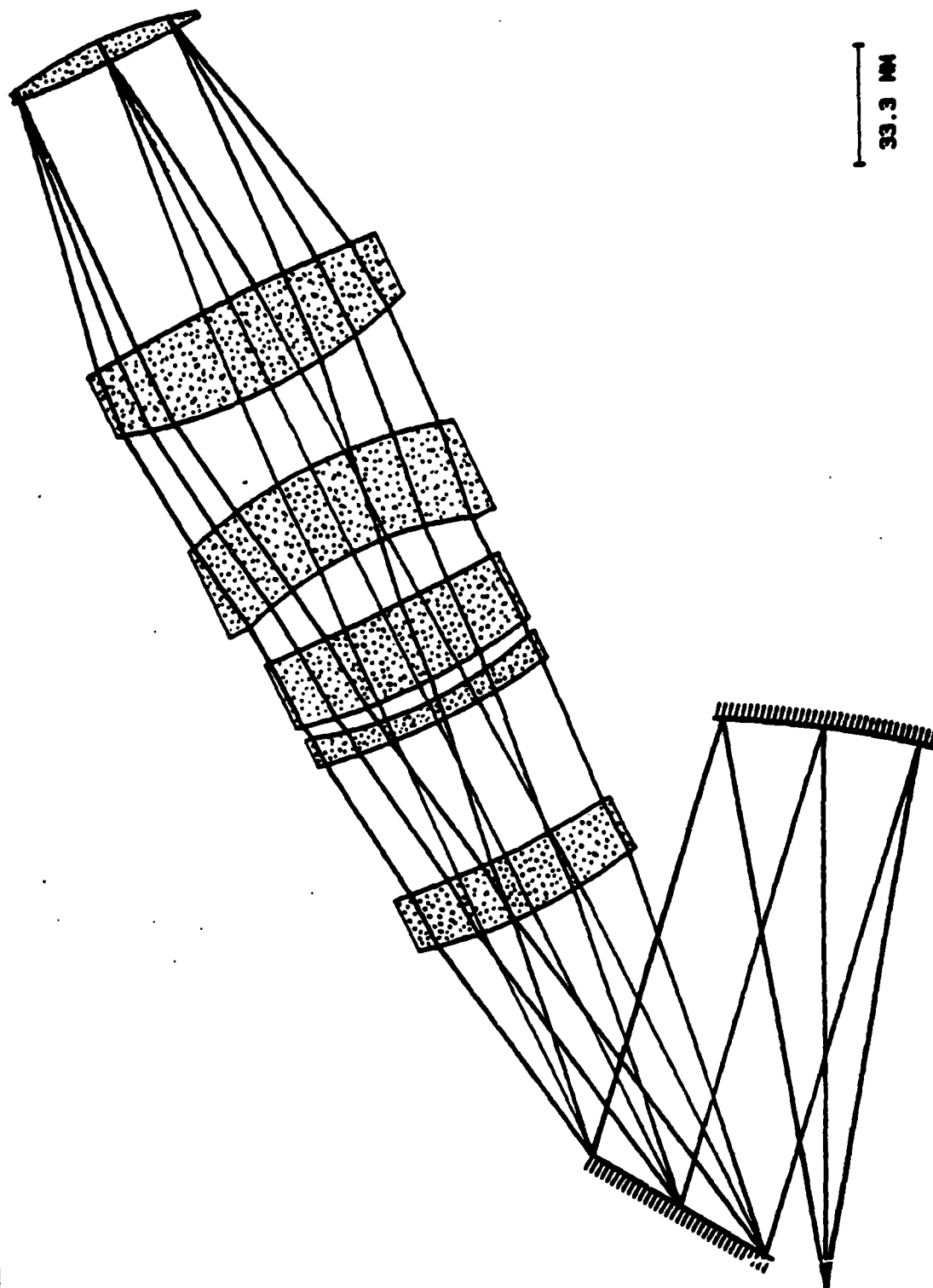
Diameter:	28.7221	28.6853	28.6463
Thickness:	135.5759	135.1616	134.7182
Stop Diameter:	52.0000	52.0000	52.0000

## **1.5 UAH Single-Mode WDM System**

UAH Single-mode WDM System

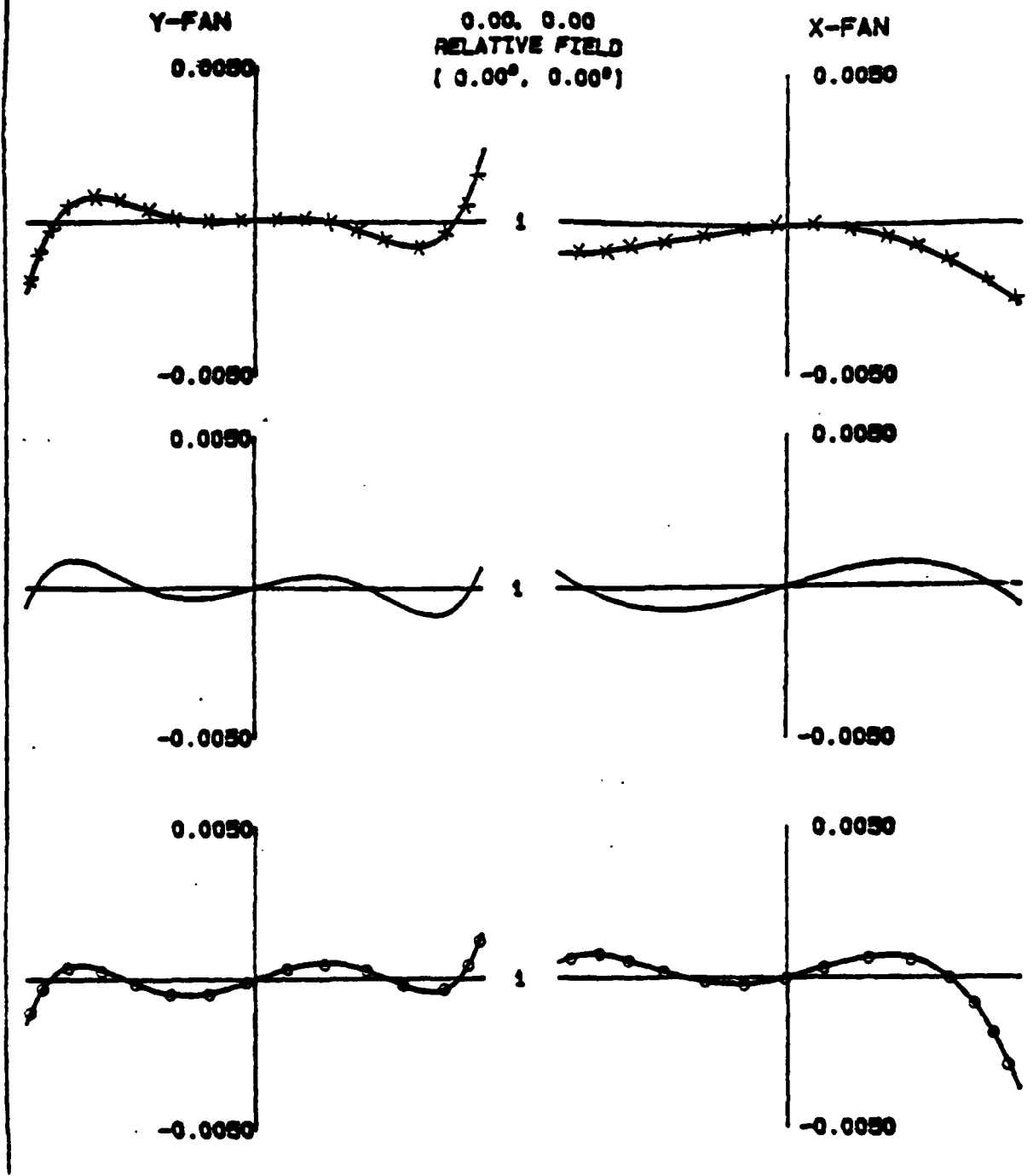
SCALE 0.600

DEC-87



# RAY ABERRATIONS

(X, Y)



UAH Single-mode WDM  
System

RAY ABERRATIONS (MILLIMETERS)

Scale: 5 microns

DEC-87

× × × × × 1400.0 NM  
— — — — — 1300.0 NM  
● ● ● ● ● 1200.0 NM

# SPOT DIAGRAM

FIELD  
POSITION

.00, 0.00  
0.0, 0.0 DS

1400 nm

.00, 0.00  
0.0, 0.0 DS

1300 nm

.00, 0.00  
0.0, 0.0 DS

1200 nm

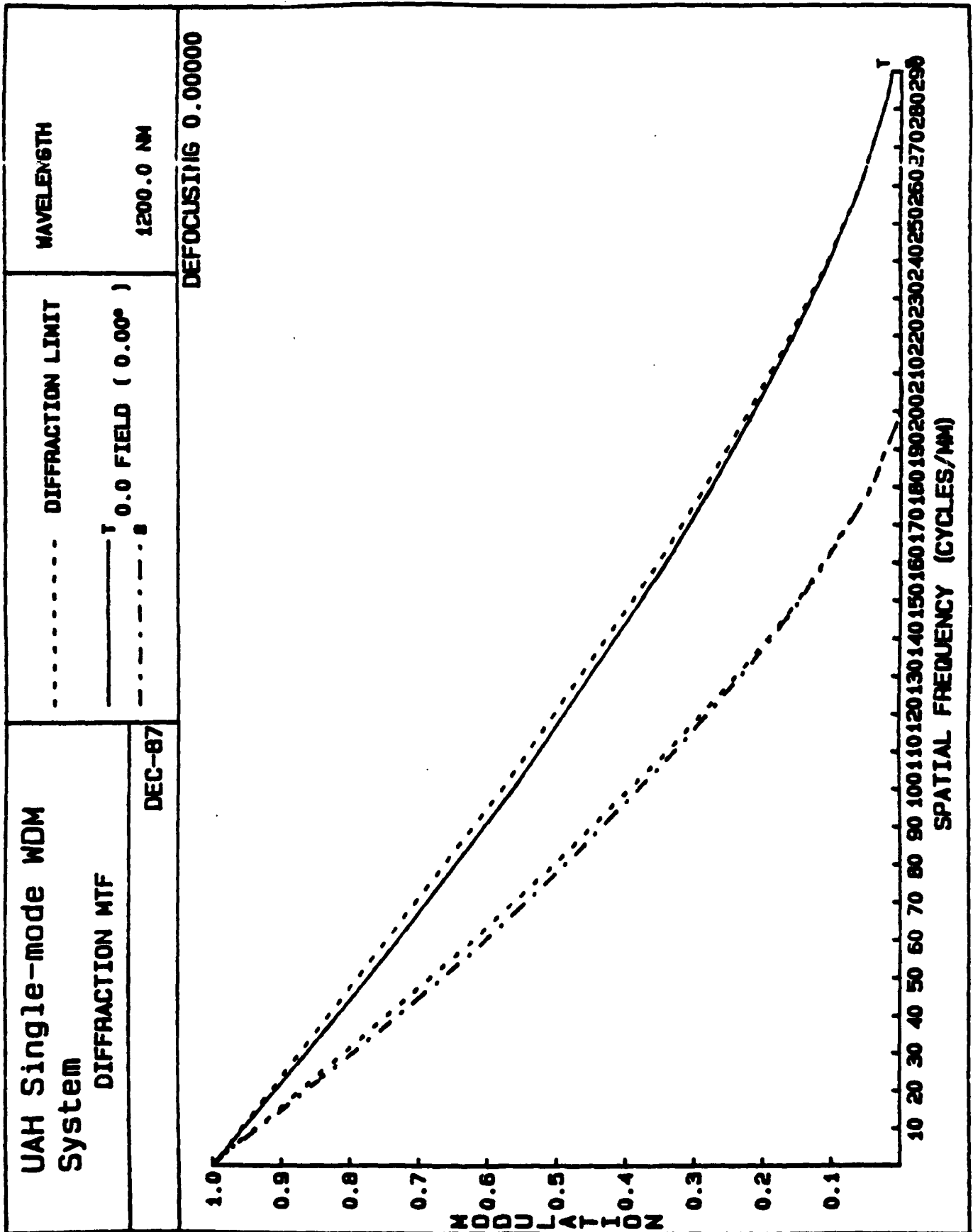
DEFOCUSING

0.00000

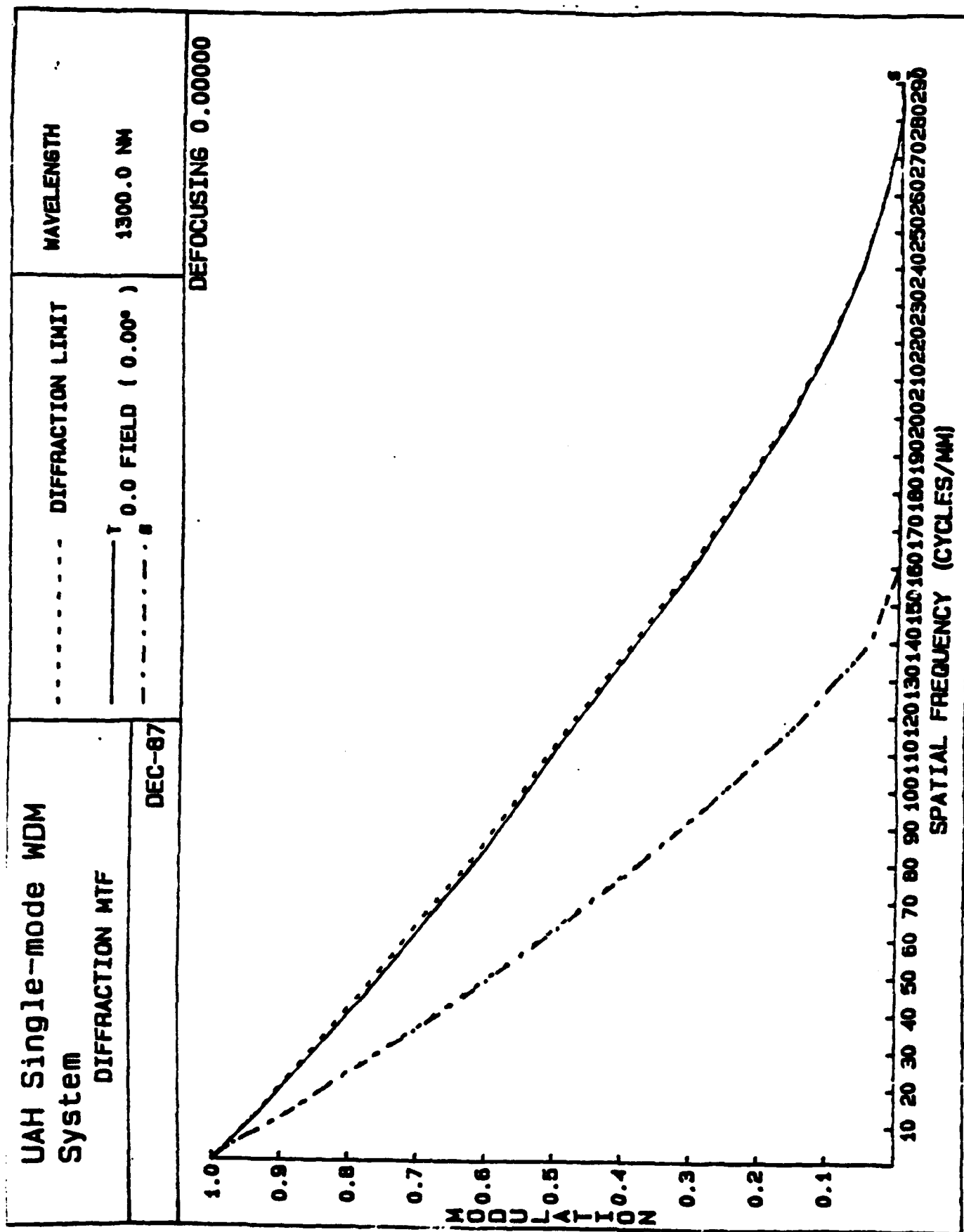
UAH Single-Mode WDM System

SCALE: 1 INCH = 0.00500 MM

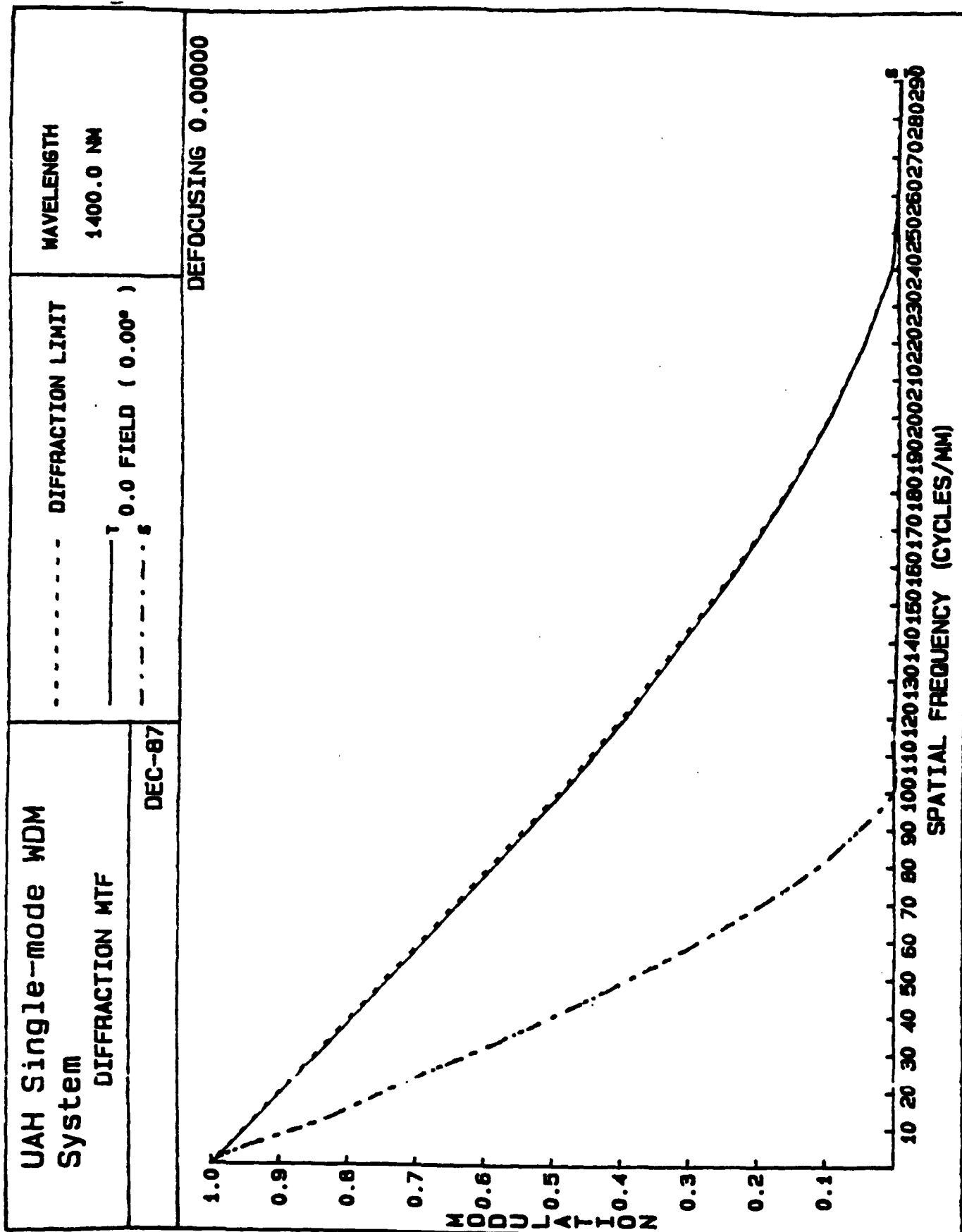
# DIFFRACTION MTF



# DIFFRACTION MTF



## DIFFRACTION MTF



# UAM Single-Mode WDM Specification Input:

ELEMENT	RADIUS	THICKNESS	GLASS	CCY	THC	GLC
Object:	INFINITY	150.000000			100	100
Stop:	INFINITY	0.000000			100	100
Surface 2:	INFINITY	-150.000000			100	100
Surface 3:	INFINITY	150.000000			100	100
XDE:	0.000000	YDE:	0.000000			
XDC:	100	YDC:	100			
ADE:	0.000000	BDE:	16.750000	CDE:	0.000000	
ADC:	100	BDC:	100	CDC:	100	
Surface 4:	-300.00000	0.000000	REFL		100	100
CON:						
K :	-1.000000	KC :	100			
Surface 5:	INFINITY	-140.000000			100	100
XDE:	44.166400	YDE:	0.000000			
XDC:	100	YDC:	100			
ADE:	0.000000	BDE:	0.000000	CDE:	0.000000	
ADC:	100	BDC:	100	CDC:	100	
Surface 6:	INFINITY	0.000000	REFL		100	100
Grating:						
K :	0.000000	KC :	100	IC :	YES	
A :	0.000000E+00	B :	0.000000E+00	C :	0.000000E+00	
AC :	100	BC :	100	CC :	100	DC :
GRO:	1	GRS:	0.001205	GRZ:	0.000000	
GRX:	1.000000	GRY:	0.000000			
XDE:	0.000000	YDE:	0.000000			
XDC:	100	YDC:	100			
ADE:	0.000000	BDE:	14.000000	CDE:	0.000000	
ADC:	100	BDC:	100	CDC:	100	
Surface 7:	INFINITY	90.000000			100	100
XDE:	0.000000	YDE:	0.000000			
XDC:	100	YDC:	100			
ADE:	0.000000	BDE:	-56.832850	CDE:	0.000000	
ADC:	100	BDC:	100	CDC:	100	
Surface 8:	149.65942	17.283206	SF11_SCHOTT		100	100
Surface 9:	280.83863	41.307700	AIR		100	100
Surface 10:	203.77882	5.954313	BK7_SCHOTT		100	100
Surface 11:	111.77415	5.432801	AIR		0	100
Surface 12:	165.94527	22.720352	SF11_SCHOTT		0	100
Surface 13:	966.65550	18.240166	AIR		0	0
Aspheric:						
K :	4.648593	KC :	100			
IC :	YES	CUF:	0.000000	CCF:	100	
A :	0.000000E+00	B :	0.000000E+00	C :	0.000000E+00	D :
AC :	100	BC :	100	CC :	100	DC :
Surface 14:	-99.23606	26.000000	BK7_SCHOTT		0	0
Surface 15:	-133.82274	23.972136	AIR		0	0
Surface 16:	148.51499	26.000000	SF11_SCHOTT		0	0
Surface 17:	-576.63963	73.203735	AIR		0	0
YTO:						
RDX:	-577.47285	CCX:	0			
K :	-20.470752	KC :	0	IC :	YES	
A :	0.000000E+00	B :	0.000000E+00	C :	0.000000E+00	D :
AC :	100	BC :	100	CC :	100	DC :

Surface 18:	492.72536	6.675050	SF11_SCHOTT	0	0
Image Surface:	-94.82372	0.000000		0	100
XDE:	0.000000	YDE:	0.000000		DAR
XDC:	100	YDC:	100		
ADE:	0.000000	BDE:	1.322295	CDE:	0.000000
ADC:	100	BDC:	0	CDC:	100

#### SPECIFICATION DATA

Eantrance Pupil Diameter:	52.00000 mm	
Wavelength:	1400.00 nm	1300.00 nm 1200.00 nm
XAN	0.00000	
YAN	0.00000	
VUX	0.00000	
VLX	0.00000	
VUY	0.00000	
VLY	0.00000	

#### REFRACTIVE INDICES

GLASS CODE	1400.00 nm	1300.00 nm	1200.00 nm
SF11_SCHOTT	1.746999	1.748879	1.750962
BK7_SCHOTT	1.502511	1.503712	1.504922

No solves defined in system

#### ZOOM DATA:

	Position 1	Position 2	Position 3
WTW W1	1	0	0
WTW W2	0	20	0
WTW W3	0	0	1
REF	1	2	3

This is a decentered system. If elements with power are decentered or tilted, the first order properties are probably inadequate in describing the system characteristics.

	Position 1	Position 2	Position 3
INFINITE CONJUGATES			
Effective Focal Length:	-381.2536	-380.0000	-378.6144
Back Focal Length:	670.6560	667.0129	662.9281
Front Focal Length:	-373.5697	-372.8913	-372.1434
F/Number	-4.1968	-4.1785	-4.1583

#### AT USED CONJUGATES

Reduction Ratio:	0.9761	0.9748	0.9734
F/Number:	2.8577	2.8540	2.8497
Object Distance:	150.0000	150.0000	150.0000
TT:	366.7895	366.7895	366.7895
Image Distance:	6.6751	6.6751	6.6751
Optical Axis Length:	210.1144	210.1144	210.1144

#### PARAXIAL IMAGE

Height:	0.0000	0.0000	0.0000
Thickness:	7.1683	6.6966	6.1574
Y Field Angle:	0.0000	0.0000	0.0000

**ENTRANCE PUPIL**

Diameter:	52.0000	52.0000	52.0000
Thickness:	0.0000	0.0000	0.0000

**EXIT PUPIL**

Diameter:	30.3776	30.3002	30.2144
Thickness:	156.5997	155.7093	154.7048
Stop Diameter:	52.0000	52.0000	52.0000

**Appendix B: July Presentation**

## Contents

### 1 Appendix B: July Presentation

1.1 WDM Presentation Cover Page . . . . .	
Multiplexing Definitions . . . . .	47
Features of an Ideal WDM System . . . . .	48
Current Commercial Multiplexer Approach . . . . .	49
RADC/UAH Approach . . . . .	49
Contract Schedule . . . . .	50
Basic WDM System Configurations . . . . .	51
Multiple Channel WDMs . . . . .	53
System Tradeoffs and Performance Measures . . . . .	54
WDM System Tradeoffs . . . . .	55
Insertion Loss . . . . .	56
Crosstalk . . . . .	57
Crosstalk Matrix . . . . .	58
WDM Lens . . . . .	59
Breadboard Wavelength Multiplexing Experiment . . . . .	60
Effective Focal Length of the WDM Lens . . . . .	61
List of Research Problems . . . . .	62
Engineering Considerations . . . . .	63
Current Effort . . . . .	69
Proposed Effort . . . . .	70
Problem 1: Lens Aberrations . . . . .	71
Problem 2 . . . . .	72
Problem 2: Scattering . . . . .	73
Improved Crosstalk with Cross-Dispersing Prism . . . . .	74
Problem 3: Laser Drift . . . . .	75
Wavelength Stabilized Diode Laser . . . . .	76
Single-Mode vs. Multi-Mode WDM Comparisons . . . . .	77
Itemized Present Effort: FY87 . . . . .	78
Itemized Proposed Effort: FY88 . . . . .	78
Overall Assessment . . . . .	79
Questions . . . . .	80

## List of Figures

<u>Block Representation of Wavelength Division Multiplexing</u> . . . . .	47
<u>Two Channel Dichroic Filter WDM</u> . . . . .	51
<u>Three Channel Dichroic Filter WDM</u> . . . . .	51
<u>Littrow Spectrograph</u> . . . . .	51
<u>Littrow Spectrograph with GRIN Lens</u> . . . . .	52
<u>Waveguide Planar Rowland Spectrometer</u> . . . . .	52
<u>Transmission Holographic WDM</u> . . . . .	52
<u>Prism WDM</u> . . . . .	52
<u>Littrow Spectrograph</u> . . . . .	53
<u>Czerny-Turner Spectrograph</u> . . . . .	53
<u>Czerny-Turner Spectrograph with Lenses</u> . . . . .	53
<u>Graphical Representation of Insertion Loss</u> . . . . .	56
<u>Graphical Representation of Crosstalk</u> . . . . .	57
<u>Crosstalk Matrix</u> . . . . .	58
<u>Mux Optical System</u> . . . . .	59
<u>Four-Element WDM Lens System</u> . . . . .	64
<u>Four-Element WDM Lens Ray Aberrations</u> . . . . .	65
<u>Five-Element WDM Lens System</u> . . . . .	66
<u>Five-Element WDM Lens Ray Aberrations</u> . . . . .	67
<u>Five-Element WDM Lens System with Parabolic Mirror</u> . . . . .	68
<u>Block Representation of Current Effort</u> . . . . .	69
<u>Block Representation of Proposed Effort</u> . . . . .	70
<u>Effects of Lens Aberrations on Insertion Loss</u> . . . . .	71
<u>Representation of Light Scattering and Efficiency Measurements of WDM's</u>	
<u>Grating</u> . . . . .	72
<u>Graphical Representation of Isolated Grating Scatter</u> . . . . .	73
<u>Picture of BRDF Instrument</u> . . . . .	73
<u>Representation of Laser Drift Across Fiber</u> . . . . .	74
<u>Laser Drift Effects on Insertion Loss</u> . . . . .	75
<u>Possible Method for Stabilizing Laser Diode</u> . . . . .	76
<u>Optical Layout of WDM System in Mux Mode</u> . . . . .	79

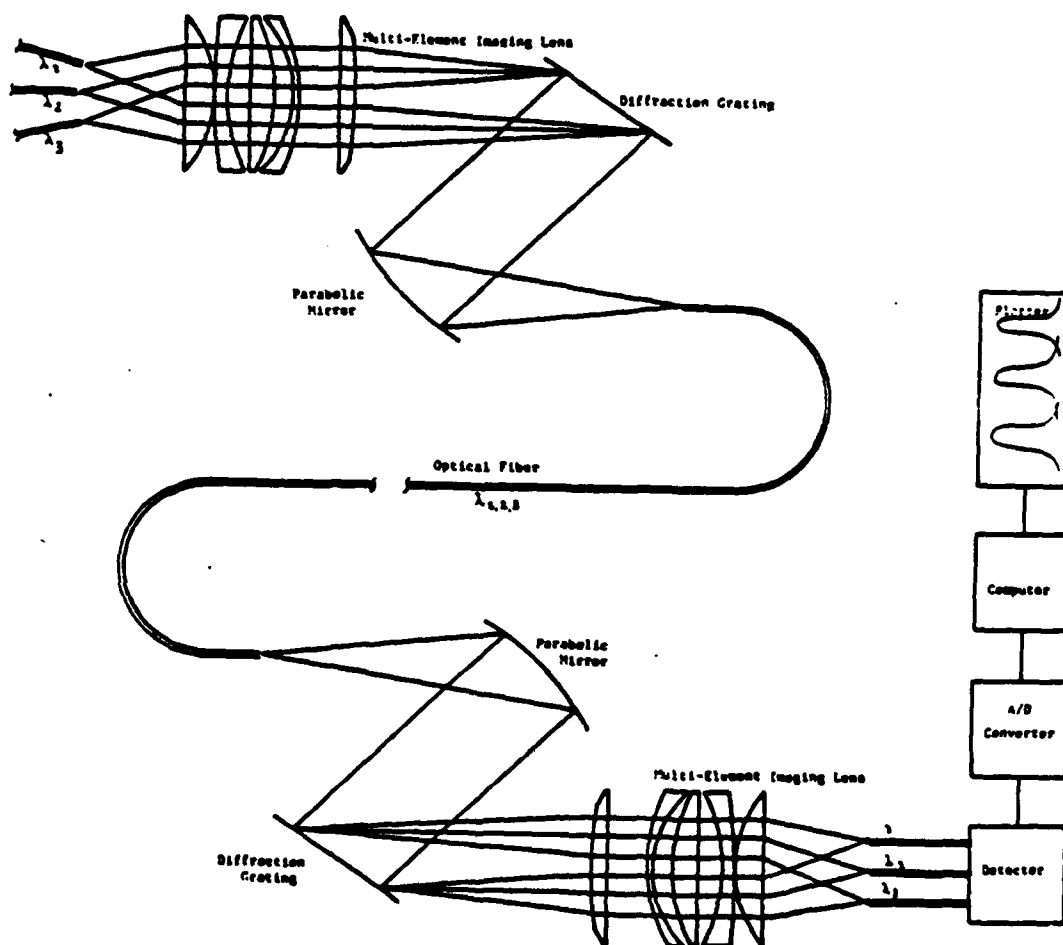
Sponsored Research from Rome Air Development Center  
Massively Multi-Channel Wavelength Division Multiplexer

at

Center for Applied Optics (CAO)  
University of Alabama in Huntsville (UAH)

Dr. Russell A. Chipman

Mr. Thomas A. Burleson



Multiplexing:

Combination of two or more signals for transmission along a single path.

Demultiplexing:

Separation of multiplexed signals.

Wavelength Division Multiplexing: (WDM)

Signals occupy separate wavelength bands.

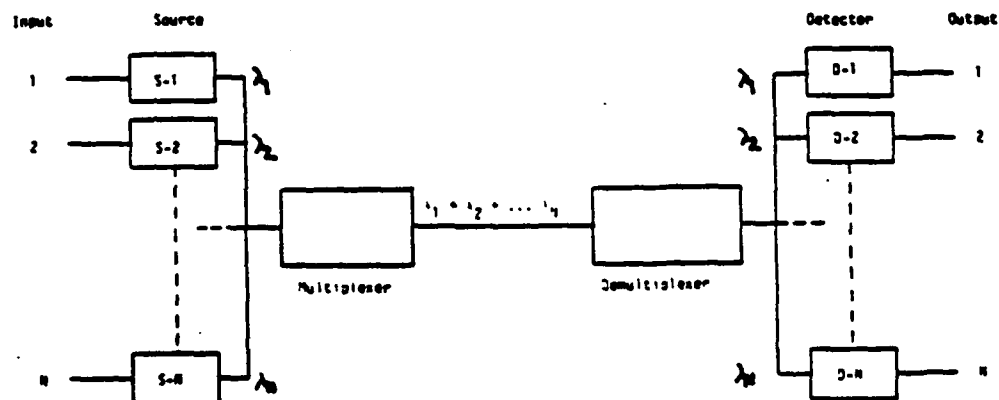
Frequency Domain Multiplexing:

Signals occupy separate frequency bands.

Time Domain Multiplexing:

Signals are compressed and shuffled in time.

WAVELENGTH MULTIPLEXING



Wavelengths can be multiplexed using:

- A.) Dichroic Filters
- B.) Prisms
- C.) Gratings
- D.) Integrated Optics



## IDEAL MASSIVELY MULTIPLEXED WDM OPTICAL SYSTEM (MM-WDM)

### Features:

- i.) Many Channels,  $>20$
- ii.) Low Insertion Loss
- iii.) Low Crosstalk
- iv.) Compact and Inexpensive

### For Example:

- i.) 200 Channels with 1.5nm Channel Separation
- ii.) 3 dB Insertion Loss
- iii.) 35 dB Crosstalk
- iv.) 200mm x 125mm x 100mm

## CURRENT COMMERCIAL MULTIPLEXER APPROACH

- 1.) 2 to 4 Channels
- ii.) No Published Design For More Than 12 Channels

## RADC/UAH APPROACH

### Current:

- 1.) Intelligent Utilization of Off-the-Shelf Components  
for the Breadboard WDM
- ii.) Design 60 Channel WDM

### Proposed:

- 1.) Design/Build 60 or 100 Channel WDM System
- ii.) Design/Build Test Laboratory at RADC for:
  - A.) WDM Components
    - 1.) Fibers
    - 2.) Laser Diodes
    - 3.) Lenses
    - 4.) Gratings
  - B.) WDM Systems
    - 1.) Insertion Loss
    - 2.) Crosstalk

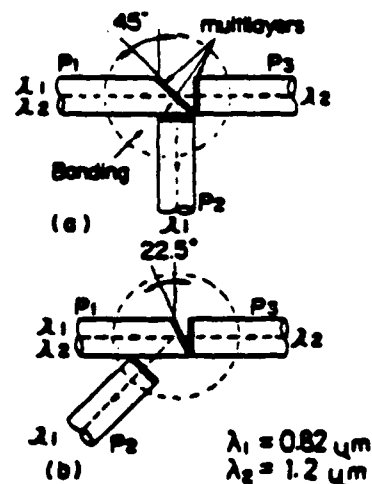
## CONTRACT SCHEDULE

February 10, 1987	----	Graduate Student Begins
May 25, 1987	----	Contract Start Date at UAH
June 30, 1987	----	Breadboard System Designed, Equipment Ordered for Insertion Loss and Crosstalk Measurements
July 10, 1987	----	Presentation on System Tradeoffs
August 1, 1987	----	Begin Assembling Breadboard 30 Channel WDM
August 15, 1987	----	Complete Lens Design for 60 Channel Multiplexer Lens
August 30, 1987	----	Begin Measurements on Breadboard WDM, Insertion Loss and Crosstalk Study
September 31, 1987	----	End Contract, Deliver Final Report:  1.) 30 Channel WDM Performance Data ii.) 60 Channel Lens Design

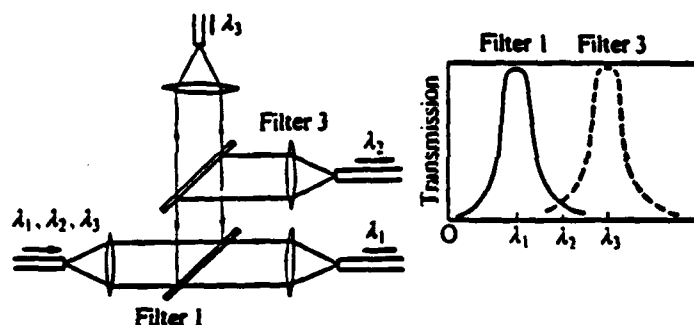
## BASIC SYSTEM CONFIGURATIONS USED IN WDM SYSTEMS with a limited number of channels

### 1.) Two Channel Dichroic Filter WDM:

Multimode optical fiber pieces with dielectric multilayers evaporated on the ends of the fibers, which have been polished obliquely or squarely.

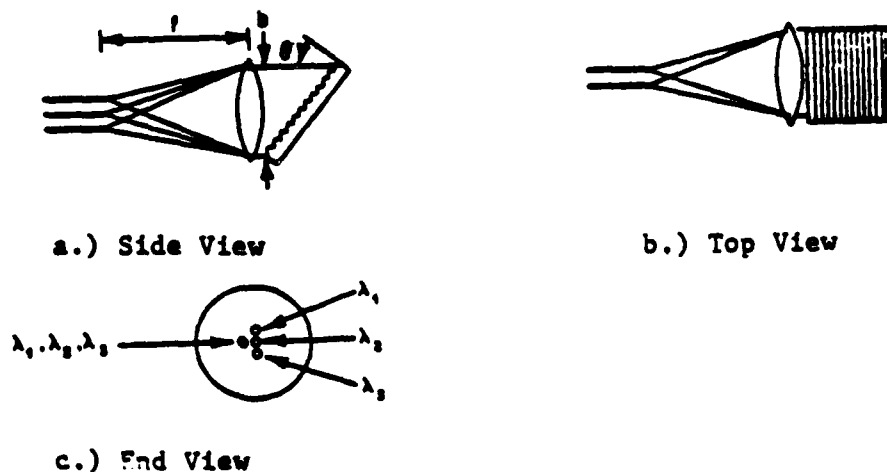


### 2.) Three Channel Dichroic Filter WDM:



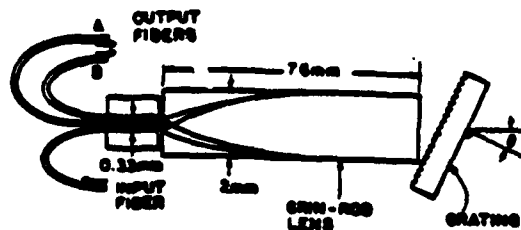
### 3.) Littrow Spectrograph:

Consisting of a plane reflection grating. The lenses have a relatively short effective focal length.



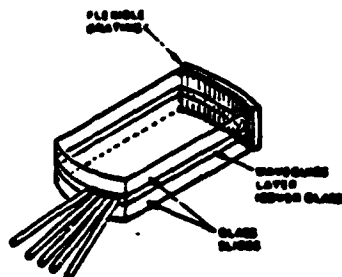
#### 4.) Littrow Spectrograph:

Consisting of a GRIN-rod lens with a plane reflection grating.



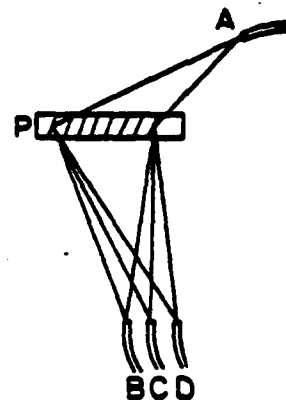
#### 5.) Waveguide Planar Roland Spectrometer:

With a concave reflection grating.



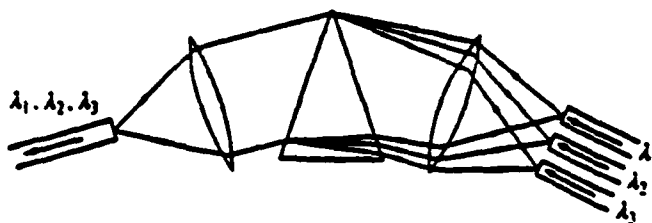
#### 6.) Transmission Hologram WDM:

Single-element thick hologram demux in operation. Note that the inclination of the fringes varies across the HOE.



#### 7.) Prism WDM:

Moderate number of channels, but limited by the prism dispersion.

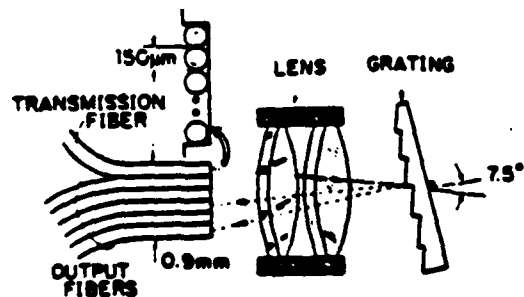


These Systems Are Small, Compact, and Inexpensive. But Limited To Few Channels By Either Dichroic Filter Constraints or Aberrations.

MULTIPLE CHANNEL WDM'S are basically spectrographs

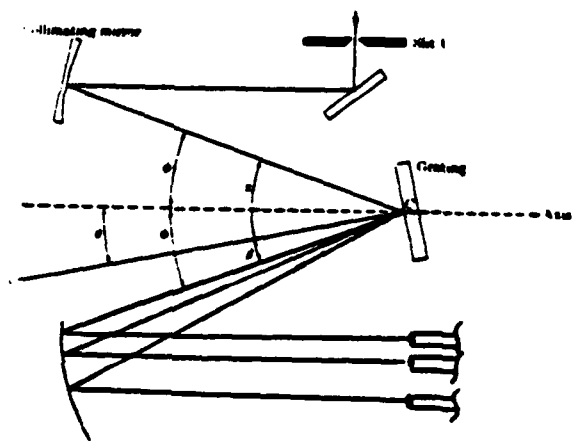
1.) Littrow Spectrograph:

Lenses have a longer effective focal length in order to provide a large number of channels.



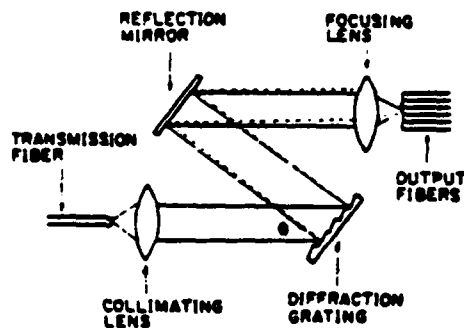
2.) Czerny-Turner Spectrograph:

Grating monochromator where CN is the grating normal. Angle  $\alpha$  is fixed.



3.) Czerny-Turner Spectrograph with Lenses:

Lenses have larger fields of view than mirrors.



## SYSTEM TRADEOFFS and PERFORMANCES MEASURES

### Outline:

- i.) Number of Channels
- ii.) Spectral Range
- iii.) Insertion Loss
- iv.) Crosstalk
- v.) Volume
- vi.) Sensitivity to Laser Drift
- vii.) Cost

## WDM SYSTEM TRADEOFFS

1.) Number of Channels depend on:

A.) Spectral Range

B.) Channel Wavelength Separation

A.) Spectral Range depends on:

1.) Laser Wavelengths

2.) Transmission of Optical Elements

3.) Efficiency of the disperser (diffraction grating or prism)

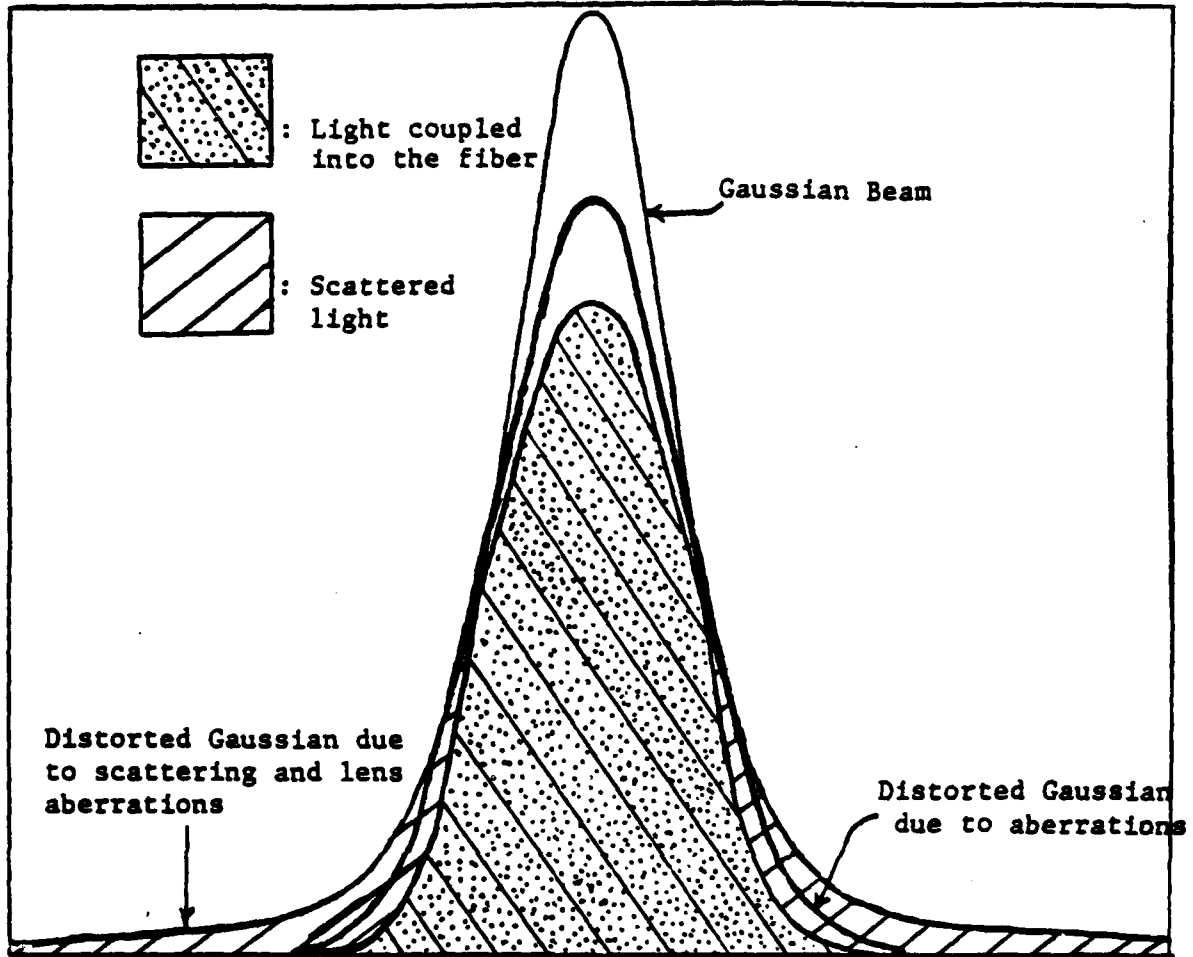
4.) Lens' Aberrations

5.) Lens' Apertures

6.) Fiber Dispersion

B.) Minimize Channel Wavelength Separation

## INSERTION LOSS

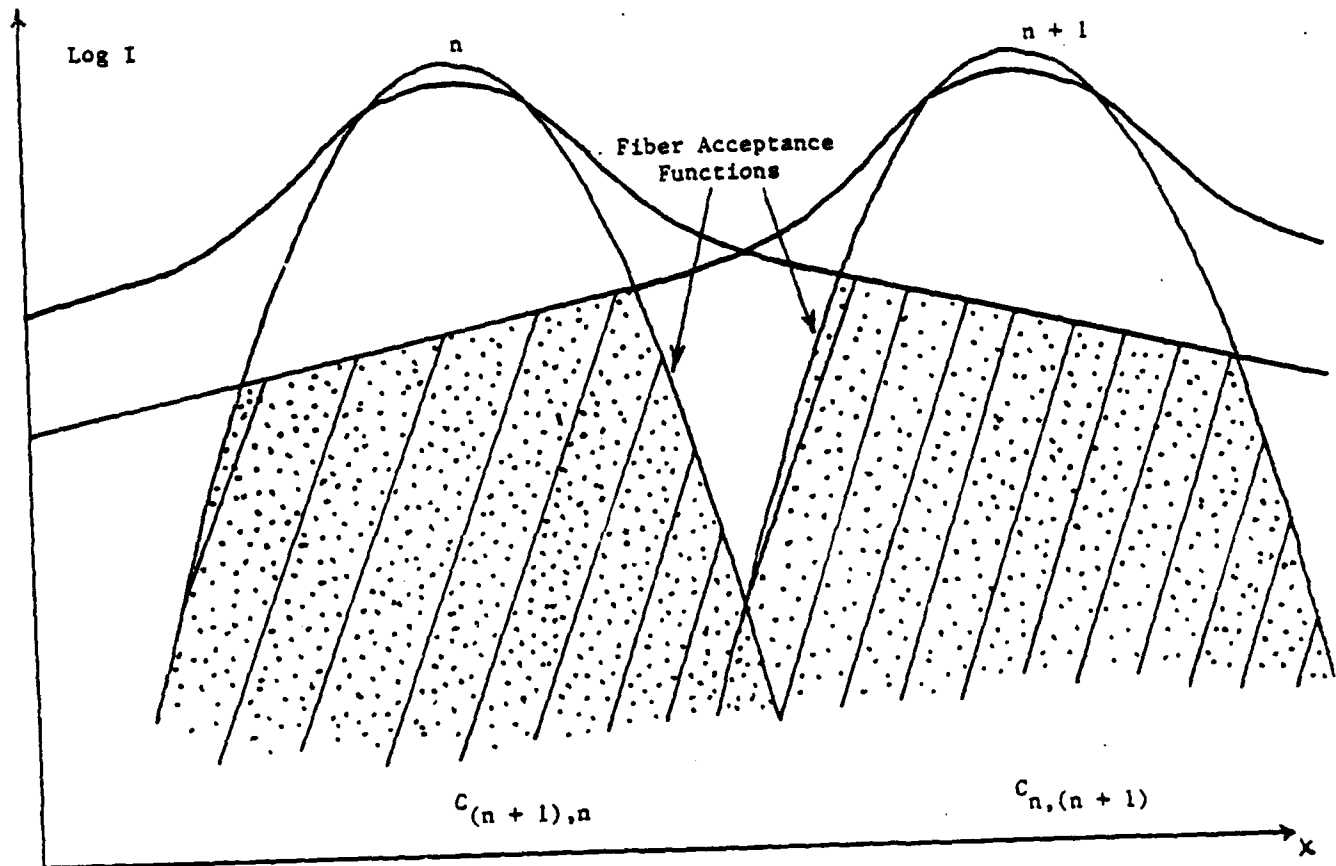


$$\text{Insertion Loss} = \frac{I}{I_0}; \quad \begin{array}{l} I : \text{Light actually coupled into the fiber} \\ I_0 : \text{Intensity incident at the multiplexer} \end{array}$$

ii.) Insertion Loss is determined by:

- A.) System Transmission and Efficiency
- B.) Recieving Fiber Diameter
- C.) Beam F/Number
- D.) Lens' Aberrations
- E.) Fiber Alignment with respect to the image
- F.) Laser Wavelength Drift

## CROSSTALK



Note: Larger Channel Separation Decreases Crosstalk

### iii.) Crosstalk Tradeoffs:

- A.) Channel Wavelength Separation
- B.) Grating Scattering
- C.) Optics' Scattering
- D.) Lens' Aberrations

CROSSTALK MATRIX (in dB)

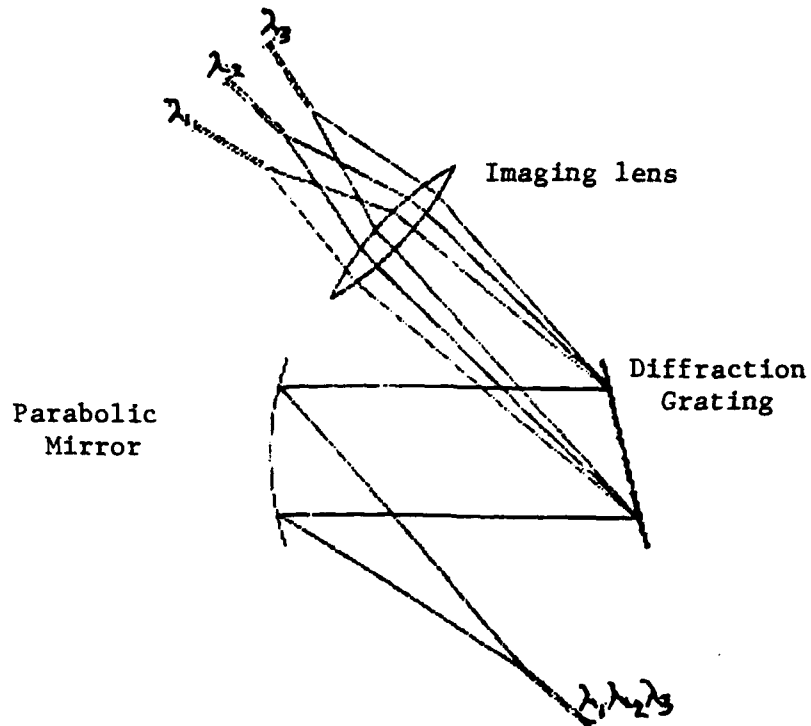
Wavelengths	Fibers				
	1	2	3	4	. . .
1	3.0	30	32	35	. . .
2	28	3.3	29	32	
3	31	29	2.9	29	
4	34	34	30	2.8	
.	.				
.	.				
.	.				

INSERTION LOSS =  $\frac{I_{n,n}}{I_n}$  ;  $I_{n,n}$  : Light of wavelength  $\lambda_n$  into fiber n.

CROSSTALK =  $\frac{I_{n,k}}{I_n}$  ;  $I_{n,k}$  : Light of wavelength  $\lambda_n$  into fiber k.

=  $C_{n,k}$

## MULTIPLEXER



Combining Side, Collimating Lens, ---- very small field of view.

Dispersing Side, Imaging Lens, ---- large field of view... proportional to the spectral range.

### 1.) Imaging Lens: very unusual lens requirements

A.) Disadvantages: stop is at the diffraction grating

- 1.) Makes lenses' apertures large.
- 2.) Introduces large amounts of coma and astigmatism.

B.) Advantages: only one wavelength at each field of view

- 1.) Chromatic Aberration unimportant
- 2.) Can position fiber arrays across image surface: flat field not required --- Field Curvature unimportant

Conclusion: the imaging lens is not an off-the-shelf or standard lens

## BREADBOARD WAVELENGTH MULTIPLEXING EXPERIMENT

Fiber:	60 $\mu$ m, Multimode Fiber
Grating:	830 lines/mm, Plane Reflection
Blaze Wavelength:	1200nm
Grating Diameter:	80mm
Laser Wavelengths:	1300nm, 1330nm
Laser Diodes:	InGaAsP, Intensity Feedback, TE Cooler, MM Pigtailed, M/A Com
Spectral Range:	1250nm - 1350nm
Magnification:	1, Variable
Angular Dispersion: (at 1300nm)	.0871 deg/nm      or      1.521 millirad/nm
Linear Dispersion: (at 1300nm)	.228mm/nm
Dispersion/Fiber: Diameter	.214nm
Laser Drift Tolerance:	$\pm$ .05nm

Multi-Element Lens: 6 Element Petzval Lens, Commercial Lens, Aberrations Unknown

Focal Length:	150mm
F/Number:	F/2.5

## EFFECTIVE FOCAL LENGTH of LENSES

### 1.) Advantages of Long Effective Focal Length ( EFL ): ( F/Number fixed )

- 1.) Large Linear Dispersion
- 2.) Closer Channel Separation ( in Wavelengths )
- 3.) High Channel Capacity
- 4.) Coarser Grating Spacing... Higher Grating Efficiency
- 5.) Smaller Effective Stop Shift ( measured in focal lengths )

### ii.) Advantages of Short EFL: ( F/Number fixed )

- 1.) Compact System
- 2.) Smaller Lens Apertures
- 3.) Less Sensitive to Laser Drift
- 4.) Lower Cost

### PROBLEM 1

Lens Design:

A.) Lens aberrations one of main limiting factors... ideal lens unlikely

### PROBLEMS 2

Scattering:

A.) Sources:

- i.) Gratings
- ii.) Coatings
- iii.) Lens Apertures
- iv.) Fiber Faces

### PROBLEM 3

Laser Drift

### PROBLEM 4

Mechanical Tolerances

ENGINEERING CONSIDERATIONS under current study

i.) Lens Design

A.) Imaging Performance Evaluation of Multiplexer Lens

1.) Transverse Aberration Plots

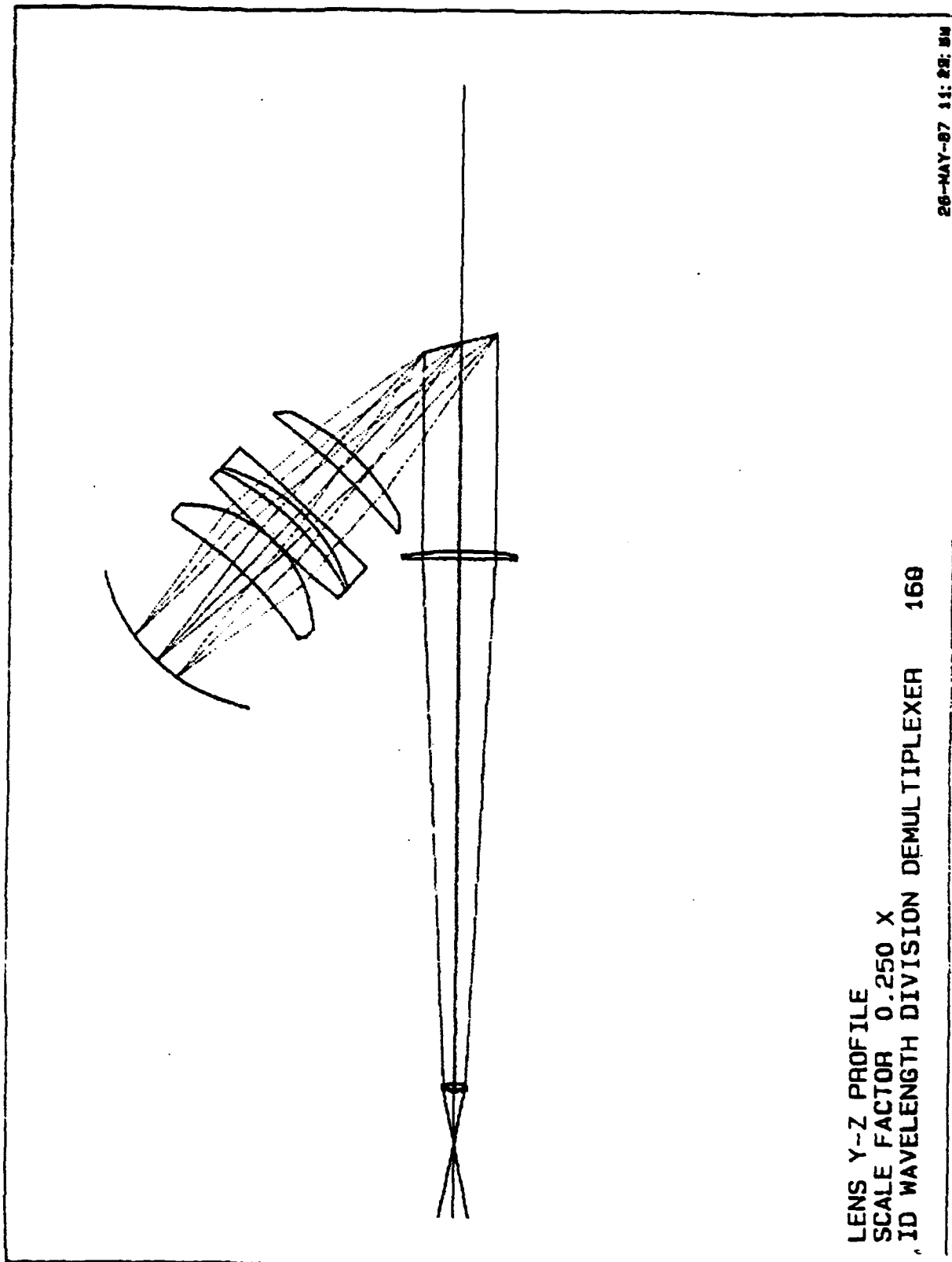
2.) RMS Spot Size

ii.) Scattering

A.) Conduct Initial Scattering Measurements on Breadboard  
Multiplexer via Insertion Loss and Crosstalk Study

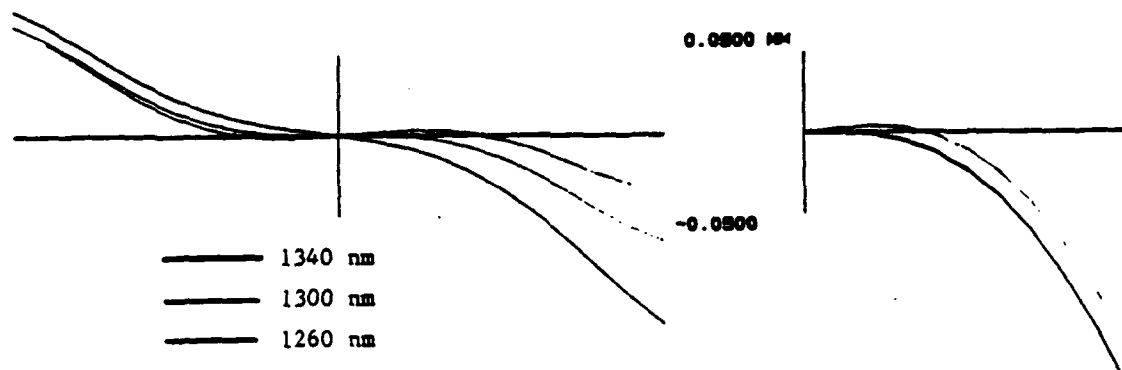
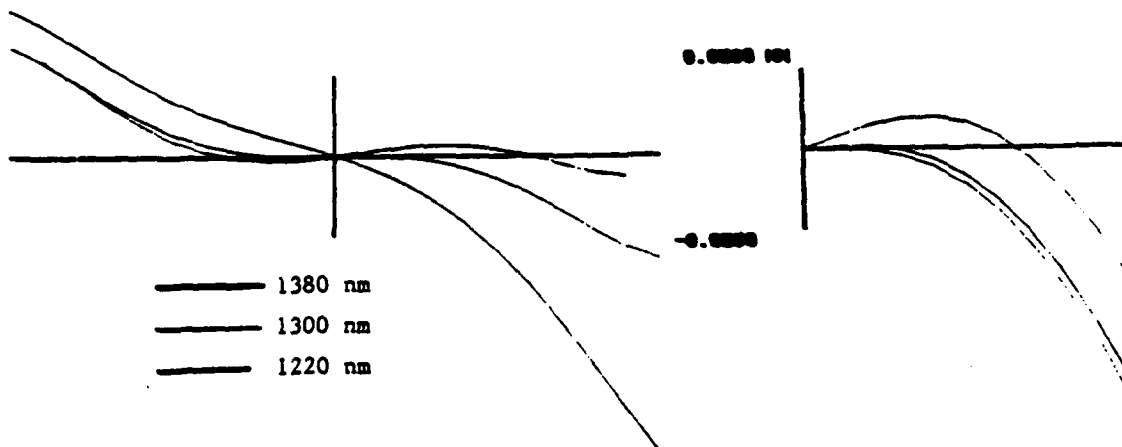
iii.) Laser Drift

A.) Acquire Baseline Data from Breadboard



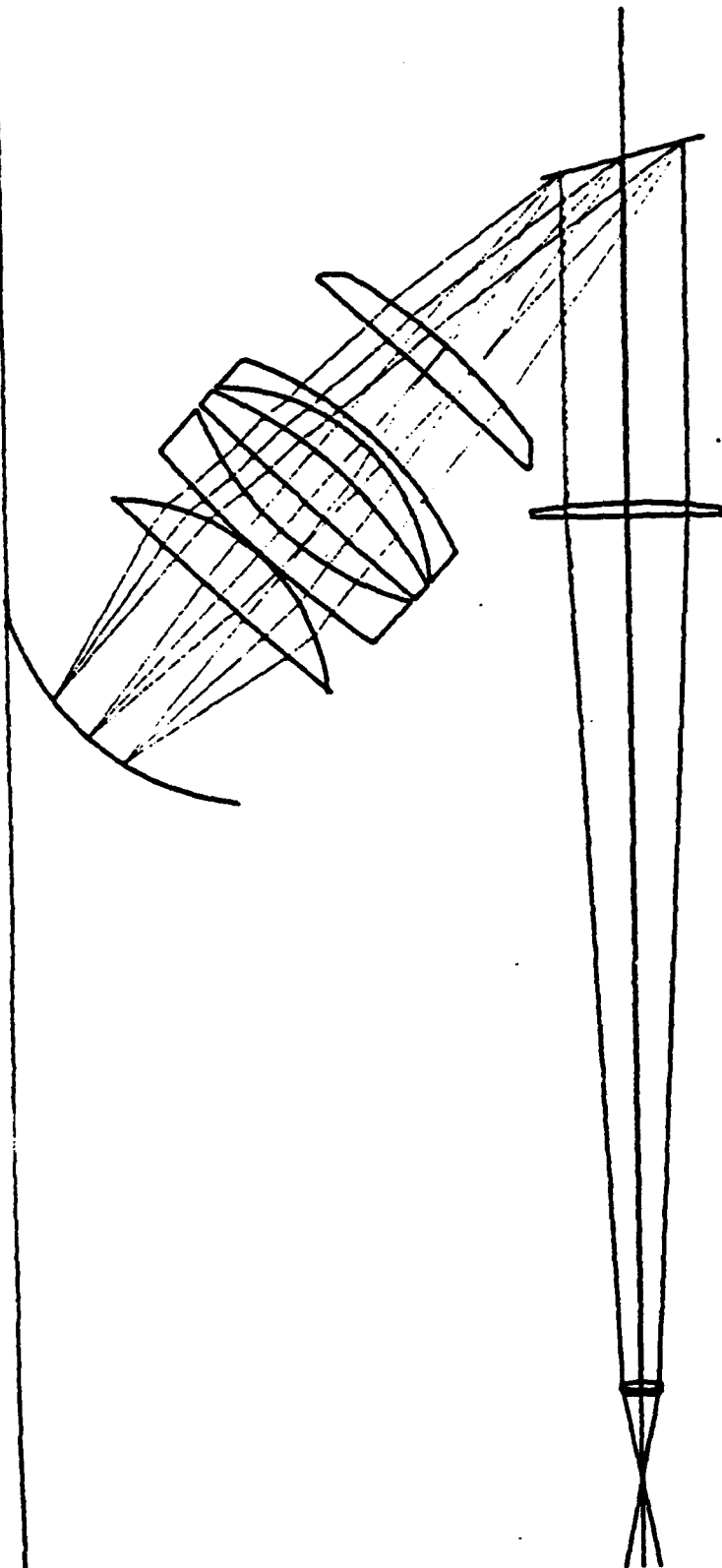
LENS Y-Z PROFILE  
SCALE FACTOR 0.250 X  
ID WAVELENGTH DIVISION DEMULTIPLEXER 160

26-MAY-87 11:22:56



ID WAVELENGTH DIVISION DEMULTIPLEXER 417

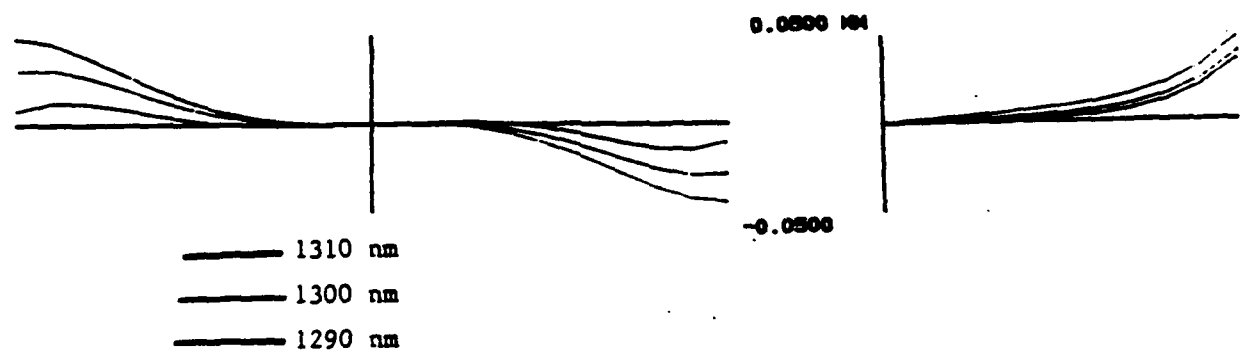
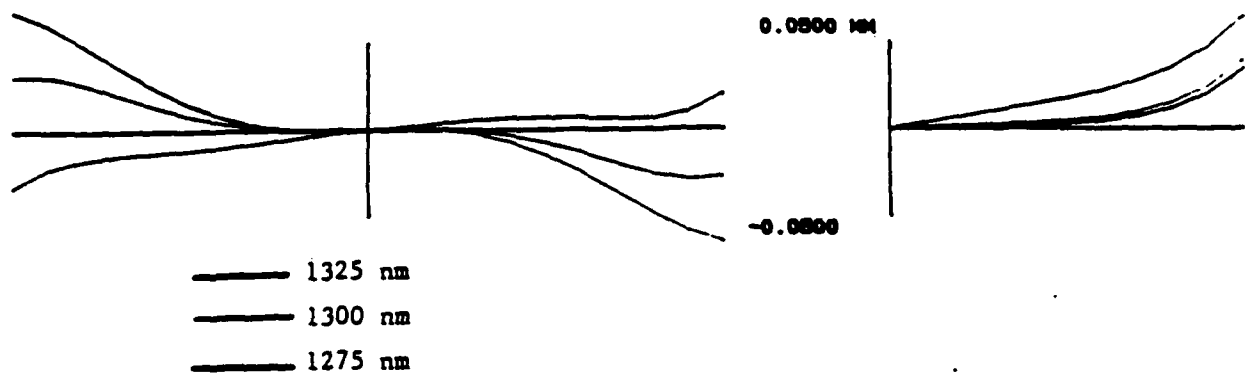
13-JUL-87 11:28:38



LENS Y-Z PROFILE  
 SCALE FACTOR 0.300 X  
 ID 7TH: 13TH OPTIM WDM

409

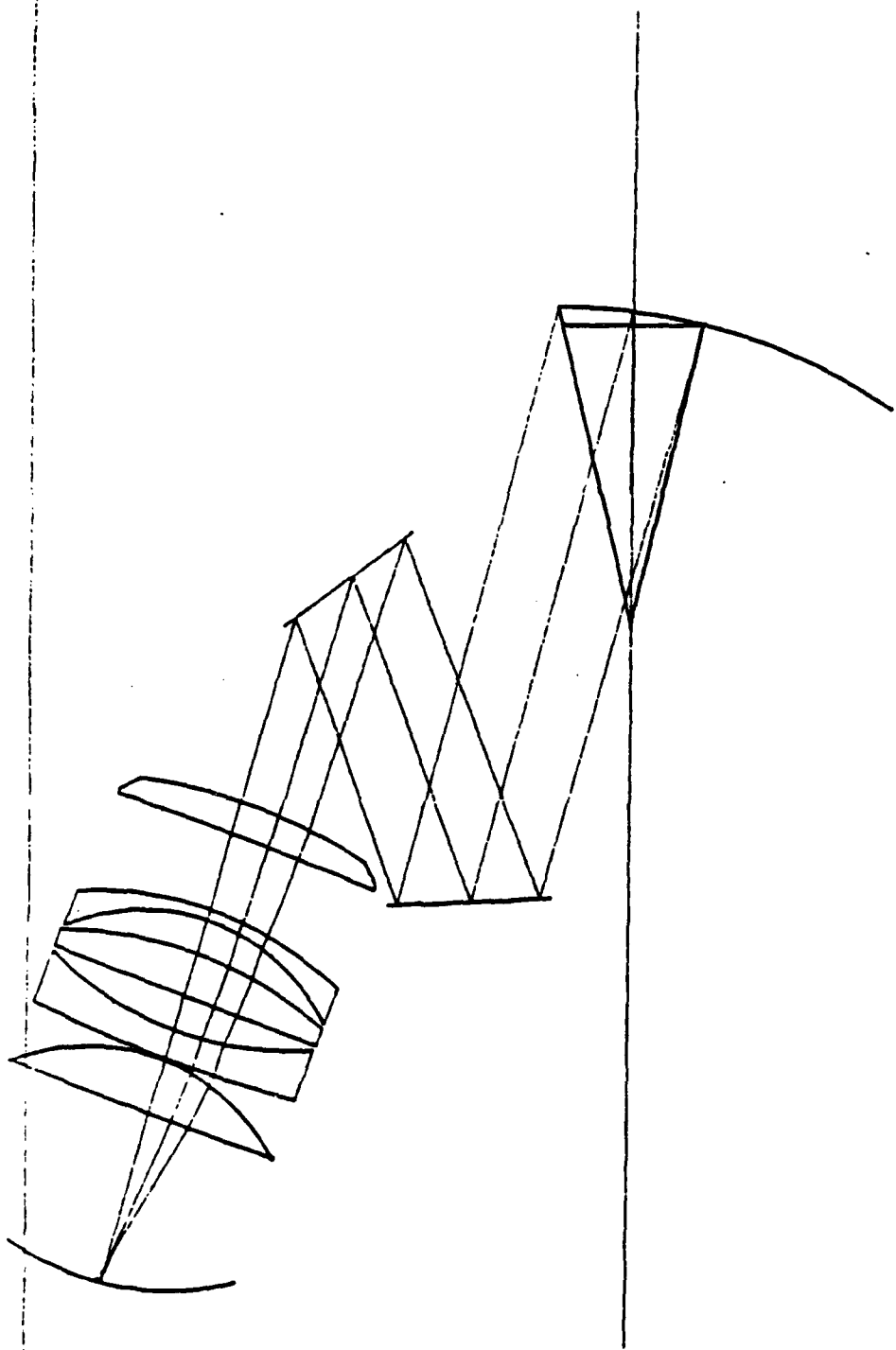
9-JUL-87 08:28:52



ID 7TH: 13TH OPTIM WDM

417

13-JUL-87 11:58:58



LENS Y-Z PROFILE  
SCALE FACTOR 0.300 X  
ID 7TH: 13TH OPTIM WDM

409

9-JUL-87 08:18:04

# CURRENT EFFORT

## Insertion Loss, Crosstalk, and Laser Drift Studies on Breadboard WDM

### Definitions:

LIA : Lock-in-Amplifier

LPS : Laser Power Supply

LD : Laser Diode

LC : Light Chopper

DC : Diffraction Grating

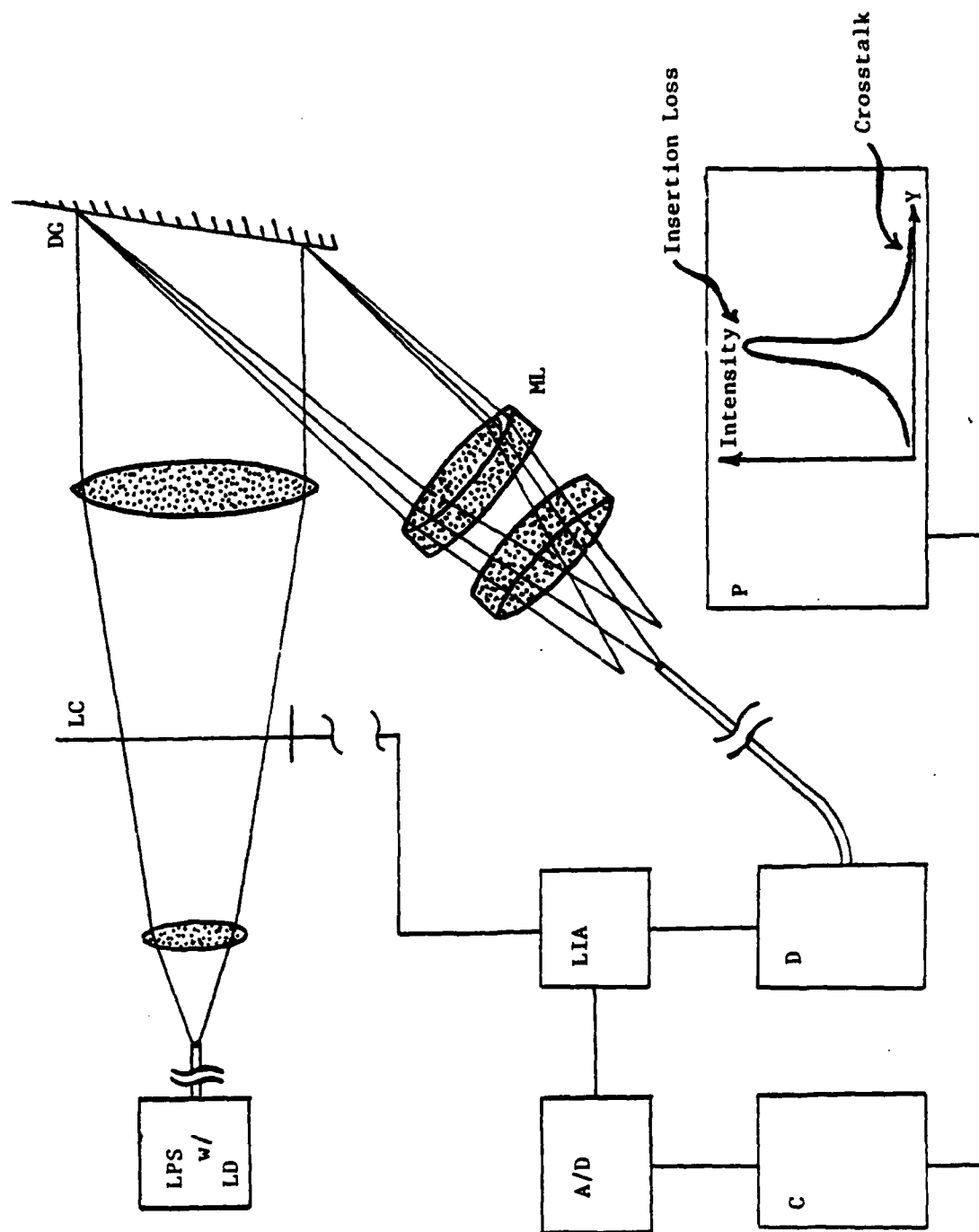
ML : Multi-element Lens

A/D : A/D Converter

C : Computer

D : Detector

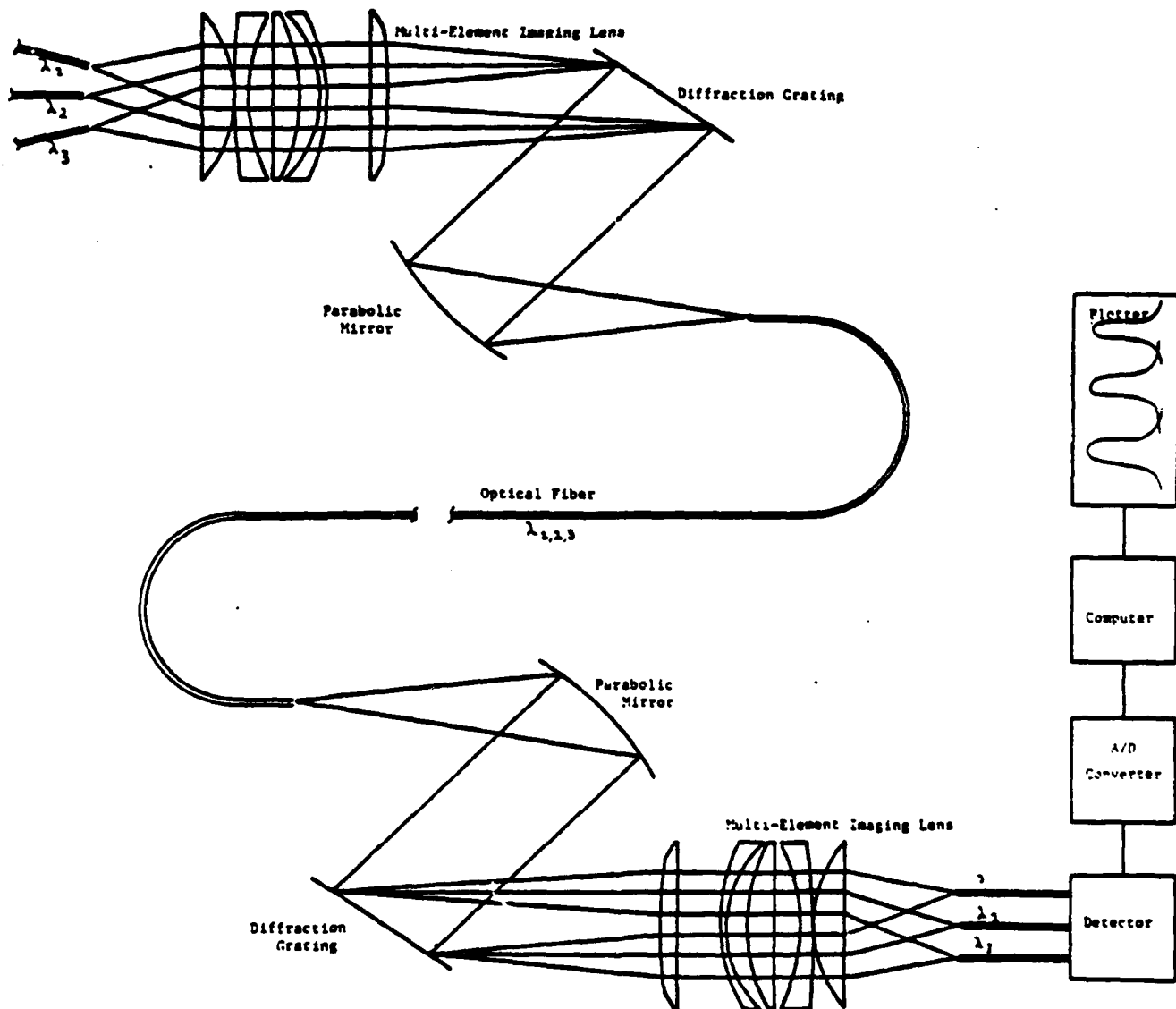
P : Plotter



PROPOSED EFFORT

Massively Multiplexed WDM Fiber Optic Communication System (MM-WDM-FOCS)

Center for Applied Optics (CAO)  
University of Alabama in Huntsville

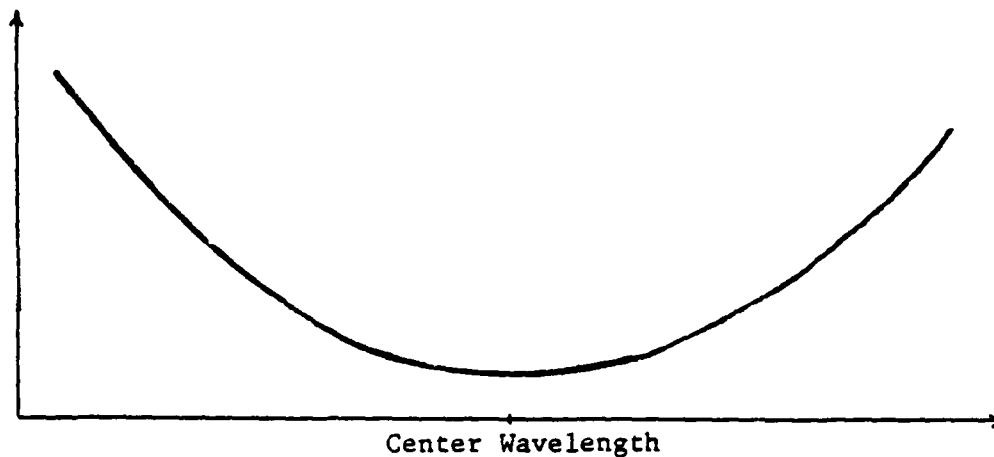


# PROBLEM 1

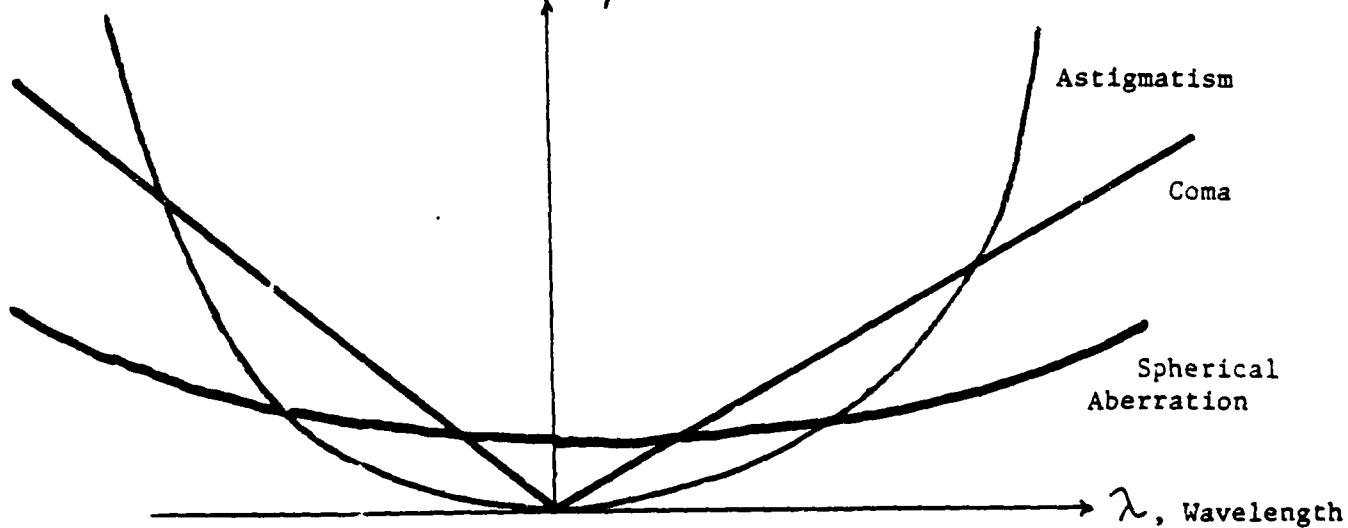
## Lens Aberrations

### Effect of Aberrations on Insertion Loss

Insertion  
Loss, dB



Aberration,  $\mu\text{m}$

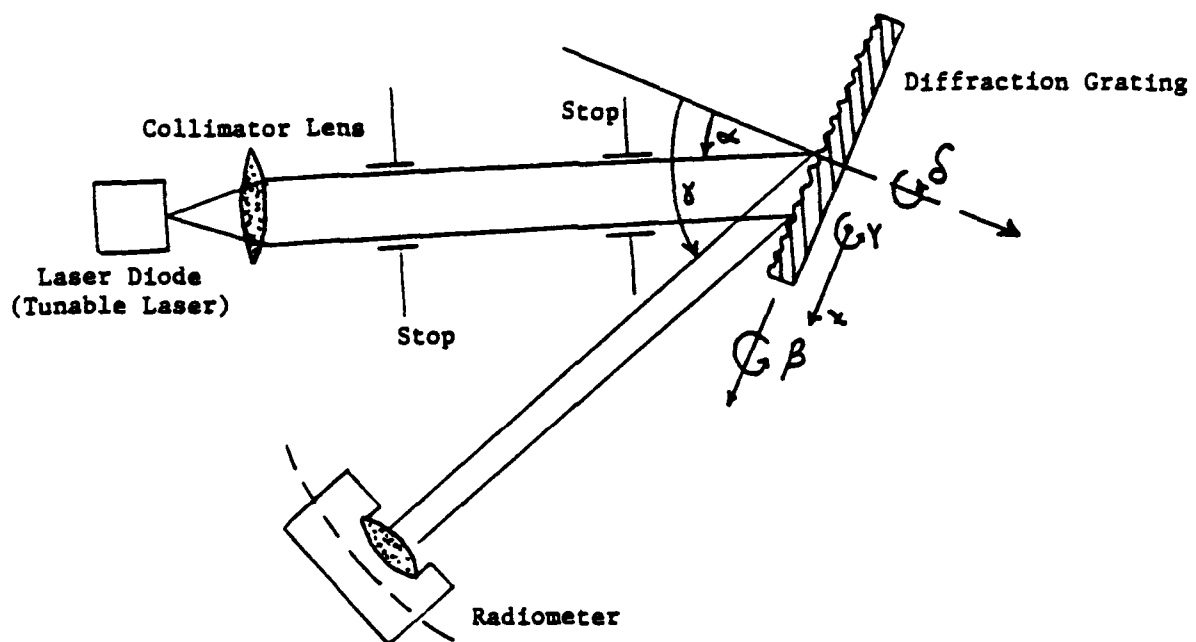


Aberrations limit Wavelength Range for a given Insertion Loss

## PROBLEM 2

### Scattering

Light Scattering and Efficiency Measurements of Multiplexer Gratings, Lenses, ect..., using the CAO BRDF Instrument

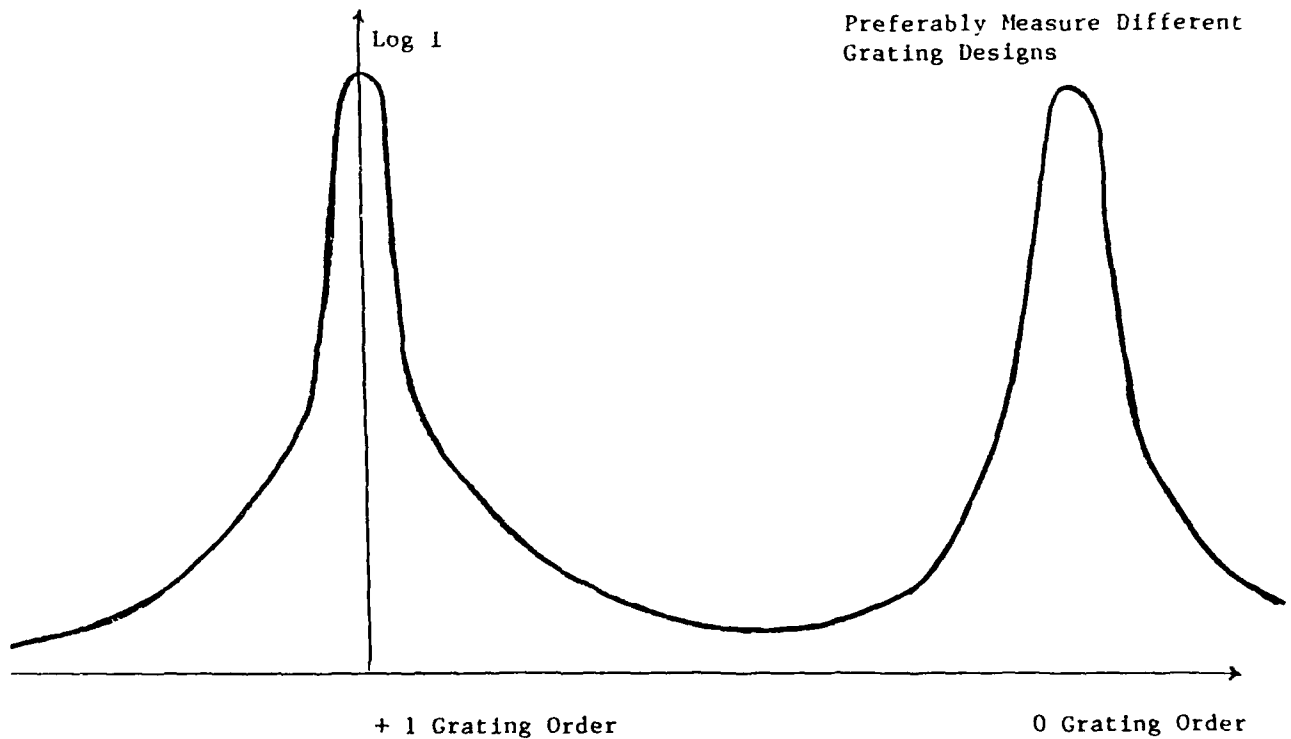


BRDF (Bidirectional Reflectance Distribution Function) describes  $I(\alpha, \gamma, \beta, \delta, \chi, \psi, \lambda)$

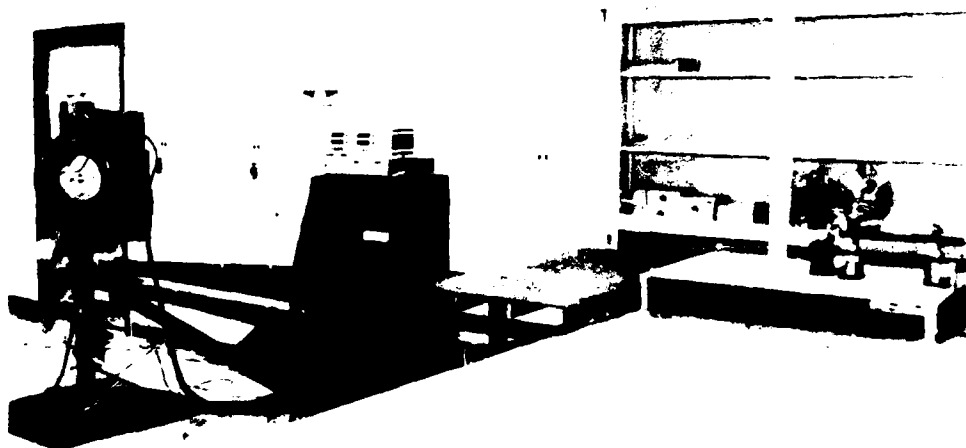
- $I$  : light intensity as a function of ----->
- $(\lambda)$  ----- wavelength
  - $(\alpha, \beta)$  ----- the 2 angles of incidence
  - $(\gamma, \delta)$  ----- the 2 angles of scattering
  - $(\chi, \psi)$  ----- the variations of scattering across the grating surface

Scattering: Principle Source Expected to be the Grating.

Scattering from Diffraction Grating in Isolation

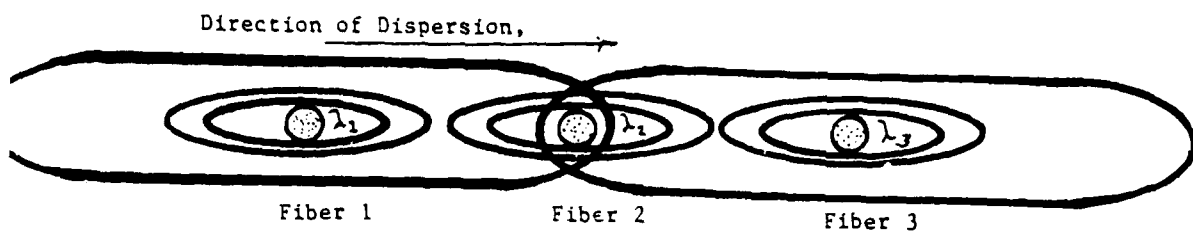


CAO BRDF INSTRUMENT

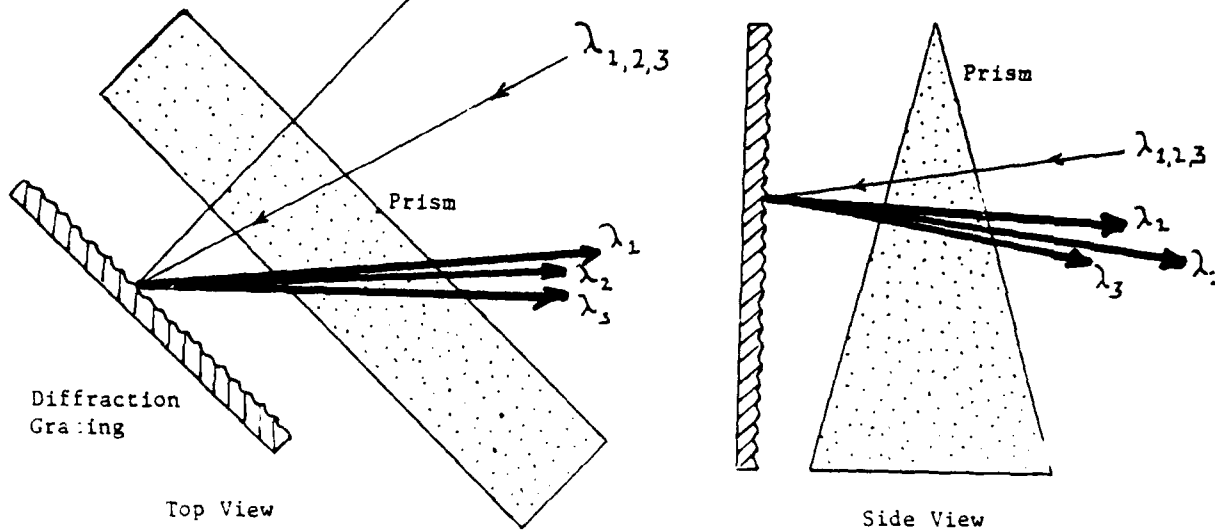


# IMPROVED CROSSTALK with a CROSS DISPERSING PRISM

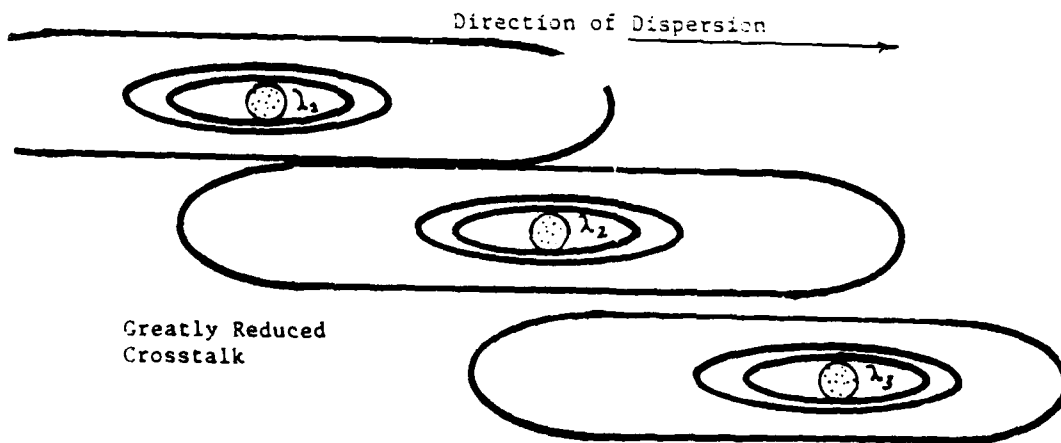
Grating Scatter Function in 2 Angles of Scatter:  $\gamma, \delta$



With CROSS DISPERSING PRISM:



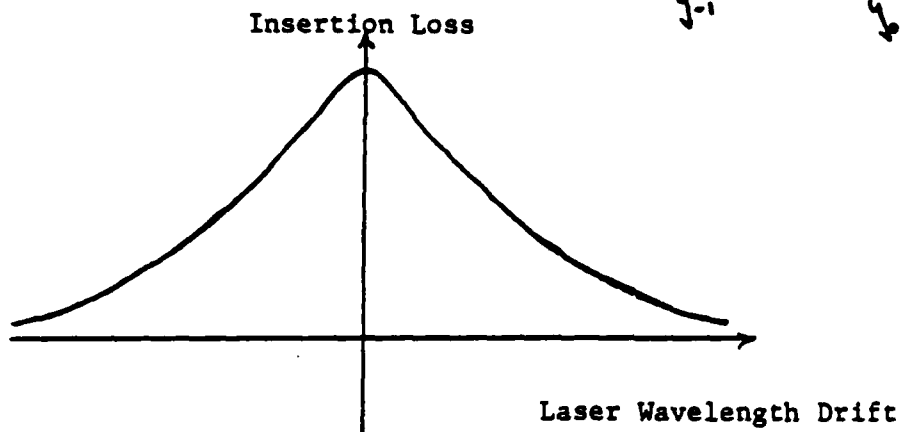
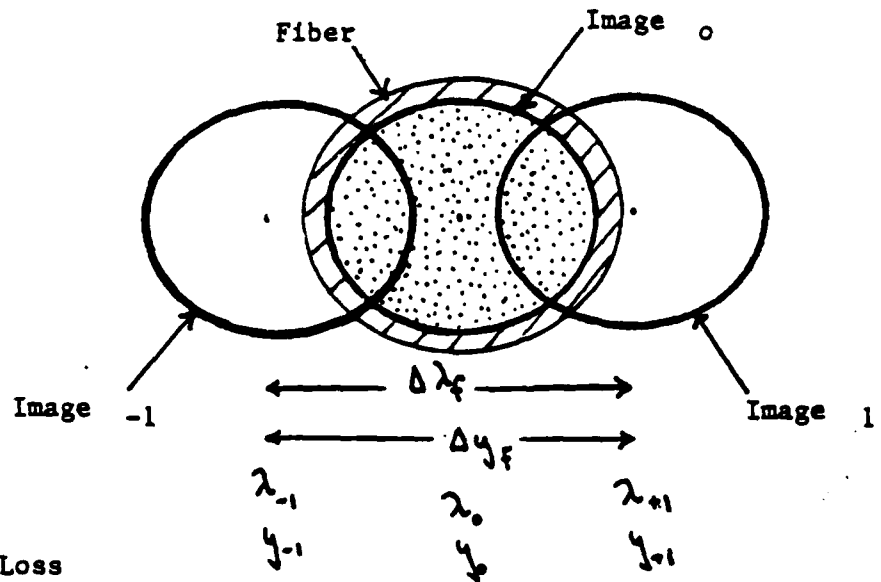
Shifted Scattered Light Distribution:



### PROBLEM 3

#### LASER DRIFT

$$\Delta y_f = \Delta \lambda_f \frac{dy}{d\lambda}$$



Specifications on:

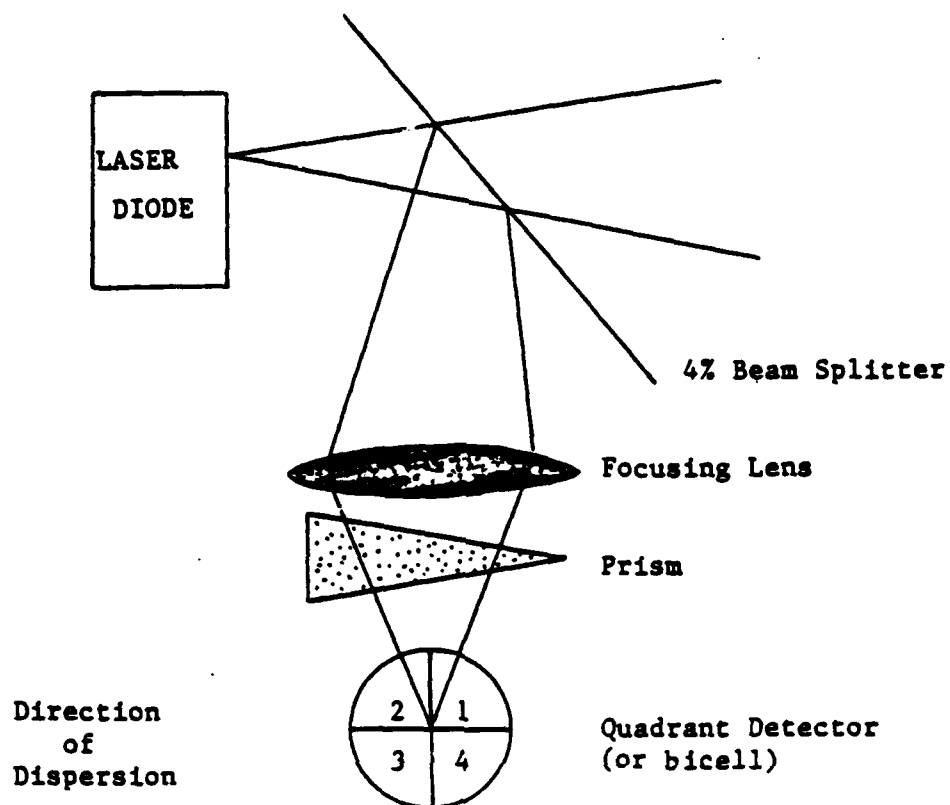
- i.) Insertion Loss
- ii.) Laser Drift

A.) Limited by (Fiber Diameter \* Linear Dispersion)

Thus Laser Drift Limits the Number of Channels

Low Laser Drift Essential

# WAVELENGTH STABILIZED DIODE LASER



$$V_1 + V_4 - V_2 - V_3 = V_y$$

$$V_y \propto \lambda$$

## SINGLE MODE vs. MULTIMODE WDM COMPARISONS

Between Systems with Equivalent Effective Focal Lengths (EFL)

	Multimode	Single Mode
Fiber:	60 $\mu\text{m}$	6 $\mu\text{m}$
Numerical Aperture:	.22	.35
F/Number:	F/2.50	F/1.43
Sensitivity to Laser Drift:	1	10
Lens Image Quality: (Spot Size)	1	.1
Mechanical Tolerances:	10 $\mu\text{m}$	1 $\mu\text{m}$

Single Mode Multiplexer is ~20 times more difficult.

PRESENT EFFORT: (FY87)

- i.) Explore System Tradeoffs for the MM-WDM
- ii.) Assemble a 30 Channel Breadboard System
  - A.) Use Off-the-Shelf Items
  - B.) Measure Insertion Loss, Crosstalk, and Laser Drift
- iii.) Design High Capacity System: 60 Channel
  - A.) Design a Multi-Element Multiplexer Lens
  - B.) Estimate WDM Performance using Data from Breadboard Studies

PROPOSED EFFORT: (FY88)

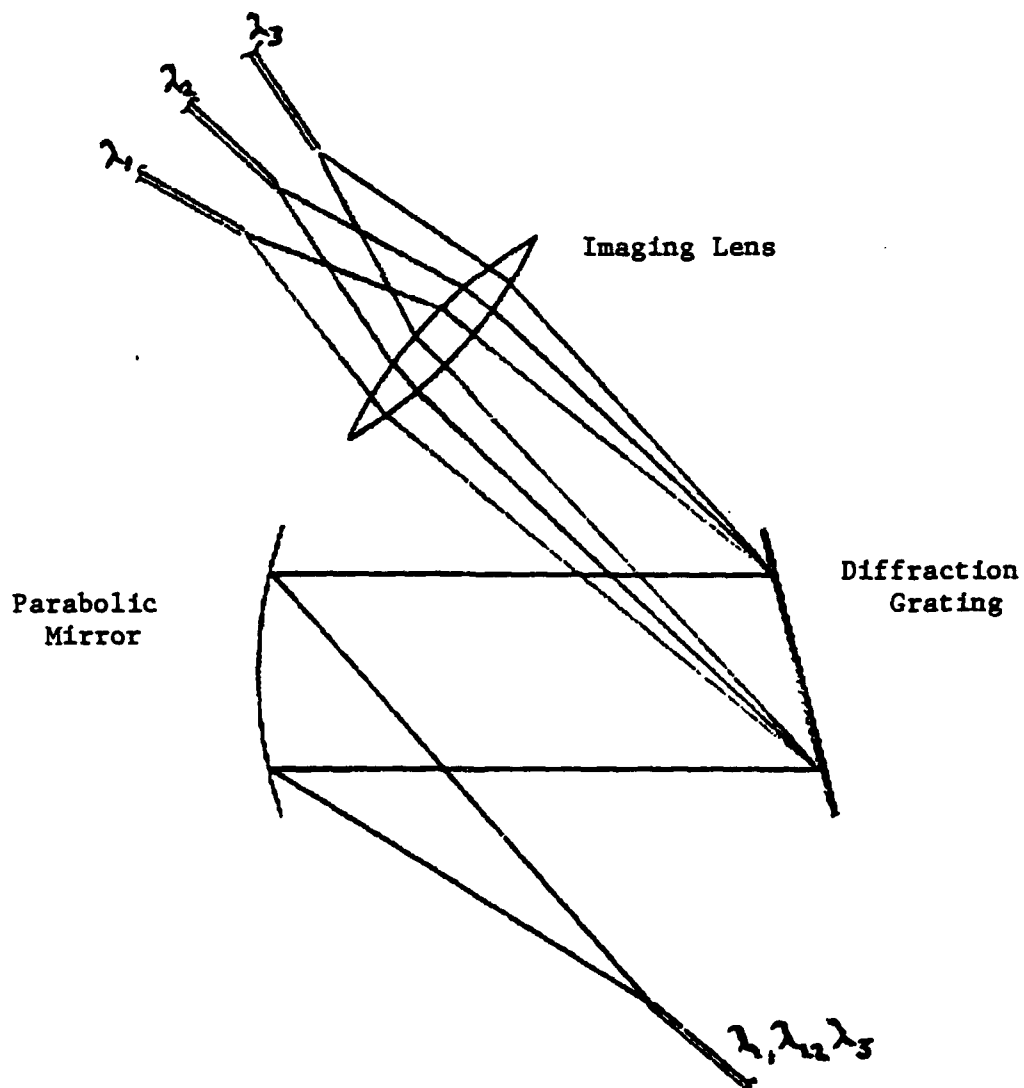
- i.) Continue Design of MM-WDM Optical Systems, 60 - 200 Channels
  - A.) Continue Lens Design
  - B.) Diffraction Grating Optimization Study
- ii.) Demonstration of MM-WDM System
- iii.) Light Scattering Studies of Gratings, ect...
- iv.) Establish Reasonable Performance Standards for a Commercial MM-WDM
- v.) Startup RADC WDM Test Laboratory

## OVERALL ASSESSMENT

I.) A Roadmap for a RADC/UAH Program to Assemble and Test  
100 - Channel WDM Systems

II.) Probability of Success is Extremely High

A.) If aim for 100 Channels and achieve 70 --- Super!



QUESTIONS:

- i.) What Insertion Loss and Crosstalk Do Air Force Applications Require?
- ii.) How Important are Volume and Unit Cost?
- iii.) What Applications use Single vs. Multi-Mode Fibers?
- iv.) What Range of Laser Wavelengths are most Important?
- v.) What Benefits Accrue from Hundreds vs. Dozens of Channels?

Appendix C: Dispersive Elements

## Contents

<b>1</b>	<b>Introduction</b>	<b>81</b>
<b>2</b>	<b>Dispersive Elements</b>	
2.1	Diffraction Gratings . . . . .	81
2.2	Planar Reflection Grating . . . . .	82
2.3	Concave Diffraction Grating . . . . .	84
2.3.1	Aberration Corrected Concave Grating . . . . .	87
<b>3</b>	<b>Echelle Grating</b>	<b>88</b>
<b>4</b>	<b>Grating Characterization</b>	<b>92</b>
4.1	Grating Resolution . . . . .	92
4.2	Spectral Purity . . . . .	93
4.2.1	Diffraction Effects . . . . .	94
4.2.2	Grating Defects . . . . .	95
4.3	Grating Efficiency . . . . .	96
4.3.1	Blazing Factors . . . . .	96
4.3.2	Polarization Considerations . . . . .	98
<b>5</b>	<b>System Resolution</b>	<b>98</b>

## List of Figures

1	<u>The Grating Profile</u> . . . . .	83
2	<u>Concave Grating Profile</u> . . . . .	84
3	<u>A Concave Grating with a Rowland Circle</u> . . . . .	85
4	<u>Parameters for the Calculation of the Aberration Correction of a Holographic Grating</u> . . . . .	87
5	<u>Free Spectral Range</u> . . . . .	88
6	<u>An Echelle Spectrogram with Overlapping Orders</u> . . . . .	90
7	<u>Grating Resolution of Different Wavelengths</u> . . . . .	93
8	<u>Forms of Spectral Impurity</u> . . . . .	94
9	<u>The Function <math>I(u)</math></u> . . . . .	96
10	<u>Blazing of a Diffraction Grating</u> . . . . .	97

## 1 Introduction

An a priori approach to the design of an optical fiber wavelength division demulti/multi-plexer ( WDM ) compares the performance of the WDM to that of a spectrometer - a similarity is immediately noticed. A spectrometer's function consists of the separation of the wavelengths of a broad-band spectrum in order to analyse a particular wavelength via an exit slit. In terms of a fiber-optic WDM, the broad-band spectrum is contained in a single optical fiber, the wavelengths are separated via some wavelength dependent dispersive device, and individual fibers replace the function of the exit slit.

The design approach to the fiber-optic WDM will be from the standpoint of the physical principles that are embodied by spectrometers: differential refraction, diffraction, or interference. The ideal spectrometer, in general, consists of:

1. An entrance aperture
2. A collimating element
3. A dispersing element
4. A focusing element
5. An exit aperture

For the case of the fiber-optic WDM, the entrance and exit apertures would be optical fibers.

## 2 Dispersive Elements

Dispersive spectral systems use prisms or gratings in order to form the frequency spectrum of polychromatic light onto an image plane. Published results of optical performances of devices which incorporate prisms have indicated that insertion losses and crosstalk levels are strong functions of the collimating optics' aberrations, and the dimensions and locations of the optical fibers on the object and image planes. The linear displacement of the refocused beam will be dependent upon prism width, wavelength separation, material dispersion, and collimating optics' characteristics. Prisms have low dispersion and highly non-linear angle functions based on the index of refraction of the glass (proportional to  $\lambda^{-3}$ ). In contrast, gratings have high resolution and linear dispersion, and are generally between 70% and 99% more effective than prisms.

### 2.1 Diffraction Gratings

Fermat's principle, which states that the light traveled between two points along an optical path is an extremum, implies that optical configurations with the highest symmetry will also be those

with the best imaging properties because the the number of equivalent optical paths between object and image will be maximized. This suggests that the design of a low-aberration optical system should begin with rotational symmetry about a common axis joining the principal source point to its conjugate image. It is clear that the condition of rotational symmetry cannot be achieved with a plane grating under any circumstances. While rotational symmetry can be achieved for spherical, elliptical, or toroidal gratings due to the fact that they can be tuned by varying the angle of incidence; aberrations (including resolution or wavelength errors as well as geometrical focusing errors) can reach their theoretical minimum values at only a single wavelength.

It is known that a traveling wave encountering an obstruction with dimensions similar to its wavelength has its energy scattered; in fact, a periodic variation of any parameter which affects the propagation of the wave scatters the energy into various discrete directions or "diffracted orders." Such a structure is referred to as a diffraction grating.

From the point of view of a wave in a diffracted order, the effect of the grating is to change the direction of propagation, and the amount by which it does so depends upon the relationship between the wavelength and the period. Thus the function of a diffraction grating is to provide appropriate modification to the incident wavefront in order to generate new wavefronts in a series of well defined directions. In this way a grating may disperse a variety of wavelengths to form a frequency spectrum. There are three types of diffraction gratings that can be considered for a spectral system - the concave grating, the holographic optical element (HOE), and the plane grating.

## 2.2 Planar Reflection Grating

A planar reflection grating consists of a suitable rigid substrate with an optical surface upon which are produced a series of equispaced parallel grooves. Such a grating would be optimum for use in a spectral system that is to be used over a relatively large range of wavelengths. Rotational symmetry is lost. The aberration over a large wavelength range could be minimized.

The diffraction efficiency - defined as the magnitude of a wave in a particular order - is groove-shape dependent. Grating technology has advanced so that 80% to 90% of the incident light power is routinely diffracted into the first order. This means that no more than 1.0 dB insertion loss will be directly attributable to the diffraction grating.

The condition that a diffracted order should exist is that the optical path difference from the source to the focused image via successive grating grooves should be equal to a whole number of wavelengths, i.e. the OPD should be out of phase by an integral number of  $2\pi$  radians. Thus, the formation of the frequency spectrum and the formation of the diffracted orders are both described by the Equation (1) and Figure 1 below:

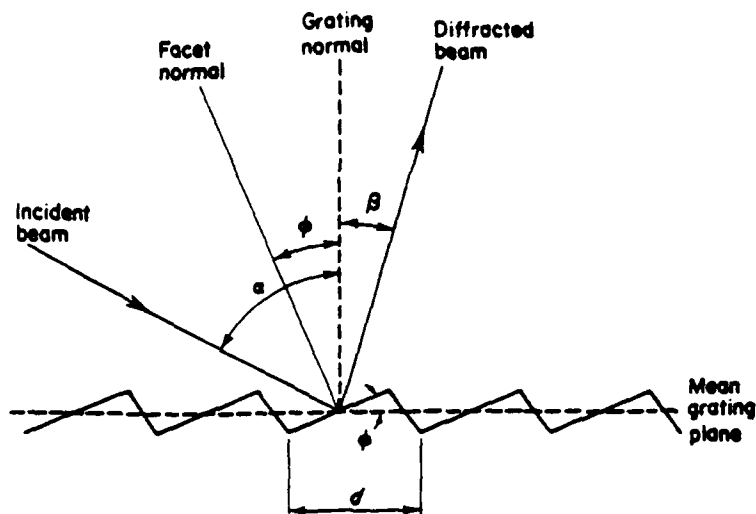


Figure 1. The Grating Profile

$$\sin\alpha + \sin\beta = \frac{(m \lambda)}{d} \quad (1)$$

where  $m$  = negative integer order number, since we are considering an order on the opposite side of the normal with respect to the zeroth order; and the variable  $d$  = distance between successive grooves.

Evident from Equation (1), the formation of a diffracted order is wavelength dependent. The formation of the frequency spectrum is dependent upon the angular dispersion which is the variation of the diffraction angle with the change in wavelength. Thus the angular dispersion of a grating is:

$$\frac{\delta\beta}{\delta\lambda} = \frac{m}{(d \cos\beta)} \quad (2)$$

When the angle of incidence is fixed, i.e.  $\delta\alpha/\delta\beta = 0$ .

The linear dispersion, the distance in the plane of the focused spectrum which corresponds to a change in wavelength, of the spectral system is:

$$\frac{\delta x}{\delta\lambda} = f * \frac{\delta\beta}{\delta\lambda} \quad (3)$$

where  $f$  = focal length of the imaging optics, with tilts or decentering with respect to the optical axis assumed to be zero. If the focal plane is not normal to the diffracted beam but inclined at an angle  $\phi$ , then the linear dispersion must be multiplied by an "obliquity factor",  $F = 1/(\cos\Theta)$ .

$$\frac{\delta x}{\delta\lambda} = F * f \left( \frac{\delta\beta}{\delta\lambda} \right) \quad (4)$$

The obliquity angle,  $\Theta$ , is commonly zero for in plane systems, giving the linear dispersion as defined in Equation (3).

### 2.3 Concave Diffraction Gratings

A concave grating can eliminate the need for auxillary optics since the grating itself, by its very design, provides collimation, diffraction, and focusing. Scalar theory for a concave grating, refer to Figure 2, considers a grating lying along the arc of a circle PCQ with the center of curvature O, ruled with equidistant lines with separation  $d$  in the direction of the tangent at C.

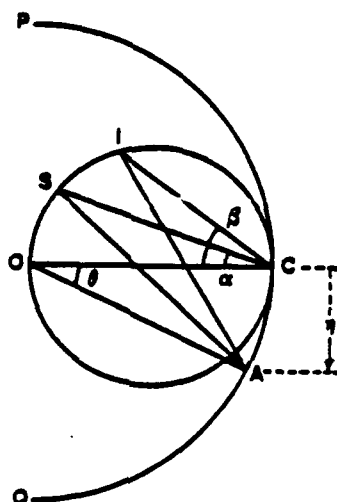


Figure 2. The Grating Profile

The angles  $\alpha$  and  $\beta$  are related by the grating equation:

$$(\sin\alpha + \sin\beta) = \frac{m\lambda}{(n d)} \quad (5)$$

With the linear dispersion given by:

$$\frac{\delta\beta}{\delta\lambda} = \frac{R \cos\beta}{r} \left( \frac{\delta\beta}{\delta\lambda} \right) \quad (6)$$

Thus for the case of a classically ruled concave grating, the spectrum falls upon the Rowland circle as shown in Figure 3 below. For optimum insertion of the dispersed spectrum into their

respective optical fibers, the fibers need to be positioned on the Rowland circle.

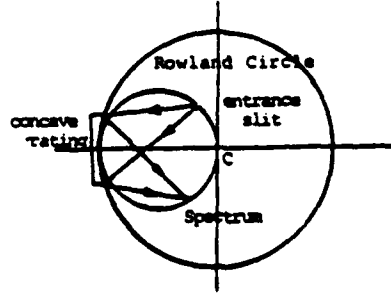


Figure 3. A Concave Grating with a Rowland Circle

Thus the grating lines are not equidistant when measured around the circular arc, and the actual line spacings will be smaller than those of a planar grating by a factor of  $\cos\theta$ . This introduces an aberrant term in the optical path equal to:

$$\frac{m \lambda R \left(\frac{\eta}{R}\right)^3}{6 d} = (SA + AI) \quad (7)$$

where  $R$  = the distance  $OC$  and  $\eta$  is the displacement of  $A$  perpendicular to  $OC$ . A small displacement of the grating away from the circular arc, i.e. the addition of an aspheric term, can be used to alter the optical path and eliminate the aberrant term in Equation (7).

A second optical aberration arises from the lack of collimation in the direction perpendicular to the plane of incidence. As a result, radiation will be incident on the grating over a range of angles with respect to the horizontal given by the numerical aperture of the object (in our case the object would be the transmitting fiber). Since radiation incident at an angle  $\theta$  to the horizontal plane will be diffracted at the angle in that plane characteristic of a wavelength  $\lambda/\cos\theta$ , this will result in a broadening of the diffraction maxima.

The optical path for a cylindrical grating with large apertures contains an aberrant term analogous to spherical aberration, given by:

$$\eta \left(\frac{n}{8}\right) + \left(\frac{\eta}{r}\right)^3 + \left[ \frac{\sin^2 \alpha}{\cos \alpha} + \frac{\sin^2 \beta}{\cos \beta} \right] \quad (8)$$

But this term may be neglected for typical values of  $\eta$ ,  $R$ ,  $\alpha$ , and  $\beta$ .

It must be noted that the image quality deteriorates if the receiver fibers do not lie exactly on the Rowland circle. And the width of the grating must be sufficient to intercept all the radiation emitted by the transmitter fiber, i.e. overfilling the grating will cause irretrievable radiation loss. Thus  $\eta_{max}$  is on the order of  $r(NA)/n$ .

• The major optical aberrations in the ideal case of a perfect concave grating are:

1. The non-ideal line spacing when a standard grating used gives rise to an aberrant optical path,  $\Delta(n)$  proportional to  $(\frac{\eta}{R})^3$ . When radiation is incident on a portion of the grating characterized by some value of  $\eta$ , the diffracted image at the Rowland circle is shifted from the ideal by a distance:

$$\Delta(x) \approx R\beta \left(\frac{\eta}{r}\right)^2 \text{ for small } \alpha, \beta, \text{ and } \left(\frac{\eta}{R}\right). \quad (9)$$

To correct for this aberration, every point on the grating surface would need to be displaced a distance parallel to OC.

2. The lack of vertical collimation results in a vertical angular spread of the beam. This leads to a maximum apparent wavelength change for horizontal diffraction, and hence to an image shift.
3. The aberrant optical path due to the grating's shape can be ignored if it is no larger than  $.25\lambda$ , since the imaging properties of an optical system do not depart significantly from the ideal while the wavefront aberration is less than  $\lambda/4$ .
4. The primary diffraction maxima for a point source using a concave grating will incur broadening effects dependent upon the grating's dimensions.
5. Even with the fibers on the Rowland circle, spherical aberration, astigmatism, and 6<sup>th</sup> order coma still exist.

The grooves of the concave grating are parallel and the grating, if ruled on a ruling engine, may have been produced with up to seven zones to optimize blaze angles over the whole surface of the grating. Rarely are these zones phase matched, with the result that the maximum possible resolution is reduced by a factor equivalent to the number of non-phased zones present.

The use of a concave grating in a small-sized spectral system requires short focal lengths. Such gratings are difficult to rule accurately and exhibit low diffraction efficiencies due to rapidly changing blaze angles across the curved surfaces. Published performance data for this type of grating incorporated into a mux-demux system indicated unsatisfactory performance in terms of efficiency and insertion loss.

### 2.3.1 Aberration Corrected Concave Grating

In order to reduce the problems of non-phased matched zones, induced aberrations, and other problems briefly mentioned in Section 2.3, it is possible to produce gratings "holographically." This technique requires two intersecting beams from a single longitudinal mode laser to produce interference fringes in a photosensitive material that has been deposited on an optically flat substrate — typically glass. Holographic techniques can modify the grooves' distribution in such a way that the locus of the spectrum can be relocated, resulting in the reduction or elimination of aberrations.

To accomplish these aberration corrections, it is necessary to rule grooves that, instead of being parallel, are a series of grooves located at the intersection of families of revolution hyperboloids with a spherical blank. The production of an aberration corrected grating utilizing the Rowland circle geometry yields a grating configuration that has astigmatism eliminated at one wavelength.

Under the circumstances defined in Figure 4, the aberrant optical path would be defined by the following expression:

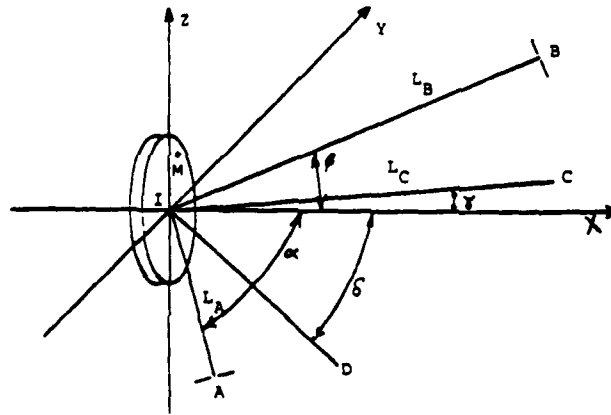


Figure 4. Parameters for the Calculation of the Aberration Correction of a Holographic Grating

$$\Delta(M) = MA + MB - \frac{K \lambda}{\lambda_0} * (MC - MD) - \left( IA + IB - \frac{K \lambda}{\lambda_0} * (IC - ID) \right) \quad (10)$$

$\Delta(M)$  can be expressed as a function of  $Y, Z, L_A, L_B, L_C, L_D, \beta, \gamma$ , and  $\delta$ . Total or partial correction of the aberrations without changing the working parameters could be obtained by properly choosing the values of  $L_C, L_D, \beta, \gamma$ , and  $\delta$ . In this way the  $Z^2/2$  term (astigmatism) can be reduced or even eliminated. If the height of the tangential focus is near zero at the center of the spectral range, astigmatism over the whole spectral range can be reduced overall by up to a factor of 10.

An HOE can be used as a diffraction component and encoded to eliminate auxiliary collimating and focusing optics in order to yield concave gratings with  $f$ /numbers as fast as  $f/2.0$ . The grooves of such a grating are curved and non-uniformly spaced in such a way that astigmatism is virtually eliminated and optical throughput is significantly increased. However, excellent diffraction efficiency and aberration correction is exhibited by an HOE only over pre-selected narrow, limited wavelength ranges, and materials are not readily available for the 1100 nm to 1600nm wavelength range. Published results of multichannel HOE multiplexers-demultiplexers (mux-demux) have indicated unsatisfactory performance in terms of efficiency and insertion loss.

### 3 Echelle Gratings

Echelles are coarse but precisely ruled diffraction gratings (usually 300 grooves or less per mm) which are used at high angles of incidence (over  $45^\circ$ ) and in high diffraction orders — typically 10 to 1000. Such high angles demand a degree of precision almost an order of magnitude greater than for ordinary gratings.

The concept of an echelle grating was first proposed as a highly useful intermediate step between an echelon and an ordinary grating, with the object of obtaining very high dispersion and resolution in small spaces. In principle, it is close to a Michelson reflection echelon, a device not likely ever to be made to the accuracies required. Echelles, however, have the virtue of much greater free spectral range. Free spectral range,  $\Delta\lambda$ , is defined as the distance between neighbouring peaks on the wavelength scale; see Figure 5 below.

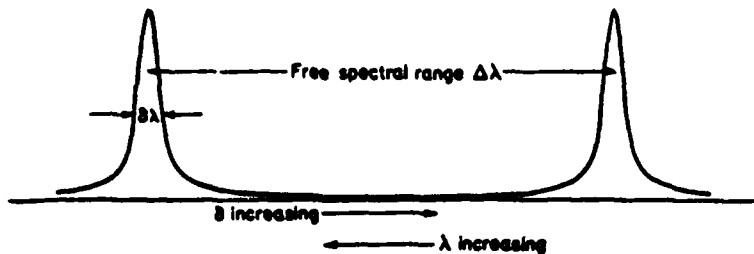


Figure 5. Free Spectral Range

Echelle resolution levels of 500,000 to 2,000,000 are exceeded only by Fabry-Perot etalons with long spacers, whose extremely short free spectral range and highly variable dispersions are basic handicaps. In addition, like most gratings, echelles operate in reflection and therefore do not have wavelength limitations imposed by transparency requirements.

The advantage of echelle spectroscopy vs. "ordinary" gratings is the angular resolution and dispersion of diffraction gratings. Theoretical grating resolution  $R$  is defined in Section 4.1 as:

$$R = mN \quad (11)$$

or

$$R = \left( \frac{2W}{\lambda} \right) * \sin\beta \quad (12)$$

Both are correct and equivalent to each other; the second is rewritten for the autocollimating (Littrow) mode of operation. Equation (11) states that grating resolution, for a given order  $m$ , increases with the number of lines,  $N$ , ruled on the grating. Equation (12) states that for a grating of width  $W$  and at a given wavelength  $\lambda$ , resolution is purely a function of the sine of the diffraction angle  $\beta$ . Many echelles operate at  $60^\circ - 80^\circ$ , compared to a typical  $5^\circ - 15^\circ$  angle for Littrow mounts, so their resolution tends to be about 3 times greater; other parameters, except  $m$ , being equal.

Defined in Equation (2), the angular dispersion of a grating used in the autocollimating mode is given by:

$$\frac{d\beta}{d\lambda} = \frac{m}{a \cos\beta} \quad (13)$$

or

$$\frac{d\beta}{d\lambda} = \frac{2}{\lambda} \tan\beta \quad (14)$$

Again, both equations are equivalent. From Equation (13), it is obvious that large dispersions can be obtained with small grating constants,  $d$ , or a large order,  $m$ . Equation (14) indicates that for a given wavelength  $\lambda$ , dispersion will be a function only of  $\tan\beta$ . For the typical angles previously mentioned the echelle dispersion is more than seven times as large as that of the conventional grating.

Changes in spacing and numbers of grooves have no effect on resolution and dispersion when a grating or echelle is used at a given angle. The increased resolution and dispersion, resulting from high angle illumination, are what makes echelles so useful for building luminous, compact, high resolution instruments. The advantage of echelles can be understood as having the coarse groove faces acting like a multiple reflection interferometer. The narrow angular range over which echelles are used results in their being effectively blazed (see Section 4.3.1) over a very large wavelength range. Each order has a short free spectral range, with the actual amount

depending on the groove spacing chosen, and the wavelength. With few exceptions, echelles are used with an auxiliary cross-dispersion device in the form of a prism, grating, or even a second echelle. The purpose is to separate overlapping orders with each line corresponding to one spectral order of wavelengths. Some of the throughput advantage is lost because of the resulting inevitable light loss. But in return, one obtains a neatly stacked spectrum and the possibility of recording virtually all wavelengths to which the detector is sensitive.

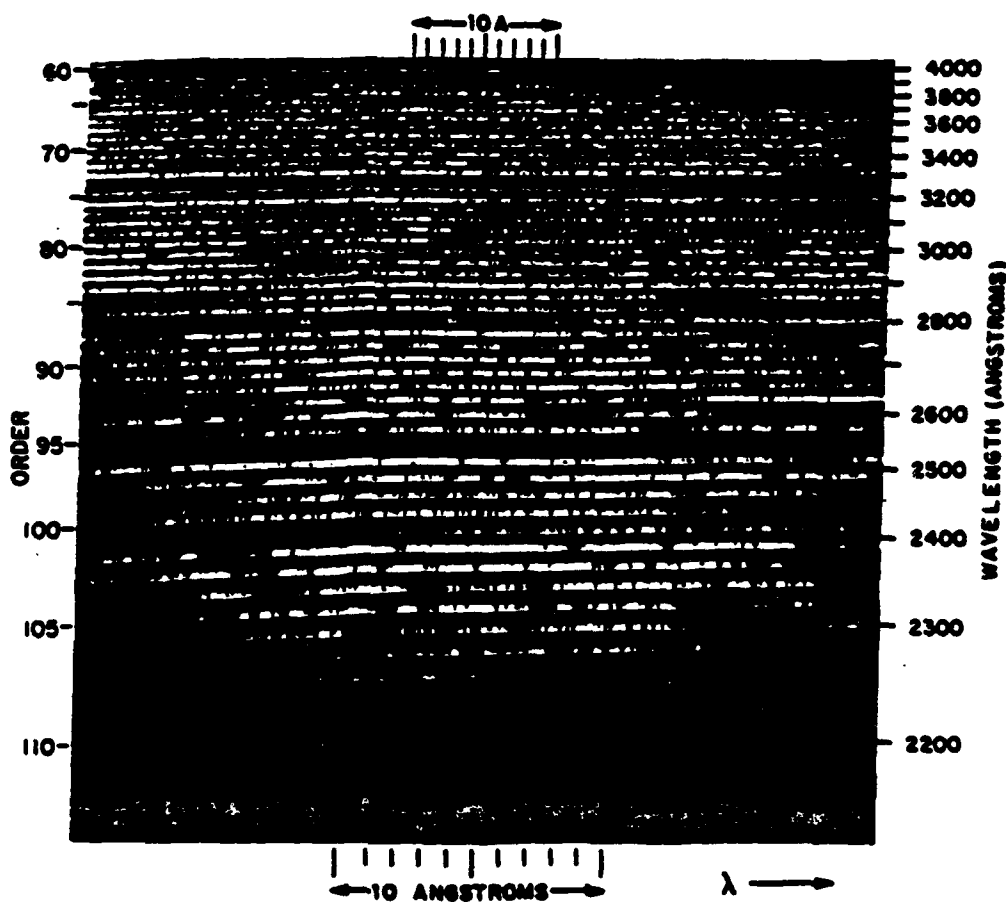


Figure 6. An Echelle Spectrogram with Overlapping Orders

Just as printed words are conveniently split up into subsequent lines, rather than printed

on one long tape, so a high dispersion spectrum is typically arranged in a series of 20 to 80 orders, each a few inches long and covering a short portion of the spectrum. Thus, an enormous amount of data can be concentrated into a convenient rectangle, for photographic or electronic detection (see Figure 6).

The ruling of echelle gratings is the ultimate challenge in a field notorious for its many difficulties. For a 10" echelle to achieve diffraction-limited performance, the location of all grooves must be uniform within  $\lambda/8$ , since it is used in reflection. Blaze efficiencies generally reach a maximum when the number of grooves per millimeter is in the 30 - 100 range. At 4000Å, this is equivalent to 1 part in 5,000,000. For a 16" echelle this requirement increases proportionately to 1 part in 8,000,000. Such precision is attainable only with an engine equipped with interferometric control, and using a stabilized single frequency laser as the light source. There is also a stringent need to control periodic errors. For the case of a single error period of amplitude  $\epsilon$ , the relative ghost intensity to that of the parent line is given by:

$$\frac{I_g}{I_p} = \left( \frac{\pi \epsilon \sin \theta}{\lambda} \right)^2 \quad (15)$$

where  $\theta$  is the angle of use, typically 63°. If the intensity is kept to 0.01%, then for  $\lambda = 5000\text{Å}$ , the maximum value of  $\epsilon$  is only about 16Å, or 0.005 fringes of the laser wavelength. These requirements demand superb ruling engine, a high grade laser interferometer and associated servo feedback control, together with state-of-the-art environmental control of temperature and vibration.

It has become customary to characterize echelle gratings by an  $r$ -number: the ratio of groove width to groove height. This controls the dispersion. Thus an  $r/2$  echelle is one whose grooves are blazed at 63° 26', the angle at which the tangent is 2, so the ratio of groove width to groove height is 2:1. Echelles are usually furnished with a width twice the groove length. In instances where maximum energy is important enough to waste collimator aperture, echelles with excess groove length are useful. An  $r/4$  echelle is blazed at 75° 56', and as a result will have twice the dispersion of an  $r/2$  echelle. At such a sharp angle it is not practical to linearize the dispersion equation, even for short ranges, as is common practice for ordinary gratings. Echelles have been ruled up to  $r/5$ , corresponding to a blaze angle of 78° 41' minute.

With echelles blazed at 76° ( $r/4$ ) or higher, the dispersion is so great that only a relatively narrow band of wavelengths will be diffracted near the blaze angle. Therefore, the free spectral range must also be made small, so that a shift to the next order will occur near the blaze angle. In practice this means  $r/4$  echelles should not be ruled much finer than 79 grooves/mm for wavelengths in visible range.

For a given wavelength region the choice of groove spacing determine the orders  $m$  in which the echelle will be used, and this in turn controls the free spectral range  $F_\lambda$ , since  $F_\lambda = \frac{\lambda}{m}$ . This makes selection of groove spacing an important design decision. Since echelles normally

are used in order 10 or greater, it is necessary to use very coarse ruling when measurements are to be made in the infrared region.

## 4 Grating Characterization

A grating can be described, in terms of Fourier analysis, as a Dirac comb multiplied by an aperture function and convoluted with a groove. The Dirac comb function, which describes the position of the grooves, determines where the diffracted orders lie. The aperture function determines the degree of perfection of the focus of the spectrum and hence the extent to which the theoretical maximum grating resolution is realized. The form of the groove determines the way in which light is distributed among the diffracted orders. These features determine the three practical aspects of a grating's performance (listed respectively):

1. Grating Resolution
2. Spectrum Purity
3. Grating Efficiency

### 4.1 Grating Resolution

An important concept in the optimum utilization of a spectral system incorporating a diffraction grating as a component is its resolution. Care must be taken to differentiate between grating resolution and the resolution of the system as a whole. The grating resolution, defined when focusing optics are not used, is limited by the overlap of the diffraction pattern at infinity. The grating resolution, defined as  $\lambda/\Delta\lambda$ , is equal to the ratio between the smallest change of wavelength that the grating can resolve and the wavelength at which it is operating. For the case of two wavelengths differing by  $\Delta\lambda$ , two images will, with the use of focusing optics, be formed at the focal plane of the system separated a distance given by Equation (3). The ideal image in the focal plane of a spectrometer has a  $\text{sinc}^2$  intensity function, and Rayleigh's criterion indicates that these images are resolved when the center of one image coincides with

the first zero of the other, see Figure 7 below.

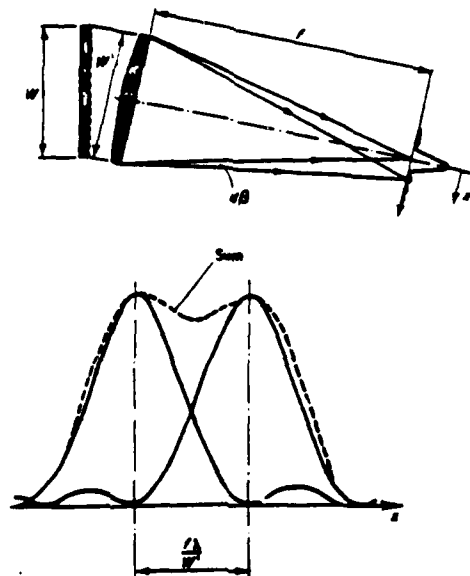


Figure 7. Grating Resolution of Different Wavelengths ( $W'$  is the grating width)

Also the grating resolution is:

$$\frac{\lambda}{\Delta\lambda} = \frac{W m}{d} \quad (16)$$

$$= \frac{W(\sin\alpha + \sin\beta)}{\lambda} \quad (17)$$

Equation (16) relates the grating resolution to the grating pitch, grating width, and order number. Thus a large grating is necessary for high-resolution work. Implied in the same equation is the possibility to achieve the same resolution with a coarse grating used in a higher order. Equation (17) expresses the grating resolution in terms of the angles of incidence and diffraction. Thus the grating resolution is the total number of wavelengths contained in the path difference between the light from the two edges of the grating, and is directly dependent on the amount of aberrations introduced by the grating into the incident wavefront.

#### 4.2 Spectral Purity

The purity of a spectrum, or the lack of stray light, is determined by two factors:

1. Diffraction effects

2. Grating defect.

#### 4.2.1 Diffraction Effects

For an ideal grating of infinite extent one would expect light to be diffracted only into the directions determined by the grating equation. However, even for a ideal grating, Fraunhofer diffraction gives rise to  $(N-2)$  secondary maxima of intensity between the main orders. Spectral impurity is best defined as any stray light observed between the main orders that is in excess of that accounted for by Fraunhofer diffraction. These "impurities" arise from various defects in the grating or the spectral instrument. Consider the components of grating defects only, in which the grating is illuminated by collimated light from a point source of monochromatic light, and then the dispersed light is focused to a series of points ( one per order ) in the image plane. Shown in Figure 8 are several distinct possible sources of stray light, along with their respective forms of unwanted scatter and aperture artifacts:

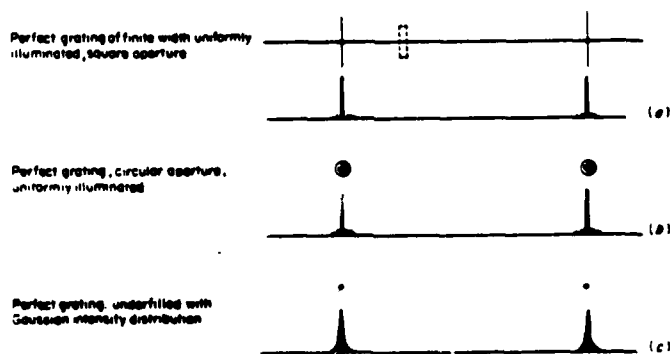


Figure 8a. Forms of Spectral Impurity

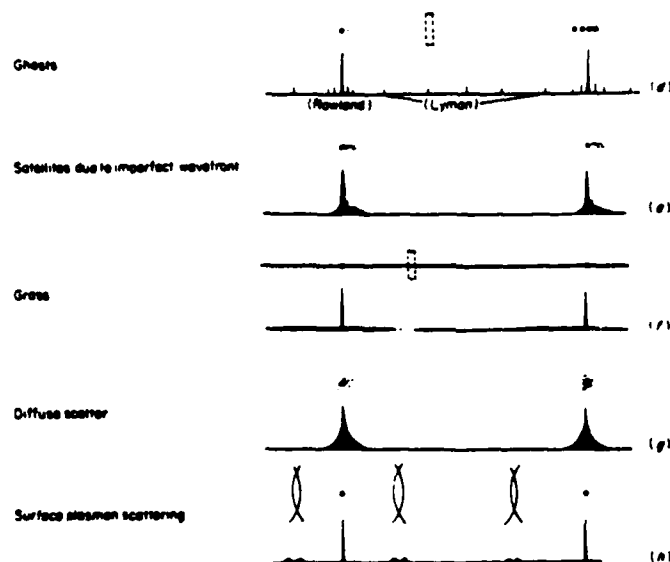


Figure 8b. Forms of Spectral Impurity

If the grating is not the limiting aperture in the system, then Fraunhofer diffraction of any other limiting aperture will give rise to a similar amount of light in the extended wings of the diffracted maxima. If, as in case (b) from Figure 8a, the aperture is circular, then a similar amount of energy goes into the wings of the diffraction pattern... the intensity will be significantly reduced. Note, that for a circular grating, the effective aperture will be elliptical because the grating is inclined to the beam. Thus, full and uniform illumination of the diffraction grating would minimize the apparent stray light, and maximize the intensity at the image point.

#### 4.2.2 Grating Defects

Periodic variations in the position or shape of the grating are defined as grating defects. These grating defects result in the formation of spurious images, commonly called ghosts, in the spectral plane of the spectrometer. *Rowland ghosts* lie close to the main orders and *Lyman ghosts* lie far away from the main orders. Since a ghost is a genuine spectral image it has the same shape as the main diffracted order and its intensity relative to that order can be measured directly. Neither differentiation between total flux and peak intensity is important, nor do their measurements depend upon the system resolution.

Non-periodic errors in the diffracted wavefront that occur over a substantial fraction of the grating aperture cause distortion of the the Fraunhofer diffraction pattern of the aperture. Apart from the distortion of the primary maxima, which results in a loss of grating resolution, the secondary maxima are distorted in both position and magnitude. These distortions in the secondary maxima are commonly known as *satellites* and are not necessarily disposed

symmetrically around the main order. Short-term random errors in the wavefront gives rise to scattered light away from the main orders. Faint lines observed joining the diffracted orders are known as *grass* and arise from grating errors that occur in a direction perpendicular to the grooves.

Recall that Fraunhofer diffraction depends on the grating size and illumination. Thus light detected at a particular point in the focal plane of an instrument will depend on Fraunhofer diffraction and stray light which arise from grating errors.

### 4.3 Grating Efficiency

Grating efficiency is affected, in general, by two factors:

1. Blazing Factors
2. Polarization Considerations

#### 4.3.1 Blazing Factors

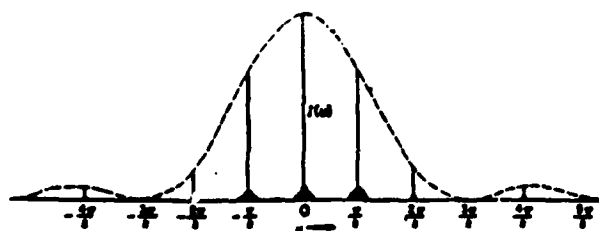
Consider monochromatic light incident normally to the plane of a grating, and a diffracted beam at an angle of diffraction  $\theta$ . The intensity in the diffracted beam is given by Equation (18) below:

$$I(\theta) = \frac{I(0)}{n^2} * \left( \frac{\sin(n k u)}{\sin(k u)} \right)^2 * \left( \frac{\sin(u)}{u} \right)^2 \quad (18)$$

where  $u = (2 \pi / \lambda) * a / 2 * \sin(\theta)$ ,  $k = (a + b) / a$  and  $n$  is the total number of transmitting lines in the grating. This equation is derived by remembering that if a converging lens

follows the grating, the spatial amplitude distribution in the focal plane of the lens is the Fourier cosine transform of the amplitude distribution in the plane of the grating.

The first term in Equation (18) is that due to interference by  $n$  equally spaced point sources, the second term is that of the diffraction of a plane wavefront by any one of the grooves of the grating. In Figure 9 below, the intensity distribution is plotted as a function of  $u$ .



The function itself is the solid line and the factor  $\sin^2 u$  which envelopes the function is shown as a broken line. In this drawing the constant  $k$  has been chosen equal to 1, so that the 3rd, 6th, 9th etc. orders are suppressed.

Figure 9. The Function  $I(u)$

While the values of  $u$ : the phase difference between wavelets arriving at the center of a ruling from those arriving at the edge, determine the directions of emergence of the diffracted beams and  $m$  is called the order of diffraction, the blaze of a grating determines the efficiency of the grating for a particular direction.

The concept of blazing a grating is that each groove should be so formed that independently, by means of geometrical optics, it redirects the incident light in the direction of a chosen diffracted order. Shown in Figure 10 is the groove profile of a blazed diffraction grating:

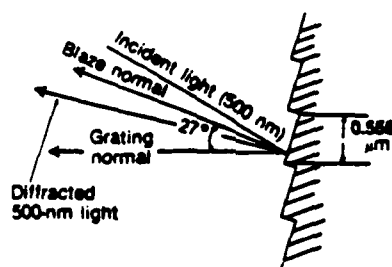


Figure 10. Blazing of a Diffraction Grating

The effect of blazing introduces an extra phase change across the width of the of the groove and alters the second term of Equation (18). This term defines the envelope of the function, refer to the dotted line in Figure 9, and for a blazed grating the principal peak of the envelope is moved sideways.

Thus, with a grating blazed at a particular wavelength, it is possible to make the groove width approach zero such that the principal maximum for that wavelength lies under the center of the envelope; all other orders of diffraction are suppressed due to the fact that they lie under the minima of the enveloping function. All incident light of this wavelength will be diffracted into the first order. No matter what blaze angle is ruled into the grating, the incident and diffracted angles are related only by the diffraction equation; blazing only determines the direction where the grating will be most efficient. Most gratings are arranged in their mountings so that the angle of incidence is very nearly equal to the angle of diffraction, and if this angle corresponds to the blaze angle there will be complete diffraction of the appropriate wavelength into that order. In the normal incidence case,  $u$  is equal to  $\pi/\lambda \sin(\theta)$ , whereas here  $u$  is zero. If the grating is rotated such that the incident and diffracted angles are equal for some other wavelength, then the phase variation over the surface of a single ruling is not zero as was the case for diffraction at the blaze angle.

The theoretical efficiency, as derived from scalar wave theory, will be greater than .5 in the

wavelength range

$$\left(\frac{2}{2m+1}\right) \lambda_b < \lambda < \left(\frac{2}{2m-1}\right) \lambda_b \quad (19)$$

where  $\lambda_b$  is the blaze wavelength in the first order, and  $m$  is the order in which the grating is to be used. This results in a reduction of the diffracted intensity since the principal maximum is no longer at the peak of the envelope. Some of the incident light will be diffracted into other orders and will be lost inside the WDM.

#### 4.3.2 Polarization Considerations

The scalar theory of diffraction for an ideal grating applies equally to light of either polarization and, even if it is modified to include the macroscopic effects of polarization upon reflection away from normal incidence, the results are only slightly changed. In practice when the groove spacing is less than about three times the wavelength the efficiency curves for the two polarizations differ dramatically and the wavelength of peak efficiency — the "blaze wavelengths" — differ.

Unpolarized incident light may be reflected with as much as 30% polarization in unfavourable cases. In general the grating approximates best to the scalar theory for light polarized with its electric vector parallel to the grooves and deviates most when the electric vector is across the grooves. The breakdown of the scalar theory with the appearance of polarization effects, in general, only affects the efficiency of the grating and does not usually affect the design of spectral instruments.

## 5 System Resolution

The resolution of a spectral system as a whole can be considered as its ability to separate wavelengths, and is frequently defined as the full width at half maximum (FWHM) of the line spread function. The line spread function being the intensity of the light at the imaging point (positioned for a particular wavelength) as a function of the wavelength readout. The line spread function is dependent on the system configuration, grating properties and efficiency, image and object areas, and wavefront aberrations.

A spectrograph is an instrument in which the image of the whole spectrum is detected on an image detector which in turn responds to the irradiance of radiation in the spectral image plane, i.e. to the flux density, whereas a spectrometer measures the total flux. Therefore a spectrograph, significantly more efficient in collecting data, requires that the given flux be brought to as small an image as possible. This in turn necessitates the design of imaging optics to focus a highly dispersed spectrum.

## **Appendix D: Optical Fibers**

## Contents

<b>1 Bandwidth Properties</b>	99
1.1 Dispersion . . . . .	99
1.1.1 Intermodal Dispersion . . . . .	100
1.1.2 Material Dispersion . . . . .	101
1.1.3 Waveguide Dispersion . . . . .	101
1.2 Attenuation . . . . .	101
<b>2 Numerical Aperture</b>	103
<b>3 Fiber Noise</b>	104
3.1 Speckle Noise . . . . .	104
3.2 Mode-Partition Noise . . . . .	105
<b>4 Multimode Fibers</b>	105
<b>5 Single-Mode Fibers</b>	106
5.1 Multimode Effects . . . . .	107
<b>6 Tradeoffs</b>	108

## List of Figures

1	<u>Propagation Aspects of Fibers with Different Structures</u> . . . . .	100
2	<u>Optical-Fiber Attenuation as a Function of Wavelength</u> . . . . .	102
3	<u>Source-Fiber Coupling in an Optical Fiber</u> . . . . .	103
4	<u>Index of Refraction Profiles and General Classifications of Multi-mode Fibers</u> .	105
5	<u>Step-index Single-mode Fiber</u> . . . . .	107

# 1 Bandwidth Properties

Bandwidth determines information transmission capacity. High-capacity systems use signals coded into binary ones and zeros, where a pulse of light represents a one and the absence of light represents a zero. The number of pulses (*bits*) per second possible is inversely proportional to the pulse duration (*pulse width*). A Fourier analysis of pulses shows that the bandwidth occupied by pulse is also inversely proportional to its duration.

The bandwidth properties of fibers can best be understood in terms of the minimum pulse width that can be used. If a sufficient time is not allowed between pulses, the pulses will interfere. This results in intersymbol interference and errors in the transmission.

Two properties of primary importance are *dispersion* and *signal attenuation*. Dispersion determines the number of bits of information that can be transmitted over a given fiber in a specified period. Attenuation (or loss) determines the distance over which a signal can be transmitted. While dispersion and attenuation are separate physical phenomena, they both cause signal distortion. In a fiber-optic communication system where bit error rate is a measure of system performance, the effects of attenuation can be traded off against the effects of dispersion.

## 1.1 Dispersion

The width (duration) of a pulse propagating in an optical fiber increases with the distance of propagation. The phenomenon of dispersion arises from the difference in the propagation velocities of the photons in the light pulse.

A mode is a transverse pattern of energy propagating at a specific velocity. Photons in a given propagation mode have the same velocity. The arrival time difference between the faster and the slower photons of a narrow pulse of light injected into a fiber increases with distance traveled, i.e. the pulse duration at the receiver increases with traveling distance. In a situation where there is a random coupling of energy between high-velocity and low-velocity propagation modes, the pulse width increases as the square root of the distance of the transmission. The duration that must be allotted between pulses to avoid intersymbol interference is proportional to the length of the fiber.

There are three classes of dispersion:

1. Intermodal Dispersion
2. Material Dispersion
3. Waveguide Dispersion

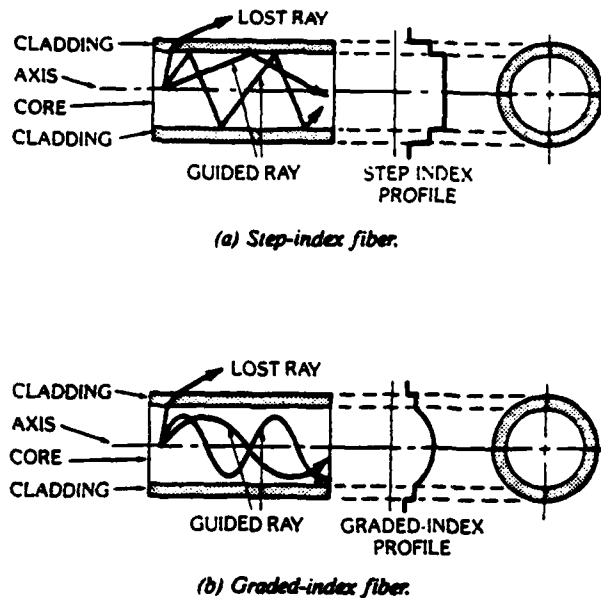


Figure 1: Propagation Aspects of Fibers with Different Structures

### 1.1.1 Intermodal Dispersion

Intermodal dispersion, the dominant source of dispersion in multimode fibers, is due to different velocities of different modes. Note that single mode fibers are not subject to intermodal dispersion. Multimode fibers support a number of modes in addition to the dominant hybrid mode  $HE_{11}$  of the linearly polarized  $LP_{01}$  mode. These modes are the discrete electromagnetic waves satisfying Maxwell's equations and the fiber's boundary conditions. Multimode fibers can be either step-index or graded-index, as shown in Figures (1):

Graded-index fibers greatly reduce intermodal dispersion. For purposes of illustration, think of modes in the fiber in terms of rays of light. Rays that deviate from the axis travel farther, but also, when they move away from the guide axis they move into a region of lower index of refraction where the velocity is greater. Thus the difference of transit times between propagating modes is accomplished by a gradation of the refractive index from the center to the outside. This causes the light to be guided not by total reflection, as in the case of step-index fibers, but by distributed refraction.

A suitably chosen index profile will result in nearly the same average velocity for all rays. The optimum index profile is nearly parabolic, which causes high-angle rays to travel a trajectory that can be characterized as more sinusoidal than angular. And, since the ray encounters glass of lower refractive index in regions away from the fiber axis, its average velocity along its trajectory can be somewhat higher than that of a paraxial ray. The net effect is that the time-of-flight differences between paraxial and skew rays are reduced, and intermodal pulse dispersion is minimized. But small deviations from this optimum profile cause significant pulse

broadening.

### 1.1.2 Material Dispersion

Material dispersion, a chromatic dispersion inherent to waveguiding processes, is due to the variation of velocity with wavelength. In other words, different wavelengths of light that occupy each particular mode travel at different velocities through the fiber. It causes an optical pulse to spread, even when all the light follows the same path. This dispersion is greater when the optical source is a broad-spectrum source, such as LED's, since the spectrum of a LED can be 50 nm full width at half maximum or more. As a result, the shortest wavelengths will travel through the fiber at substantially different speeds than the longer wavelengths. Since these wavelengths arrive at different times, an injected light pulse spreads appreciably even in the absence of modal dispersion. Two common methods to reduce material dispersion in multimode fibers are:

- Use laser diodes, which have typical FWHM values between 2-5 nm.
- Select the transmission wavelength near 1300 nm, since material dispersion has a null close to 1.3  $\mu\text{m}$ .

### 1.1.3 Waveguide Dispersion

Waveguide dispersion results from the guiding structure and is important in single-mode fibers. The guiding energy is divided between the core and the cladding. The propagation velocity in the cladding is greater than in the core. Each mode, however, has a distinct velocity that is determined by the distribution of its energy between the core and the cladding. This distribution and therefore the velocity of the mode is a function of wavelength and of the index of refraction structure used to guide the light.

Since waveguide and material dispersion depend on the source's spectral width as well as the length of the fiber, they are measure in picoseconds per nanometer per kilometer (pulse spreading divided by source spectral width divided by fiber length).

## 1.2 Attenuation

Attenuation,  $\alpha$ , is expressed in terms of decibels per unit length, and is given by:

$$\alpha = \frac{10}{L} * \ln\left(\frac{P_{in}}{P_{out}}\right) \quad (1)$$

where  $P_{out}$  is the output power,  $P_{in}$  is the input power, and  $L$  is the length of the fiber.

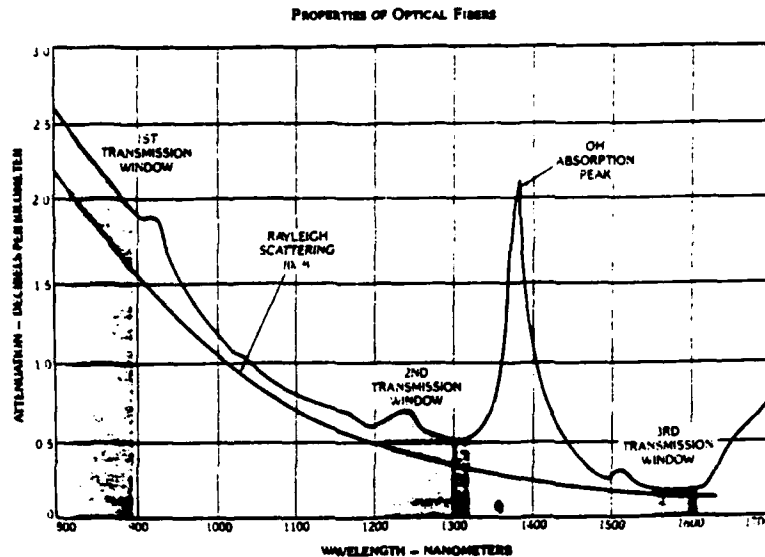


**Figure 2: Optical-Fiber Attenuation as a Function of Wavelength**

The dependence of attenuation on wavelength is shown in Figure (2). Recall that losses and dispersion are lower at the second and third transmission windows.

There are several mechanisms that lead to transmission losses in fibers:

- **Material Absorption:** part of the transmitted power is dissipated as heat.
- **Linear Scattering:** part of the power carried by one mode of the fiber is transferred linearly into another mode.
- **Nonlinear Scattering:** for very high field intensities, power is transferred to other modes shifted in frequency.
- **Waveguide Attenuation:** part of power is lost due to bending and defects at joints between axes.
- **Leaky Modes and Fiber Design:** excited modes that are neither refracted nor completely guided.
- **Ionizing Radiation Exposure:** ionization effects cause light-absorbing defect centers in fibers. Fibers with high intrinsic loss have a higher radiation sensitivity. Gamma-ray

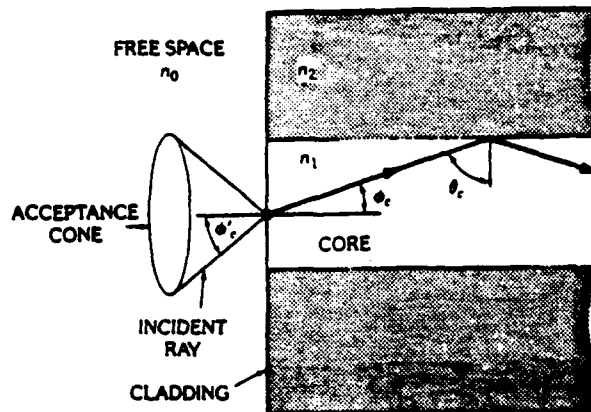


Figure 3: Source-Fiber Coupling in an Optical Fiber

damage is more pronounced at shorter wavelengths. Communication systems operating at 1300 nm suffer less damage from gamma rays than shorter-wavelength systems.

The first five are considered *intrinsic* losses and the sixth is considered an *extrinsic* loss.

## 2 Numerical Aperture

Numerical aperture is a measure of a fiber's light-gathering ability. When coupling sources to fibers, fibers to fibers, and fibers to detectors, the coupling efficiency depends on the angular distribution of energy as well as on alignment. Numerical aperture (NA) describes the angular distribution of light accepted by a fiber.

For efficient coupling to a fiber, two requirements must be satisfied. The light must be incident on the core, and it must also be injected into the fiber at an angle relative to the fiber axis that is less than the acceptance cone, formed by rotating a ray at the acceptance angle  $\phi'_c$  about the axis, as shown in Figure (3):

In step-index fibers, the guidance mechanism is total internal reflection at the core-cladding interface. In graded-index fibers, the guidance mechanism is the gradual decrease of index of refraction as a function of distance from the axis. Thus ray trajectories oscillate about the fiber axis as a function of the distance along the axis.

The amplitude of oscillation, and therefore the extent to which energy deviates from the fiber axis, is a function of the input injection angle and depends upon the entry point displacement of the light from the fiber axis. The acceptance angle for graded-index fibers is a function of where on the core face the light enters the fiber. Just as with step-index fibers, however, there is an overall limit on the angles at which light will be accepted by the fiber.

The numerical aperture of the fiber is defined as:

$$NA = \sqrt{(n_1^2 - n_2^2)} \quad (2)$$

where the light exiting from a fiber is confined to the same acceptance angle as rays entering the fiber.

### 3 Fiber Noise

Fiber propagation properties cause two types of noise: speckle or modal noise and mode-partition noise.

When fibers operate close to the cutoff of the higher-order mode, lossy propagation of the higher order mode results, which in turn, results in modal noise when short lengths of fibers, such as in pigtails are used. Mode-conversion mechanisms, such as bends and splices, cause energy to be transferred from the fundamental to the higher-order mode. Modal noise occurs when the energy in the modes varies with time in the presence of mode-dependent losses. Mode-dependent losses are speckle-dependent losses and can occur at splices and microbends.

#### 3.1 Speckle Noise

Speckle noise is the result of speckle patterns produced by interfering propagating modes. Speckle patterns occur when the time delay between fiber modes is less than the coherence time of the source. Thus, narrow-band, high-coherence sources, such as lasers, result in more modal noise than broadband sources. Note that incoherent sources do not produce modal noise. Propagating-mode changes produce speckle-pattern changes. This results in a change in the transmitted energy.

Changes in the relative strengths of propagating modes can be caused by changes in the spatial distribution of the laser output, bending, or by temperature and pressure changes in the fiber. Wavelength changes in the source, due to changes in the dielectric constant in the presence of laser drive-current electrons, are a prime cause of modal changes in the fiber.

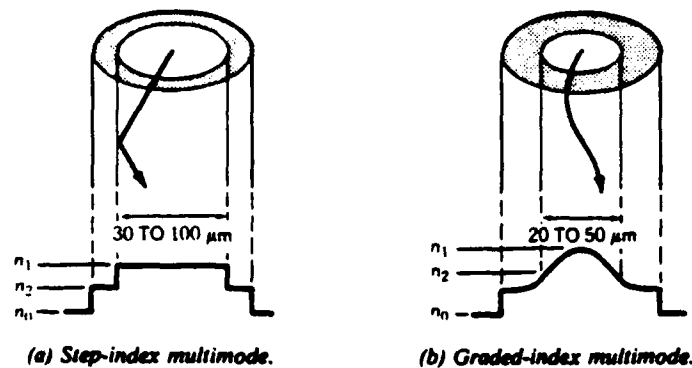


Figure 4: Index of Refraction Profiles and General Classifications of Multi-mode Fibers

### 3.2 Mode-Partition Noise

Mode-partition noise is due to a change in the distribution of energy in the laser longitudinal modes rather than in the fiber propagation modes. Mode-partition noise is the dominant noise in single-mode fibers. Light propagating at discrete frequencies is subject to relative delays determined by the chromatic dispersion of the fiber. At the laser the light is a clean pulse in time, but after propagation in the fiber, interference causes distortion. Changes in laser spectral distribution result in a change in the interference pattern at the detector. This causes a fluctuation in the detected signal even though the total laser output power is constant. Mode-partition noise is proportional to the signal power. Therefore the signal to mode-partition noise ratio cannot be improved by increasing signal power.

## 4 Multimode Fibers

Shown in Figures (4) are the two major classification of multi-mode fibers with their respective refractive index profiles.

Multimodes fibers offer the following advantages:

- They can be coupled to multimode lasers an incoherent sources as well as single-mode lasers with reasonable efficiency.
- Much wider tolerance for the alignment of these sources with the multimode fiber may be allowed than for a single-mode laser with a single-mode fiber.

- To connect and splice multi-mode fibers also requires less precision than for single-mode fibers.

Typical properties of multimode graded-index fibers include:

- Attenuation: Scattering limit increases with NA, 0.5-2.0 dB/km
- Bandwidth: Greater than 1 GHz\*km for a profile optimized for maximum bandwidth. Limited by profile control and profile change with wavelength. Bandwidth decreases with an increase in NA.
- Core: 50 to 60  $\mu\text{m}$  diameter with an NA of 0.2 to 0.3.
- Cladding:  $10\lambda$  cladding thickness and 2:1 ratio of outer diameter to core is adequate for low microbending loss (where  $\lambda$  is the wavelength of the source).
- Coupling: To Lambertian source of size equal to core, the coupling efficiency is  $(NA)^2/2$ . To laser source with coupling lens the coupling efficiency is greater than 90%. Fiber-to-fiber coupling requires alignment accurate to 10% for coupling loss to be within 1 dB. Loss is dependent on mode distribution within the fiber at the coupling point.

## 5 Single-Mode Fibers

A single-mode fiber has the ultimate wide-bandwidth capability and has a completely defined propagation characteristic. It is ideally suited for long-haul and high-capacity applications. Shown in Figure (5) is a step-index single-mode optical fiber.

The single-mode fibers carry only the dominant  $HE_{11}$  mode, but are doubly degenerate in polarization. This degeneracy results from the fact that in circular waveguides all orientations are equivalent, thus permitting two orthogonal polarization modes to exist with the same wave number.

Single-mode propagation is realized by designing core sizes to be a few wavelengths in cross-sectional dimensions and by having small index differences between the core and cladding. Single-mode fibers do not suffer from intermodal dispersion. In the case of elliptical deformation of the nominally circular fiber cross section, the two orthogonal polarization states would travel at slightly different velocities, causing an intermodal delay problem. Aside from this difficulty, the source of single-mode fiber dispersion arises from material and waveguide dispersion.

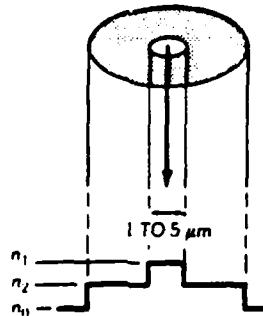


Figure 5: Step-index Single-mode Fiber

### 5.1 Multimode Effects

There are two mechanisms for multimode effects in single-mode fibers. The first is polarization, and the second is the existence of higher-order modes. Since two independent polarizations are possible, the fundamental mode of a single-mode fiber is really two modes. Thus:

- Fiber dispersion and attenuation will be different for each state of polarization.
- Imperfections cause energy to transfer between the two polarizations.
- Modal dispersion results when different polarizations have different velocities.
- Modal noise results when polarization is changing and polarization-dependent loss mechanisms are present.

The signal distortion due to polarization mode dispersion can in principle be removed by using only one polarization mode for transmission. Energy in higher-order modes propagating for some distance before being lost or transferred back to the fundamental mode can cause some pulse spreading (*modal dispersion*) of the signal in the fundamental mode.

Typical single-mode properties:

- Attenuation: Scattering limit 0.15 dB/km at 1550 nm.
- Bandwidth: Theoretically 1000 GHz\*km or more, but limited by the spectral width of the source and second order material and waveguide dispersion effects.

- Core: One to several wavelengths in diameter. Core size can be increased by lowering NA, but the radiative loss will increase at a bend and/or with dimensional variations.
- Cladding: Thickness must be at least ten times the core radius. Increased thickness eases handling and reduced susceptibility to microbending. The influence of lossy outer jacket on propagation will also be reduced.
- Coupling: Requires the light-source emission spot size to be equal to or smaller than the fiber core area for maximum efficiency.

## 6 Tradeoffs

In the choice between multimode and single-mode fibers, trade-offs between ease of coupling, bandwidth, and laser sources and stability should be considered. Large core diameter, multimode fibers, while subject to greater amounts of modal dispersion than single-mode fibers – resulting in larger bit errors at high modulation rates, will be used during the preliminary experiment construction. The initial experiment will yield preliminary crosstalk and insertion loss measurements. These measurements will be used to determine the performance of the fiber-optic wavelength division multiplexer.



# *MISSION of Rome Air Development Center*

*RADC plans and executes research, development, test and selected acquisition programs in support of Command, Control, Communications and Intelligence (C<sup>3</sup>I) activities. Technical and engineering support within areas of competence is provided to ESD Program Offices (POs) and other ESD elements to perform effective acquisition of C<sup>3</sup>I systems. The areas of technical competence include communications, command and control, battle management information processing, surveillance sensors, intelligence data collection and handling, solid state sciences, electromagnetics, and propagation, and electronic reliability/maintainability and compatibility.*